5 Geomagnetism and paleomagnetism

5.1 HISTORICAL INTRODUCTION

5.1.1 The discovery of magnetism

Mankind's interest in magnetism began as a fascination with the curious attractive properties of the mineral lodestone, a naturally occurring form of magnetite. Called loadstone in early usage, the name derives from the old English word load, meaning "way" or "course"; the loadstone was literally a stone which showed a traveller the way.

The earliest observations of magnetism were made before accurate records of discoveries were kept, so that it is impossible to be sure of historical precedents. Nevertheless, Greek philosophers wrote about lodestone around 800 BC and its properties were known to the Chinese by 300 BC. To the ancient Greeks science was equated with knowledge, and was considered an element of philosophy. As a result, the attractive forces of lodestone were ascribed to metaphysical powers. Some early animistic philosophers even believed lodestone to possess a soul. Contemporary mechanistic schools of thought were equally superstitious and gave rise to false conceptions that persisted for centuries. Foremost among these was the view that electrical and magnetic forces were related to invisible fluids. This view persisted well into the nineteenth century. The power of a magnet seemed to flow from one pole to the other along lines of induction that could be made visible by sprinkling iron filings on a paper held over the magnet. The term "flux" (synonymous with flow) is still found in "magnetic flux density," which is regularly used as an alternative to "magnetic induction" for the fundamental magnetic field vector **B**.

One of the greatest and wealthiest of the ancient Greek city-colonies in Asia Minor was the seaport of Ephesus, at the mouth of the river Meander (modern Küçük Menderes) in the Persian province of Caria, in what is now the Turkish province of western Anatolia. In the fifth century BC the Greek state of Thessaly founded a colony on the Meander close to Ephesus called *Magnesia*, which after 133 BC was incorporated into the Roman empire as *Magnesia ad Maeandrum*. In the vicinity of Magnesia the Greeks found a ready supply of lodestone, pieces of which subsequently became known by the Latin word *magneta* from which the term magnetism derives.

It is not known when the directive power of the magnet – its ability to align consistently north–south – was first recognized. Early in the Han dynasty, between 300 and 200 BC, the Chinese fashioned a rudimentary compass out of lodestone. It consisted of a spoon-shaped object, whose bowl balanced and could rotate on a flat polished surface. This compass may have been used in the search for gems and in the selection of sites for houses. Before 1000 AD the Chinese had developed suspended and pivoted-needle compasses. Their directive power led to the use of compasses for navigation long before the origin of the aligning forces was understood. As late as the twelfth century, it was supposed in Europe that the alignment of the compass arose from its attempt to follow the pole star. It was later shown that the compass alignment was produced by a property of the Earth itself. Subsequently, the characteristics of terrestrial magnetism played an important role in advancing the understanding of magnetism.

5.1.2 Pioneering studies in terrestrial magnetism

In 1269 the medieval scholar Pierre Pélerin de Maricourt, who took the Latin nom-de-plume of Petrus Peregrinus, wrote the earliest known treatise of experimental physics (*Epistola de Magnete*). In it he described simple laws of magnetic attraction. He experimented with a spherical magnet made of lodestone, placing it on a flat slab of iron and tracing the lines of direction which it assumed. These lines circled the lodestone sphere like geographical meridians and converged at two antipodal points, which Peregrinus called the *poles* of the magnet, by analogy to the geographical poles. He called his magnetic sphere a *terrella*, for "little Earth."

It was known to the Chinese around 500 AD, in the Tang dynasty, that magnetic compasses did not point exactly to geographical north, as defined by the stars. The local deviation of the magnetic meridian from the geographical meridian is called the magnetic *declination*. By the fourteenth century, the ships of the British navy were equipped with a mariner's compass, which became an essential tool for navigation. It was used in conjunction with celestial methods, and gradually it became apparent that the declination changed with position on the globe. During the fifteenth and sixteenth centuries the worldwide pattern of declination was established. By the end of the sixteenth century, Mercator recognized that

declination was the principal cause of error in contemporary map-making.

Georg Hartmann, a German cleric, discovered in 1544 that a magnetized needle assumed a non-horizontal attitude in the vertical plane. The deviation from the horizontal is now called the magnetic *inclination*. He reported his discovery in a letter to his superior, Duke Albrecht of Prussia, who evidently was not impressed. The letter lay unknown to the world in the royal archives until its discovery in 1831. Meanwhile, an English scientist, Robert Norman, rediscovered the inclination of the Earth's magnetic field independently in 1576.

In 1600 William Gilbert (1544–1603), an English scientist and physician to Queen Elizabeth, published *De Magnete*, a landmark treatise in which he summarized all that was then known about magnetism, including the results of about seventeen years of his own research. His studies extended also to the electrostatic effects seen when some materials were rubbed, for which he coined the name "electricity" from the Greek word for amber. Gilbert was the first to distinguish clearly between electrical and magnetic phenomena. His magnetic studies followed the work of Peregrinus three centuries earlier. Using small magnetic needles placed on the surface of a sphere of lodestone to study its magnetic field, he recognized the poles, where the needles stood on end, and the equator, where they lay parallel to the surface. Gilbert achieved the leap of imagination that was necessary to see the analogy between the attraction of the lodestone sphere and the known magnetic properties of the Earth. He recognized that the Earth itself behaved like a large magnet. This was the first unequivocal recognition of a geophysical property, preceding the laws of gravitation in Newton's *Principia* by almost a century. Although founded largely on qualitative observations, *De Magnete* was the most important work on magnetism until the nineteenth century.

The discovery that the declination of the geomagnetic field changed with time was made by Henry Gellibrand (1597–1637), an English mathematician and astronomer, in 1634. He noted, on the basis of just three measurements made by William Borough in 1580, Edmund Gunter in 1622 and himself in 1634, that the declination had decreased by about 7° in this time. From these few observations he deduced what is now called the *secular variation* of the field.

Gradually the variation of the terrestrial magnetic field over the surface of the Earth was established. In 1698–1700 Edmund Halley, the English astronomer and mathematician, carried out an important oceanographic survey with the prime purpose of studying compass variations in the Atlantic ocean. In 1702 this resulted in the publication of the first declination chart.

5.1.3 The physical origins of magnetism

By the end of the eighteenth century many characteristics of terrestrial magnetism were known. The *qualitative* properties of magnets (e.g., the concentration of their powers at their poles) had been established, but the accumulated observations were unable to provide a more fundamental understanding of the phenomena because they were not *quantitative*. A major advance was achieved by Charles Augustin de Coulomb (1736–1806), the son of a noted French family, who in 1784 invented a torsion balance that enabled him to make quantitative measurements of electrostatic and magnetic properties. In 1785 he published the results of his intensive studies. He established the inverse-square law of attraction and repulsion between small electrically charged balls. Using thin, magnetized steel needles about 24 inches (61 cm) in length, he also established that the attraction or repulsion between their poles varied as the inverse square of their separation.

Alessandro Volta (1745–1827) invented the voltaic cell with which electrical currents could be produced. The relationship between electrical currents and magnetism was detected in 1820 by Hans Christian Oersted (1777–1851), a Danish physicist. During experiments with a battery of voltaic cells he observed that a magnetic needle is deflected at right angles to a conductor carrying a current, thus establishing that an electrical current produces a magnetic force.

Oersted's result was met with great enthusiasm and was followed at once by other notable discoveries in the same year. The law for the direction and strength of the magnetic force near a current-carrying wire was soon formulated by the French physicists Jean-Baptiste Biot (1774–1862) and Felix Savart (1791–1841). Their compatriot André Marie Ampère (1775–1836) quickly undertook a systematic set of experiments. He showed that a force existed between two parallel straight current-carrying wires, and that it was of a type different from the known electrical forces. Ampère experimented with the magnetic forces produced by current loops and proposed that internal electrical currents were responsible for the existence of magnetism in iron objects (i.e., ferromagnetism). This idea of permanent magnetism due to constantly flowing currents was audacious for its time.

At this stage, the ability of electrical currents to generate magnetic fields was known, but it fell to the English scientist Michael Faraday (1791–1867) to demonstrate in 1831 what he called "magneto-electric" induction. Faraday came from a humble background and had little mathematical training. Yet he was a gifted experimenter, and his results demonstrated that the change of magnetic flux in a coil (whether produced by introducing a magnet or by the change in current in another coil) induced an electric current in the coil. The rule that governs the direction of the induced current was formulated three years later by a Russian physicist, Heinrich Lenz (1804–1865). Unhampered by mathematical equations, Faraday made fundamental contributions to understanding magnetic processes. Instead of regarding magnetic and electrical phenomena as the effects of centers of force acting at a distance, he saw in his mind's eye fictional lines of force

traversing space. This image emphasized the role of the medium and led eventually to the concept of *magnetic field*, which Faraday first used in 1845.

Although much had been established by the early 1830s, it was still necessary to interpret the strengths of magnetic forces by relating magnetic units to mechanical units. This was achieved in 1832 by the German scientist and mathematician, Carl Friedrich Gauss (1777–1855), who assumed that static magnetism was carried by magnetic "charges," analogous to the carriers of static electricity. Experiment had shown that, in contrast to electric charge, magnetic poles always occur as oppositely signed pairs, and so the basic unit of magnetic properties corresponds to the dipole. Together with Wilhelm Weber (1804–1891), Gauss developed a method of absolute determination of the intensity of the Earth's magnetic field. They founded a geomagnetic observatory at Göttingen where the Earth's magnetic field was observed at regular intervals. By 1837 global charts of the total intensity, inclination and declination were in existence, although the data had been measured at different times and their areal coverage was incomplete. To analyze the data-set Gauss applied the mathematical techniques of spherical harmonic analysis and the separation of variables, which he had invented. In 1839 he established that the main part of the Earth's magnetic field was a dipole field that originated inside the Earth.

The fundamental physical laws governing magnetic effects were now firmly established. In 1872 James Clerk Maxwell (1831–1879), a Scottish physicist, derived a set of equations that quantified all known relationships between electrical and magnetic phenomena: Coulomb's laws of force between electric charges and magnetic poles; Oersted's and Ampère's laws governing the magnetic effects of electric currents; Faraday's and Lenz's laws of electromagnetic induction; and Ohm's law relating current to electromotive force. Maxwell's mathematical studies predicted the propagation of electric waves in space, and concluded that light is also an electromagnetic phenomenon transmitted through a medium called the *luminiferous ether*. The need for this light-transmitting medium was eliminated by the theory of relativity. By putting the theory of the electromagnetic field on a mathematical basis, Maxwell enabled a greater understanding of electromagnetic phenomena before the discovery of the electron.

A further notable discovery was made in 1879 by Heinrich Lorentz (1853–1928), a Dutch physicist. In experiments with vacuum tubes he observed the deflection of a beam of moving electrical charge by a magnetic field. The deflecting force acted in a direction perpendicular to the magnetic field and to the velocity of the charged particles, and was proportional to both the field and the velocity. This result now serves to define the unit of magnetic induction.

Since the time of man's first awareness of magnetic behavior, students of terrestrial magnetism have made important contributions to the understanding of magnetism as a physical phenomenon. In turn, advances in the physics of magnetism have helped geophysicists to understand the morphology and origin of the Earth's magnetic field, and to apply this knowledge to geological processes, such as global tectonics. The physical basis of magnetism is fundamental to the geophysical topics of geomagnetism, rock magnetism and paleomagnetism.

5.2 THE PHYSICS OF MAGNETISM

5.2.1 Introduction

Early investigators conceptualized gravitational, electrical and magnetic forces between objects as instantaneous effects that took place through direct action-at-a-distance. Faraday introduced the concept of the *field* of a force as a property of the space in which the force acts. The force-field plays an intermediary role in the interaction between objects. For example, an electric charge is surrounded by an electrical field that acts to produce a force on a second charge. The pattern of a field is portrayed by *field lines.* At any point in a field the direction of the force is tangential to the field line and the intensity of the force is proportional to the number of field lines per unit cross-sectional area.

Problems in magnetism are often more complicated for the student than those in gravitation and electrostatics. For one thing, gravitational and electrostatic fields act centrally to the source of force, which varies in each case as the inverse square of distance. Magnetic fields are not central; their directions vary with azimuth. Moreover, even in the simplest case (that of a magnetic dipole or a small current loop) the field strength falls off inversely as the cube of distance. To make matters more complicated, the student has to take account of *two* magnetic fields (denoted by **B** and **H**).

The confusion about the **B**-field and the **H**-field may be removed by recalling that all magnetic fields originate with electrical currents. This is the case even for permanent magnets, as Ampère astutely recognized in 1820. We now know that these currents are associated with the motions of electrons about atomic nuclei in the permanent magnets. The fundamental magnetic field associated with currents in any medium is **B**. The quantity **H** should be regarded as a computational parameter proportional to **B** in non-magnetizable materials. Inside a magnetizable material, **H** describes how **B** is modified by the magnetic polarization (or magnetization, **M**) of the material. The magnetic **B**-field is also called the magnetic induction or magnetic flux density.

Historically, the laws of magnetism were established by relating the **B**-field to fictitious centers of magnetic force called magnetic poles, defined by comparison with the properties of a bar magnet. Gauss showed that, in contrast to electrostatic charges, free magnetic poles cannot exist; each positive pole must be paired with a

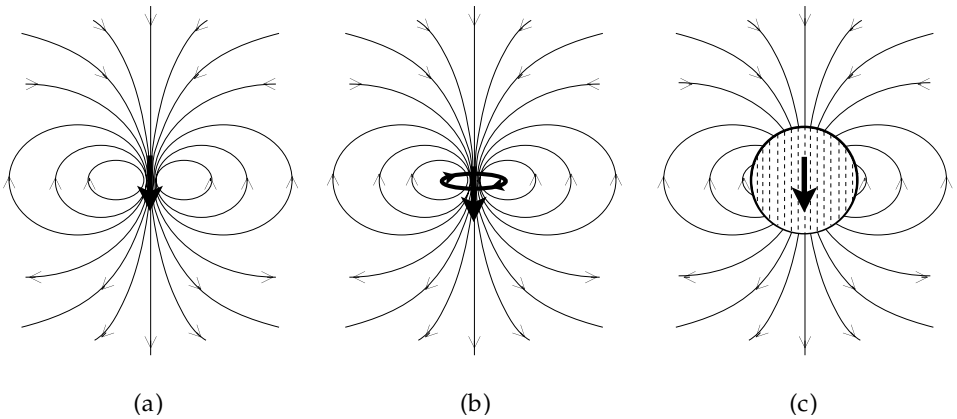

Fig. 5.1 The characteristic field lines of a magnetic dipole are found around (a) a short bar magnet, (b) a small loop carrying an electric current, and (c) a uniformly magnetized sphere.

corresponding negative pole. The most important type of magnetic field – and also the dominant component of the geomagnetic field – is that of a *magnetic dipole* (Fig. 5.1a). This is the field of two magnetic poles of opposite sense that are infinitesimally close to each other. The geometry of the field lines shows the paths along which a free magnetic pole would move in the vicinity of the dipole. A tiny current loop (Fig. 5.1b) and a uniformly magnetized sphere (Fig. 5.1c) also have dipole-type magnetic fields around them. Although magnetic poles do not exist physically, many problems that arise in geophysical situations can be readily solved in terms of surface distributions of poles or dipoles. So we will first examine these concepts.

5.2.2 Coulomb's law for magnetic poles

Coulomb's experiments in 1785 established that the force between the ends of long thin magnets was inversely proportional to the square of their separation. Gauss expanded Coulomb's observations and attributed the forces of attraction and repulsion to fictitious magnetic charges, or poles. An inverse square law for the force F between magnetic poles with strengths p_1 and p_2 at distance r from each other can be formulated as

$$F(r) = K\frac{p_1 p_2}{r^2} \tag{5.1}$$

The proportionality constant K was originally defined to be dimensionless and equal to unity, analogously to the law of electrostatic force. This gave the dimensions of pole strength in the centimeter-gram-second (c.g.s.) system as dyne$^{1/2}$ cm.

5.2.2.1 The field of a magnetic pole

The gravitational field of a given mass is defined as the force it exerts on a unit mass (Section 2.2.2). Similarly, the electric field of a given charge is the force it exerts on a unit charge. These ideas cannot be transferred directly to magnetism, because magnetic poles do not really exist. Nevertheless, many magnetic properties can be described and magnetic problems solved in terms of fictitious poles. For example, we can define a magnetic field B as the force exerted by a pole of strength p on a unit pole at distance r. From Eq. (5.1) we get

$$B(r) = K\frac{p}{r^2} \tag{5.2}$$

Setting $K = 1$, the unit of the magnetic **B**-field has dimensions dyne$^{1/2}$ cm^{-1} in c.g.s. units and is called a *gauss*. Geophysicists employ a smaller unit, the *gamma* (γ), to describe the geomagnetic field and to chart magnetic anomalies ($1\ \gamma = 10^{-5}$ gauss).

Unfortunately, the c.g.s. system required units of electrical charge that had different dimensions and size in electrostatic and electromagnetic situations. By international agreement the units were harmonized and rationalized. In the modern Système Internationale (SI) units the proportionality constant K is not dimensionless. It has the value $\mu_0/4\pi$, where μ_0 is called the *permeability constant* and is equal to $4\pi \times 10^{-7}$ N A^{-2} (or henry/meter, H m^{-1}, which is equivalent to N A^{-2}).

5.2.2.2 The potential of a magnetic pole

In studying gravitation we also used the concept of a field to describe the region around a mass in which its attraction could be felt by another test mass. In order to move the test mass away from the attracting mass, work had to be done against the attractive force and this was found to be equal to the gain of potential energy of the test mass. When the test mass was a unit mass, the attractive force was called the gravitational field and the gain in potential energy was called the change in potential. We calculated the gravitational potential at distance r from an attracting point mass by computing the work that would have to be expended *against* the field to move the unit mass from r to infinity.

We can define the magnetic potential W at a distance r from a pole of strength p in exactly the same way. The magnetic field of the pole is given by Eq. (5.2). Using the value $\mu_0/4\pi$ for K and expressing the pole strength p in SI units, the magnetic potential at r is given by

$$W = -\int_r^\infty B\,\mathrm{d}r = \frac{\mu_0 p}{4\pi r} \tag{5.3}$$

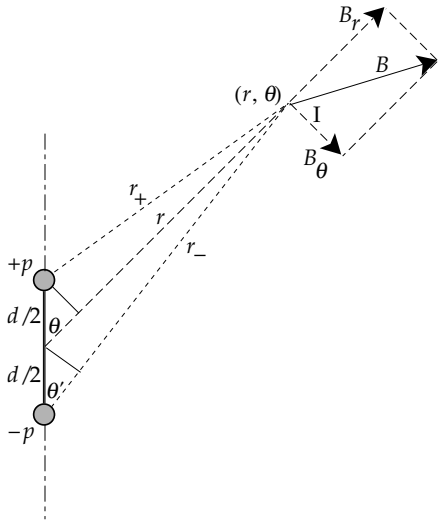

Fig. 5.2 Geometry for the calculation of the potential of a pair of magnetic poles.

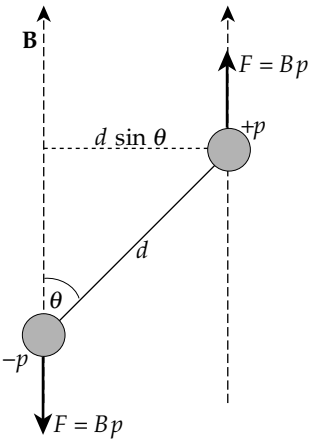

$$\text{torque} = Fd \sin\theta$$
$$\boldsymbol{\tau} = pd\ B \sin\theta = \mathbf{m} \times \mathbf{B}$$

Fig. 5.3 Definition of the magnetic moment **m** of a pair of magnetic poles.

5.2.3 The magnetic dipole

In Fig. 5.1 the line joining the positive and negative poles (or the normal to the plane of the loop, or the direction of magnetization of the sphere) defines an axis, about which the field has rotational symmetry. Let two equal and opposite poles, $+p$ and $-p$, be located a distance d apart (Fig. 5.2). The potential W at a distance r from the midpoint of the pair of poles, in a direction that makes an angle θ to the axis, is the sum of the potentials of the positive and negative poles. At the point (r, θ) the distances from the respective poles are r_+ and r_- and we get for the magnetic potential of the pair

$$W = \frac{\mu_0 p}{4\pi}\left(\frac{1}{r_+} - \frac{1}{r_-}\right) \tag{5.4}$$

$$W = \frac{\mu_0 p}{4\pi}\left(\frac{r_- - r_+}{r_+ r_-}\right) \tag{5.5}$$

The pair of opposite poles is considered to form a *dipole* when their separation becomes infinitesimally small compared to the distance to the point of observation (i.e., $d \ll r$). In this case, we get the approximate relations

$$\begin{aligned} r_+ &\approx r - \frac{d}{2}\cos\theta \\ r_- &\approx r + \frac{d}{2}\cos\theta' \end{aligned} \tag{5.6}$$

When $d \ll r$, we can write $\theta \approx \theta'$ and terms of order $(d/r)^2$ and higher can be neglected. This leads to the further simplifications

$$\begin{aligned} r_- - r_+ &\approx \frac{d}{2}(\cos\theta' + \cos\theta) \approx d\cos\theta \\ r_+ r_- &\approx r^2 - \frac{d^2}{4}\cos^2\theta \approx r^2 \end{aligned} \tag{5.7}$$

Substituting Eq. (5.7) in Eq. (5.5) gives the dipole potential at the point (r, θ):

$$W = \frac{\mu_0}{4\pi}\frac{(dp)\cos\theta}{r^2} = \frac{\mu_0}{4\pi}\frac{m\cos\theta}{r^2} \tag{5.8}$$

The quantity $m = (dp)$ is called the *magnetic moment* of the dipole. This definition derives from observations on bar magnets. The torque exerted by a magnetic field to turn the magnet parallel to the field direction is proportional to m. This applies even when the separation of the poles becomes very small, as in the case of the dipole.

The torque can be calculated by considering the forces exerted by a uniform magnetic field B on a pair of magnetic poles of strength p separated by a distance d (Fig. 5.3). A force equal to (Bp) acts on the positive pole and an equal and opposite force acts on the negative pole. If the magnetic axis is oriented at angle θ to the field, the perpendicular distance between the lines of action of the forces is $d \sin\theta$. The torque $\boldsymbol{\tau}$ felt by the magnet is equal to $B(pd)\sin\theta$ (i.e., $\boldsymbol{\tau} = mB \sin\theta$). Taking into account the direction of the torque and using the conventional notation for the cross product of two vectors this gives for the magnetic torque

$$\boldsymbol{\tau} = \mathbf{m} \times \mathbf{B} \tag{5.9}$$

5.2.4 The magnetic field of an electrical current

The equation used to define the magnetic **B**-field was formulated by Lorentz in 1879. Let q be an electrical charge that moves with velocity $\mathbf{v}$ through a magnetic field **B** (Fig. 5.4a). The charged particle experiences a deflecting force **F** given by Lorentz's law, which in SI units is:

$$\mathbf{F} = q(\mathbf{v} \times \mathbf{B}) \tag{5.10}$$

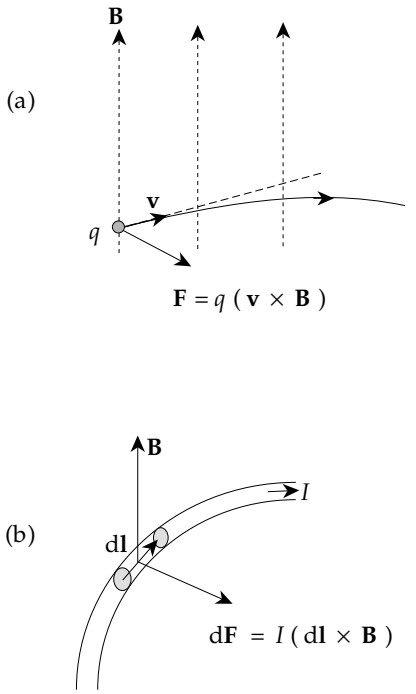

Fig. 5.4 Illustrations of (a) Lorentz's law for the deflecting force **F** experienced by an electrical charge that moves with velocity **v** through a magnetic field **B**, and (b) the law of Biot and Savart for the force experienced by an element d**l** of a conductor carrying a current *I* in a magnetic field **B**.

The SI unit of the magnetic **B**-field defined by this equation is called a *tesla*; it has the dimensions $\mathrm{N\,A^{-1}\,m^{-1}}$.

Imagine the moving charge to be confined to move along a conductor of length d*l* and cross-section *A* (Fig. 5.4b). Let the number of charges per unit volume be *N*. The number inside the element d*l* is then *NA* d*l*. Each charge experiences a deflecting force given by Eq. (5.10). Thus the total force transferred to the element d**l** is

$$\mathrm{d}\mathbf{F} = NA\,\mathrm{d}l q(\mathbf{v}\times\mathbf{B}) = NAvq(\mathrm{d}\mathbf{l}\times\mathbf{B}) \tag{5.11}$$

The electrical current *I* along the conductor is the total charge that crosses *A* per second, and is given by $I = NAvq$. From Eq. (5.11) we get the law of Biot and Savart for the force experienced by the element d**l** of a conductor carrying a current *I* in a magnetic field **B**:

$$\mathrm{d}\mathbf{F} = I(\mathrm{d}\mathbf{l}\times\mathbf{B}) \tag{5.12}$$

The orienting effect of an electrical current on magnetic compass needles, reported by Oersted and Ampère in 1820, is illustrated in Fig. 5.5. The magnetic field lines around an infinitely long straight wire form concentric circles in the plane normal to the wire. The strength of the **B**-field around the wire is

$$B = \frac{\mu_0 I}{2\pi r} \tag{5.13}$$

The Biot–Savart law can be applied to determine the torque exerted on a small rectangular loop PQRS in a

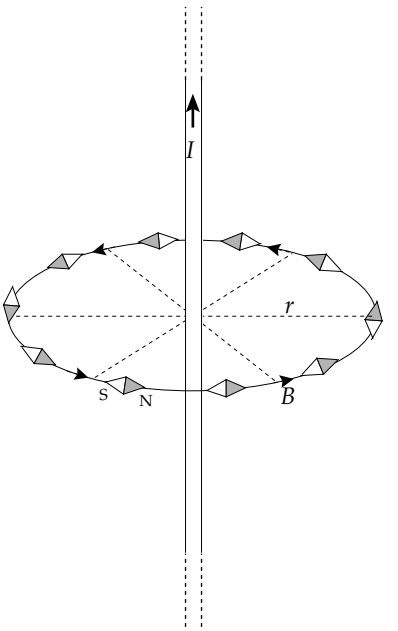

Fig. 5.5 Small compass needles show that the magnetic field lines around an infinitely long straight wire carrying an electrical current form concentric circles in a plane normal to the wire.

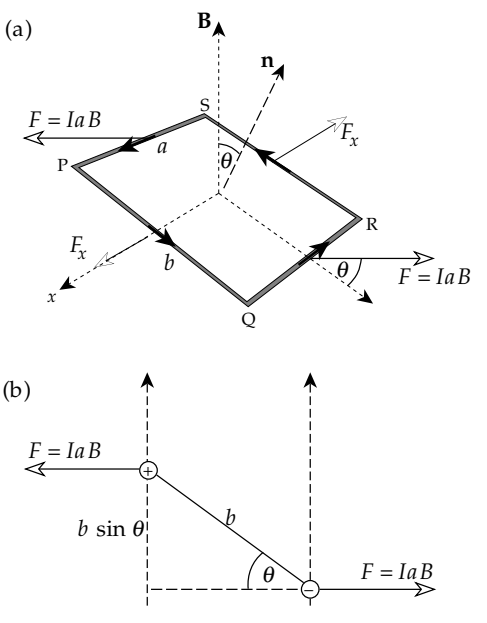

Fig. 5.6 (a) Rectangular loop carrying a current *I* in a uniform magnetic field *B*; (b) derivation of the torque **τ** experienced by the loop.

magnetic field (Fig. 5.6a). Let the lengths of the sides of the loop be *a* and *b*, respectively, and define the *x*-axis parallel to the sides of length *a*. The area of the loop can be expressed as a vector with magnitude $A = ab$, and direction **n** normal to the plane of the loop. Suppose that a current *I* flows in the loop and that a magnetic field **B** acts normal to the *x*-axis, making an angle θ with the

normal to the plane of the loop. Applying Eq. (5.12), a force F_x equal to $(IbB\cos\theta)$ acts on the side PQ in the direction of $+x$; its effect is cancelled by an equal and opposite force F_x acting on side RS in the direction of $-x$. Forces equal to (IaB) act in opposite directions on the sides QR and SP (Fig. 5.6b). The perpendicular distance between their lines of action is $b\sin\theta$, so the torque $\boldsymbol{\tau}$ experienced by the current loop is

$$\boldsymbol{\tau} = (IaB)b\sin\theta = (IA)B\sin\theta$$
$$\boldsymbol{\tau} = \mathbf{m} \times \mathbf{B} \tag{5.14}$$

The quantity $\mathbf{m} = IA$ is a vector with direction parallel to the normal to the plane of the current loop. This expression is valid for an arbitrary small loop of area A, regardless of its shape. By comparing Eqs. (5.14) and (5.9) for the torque on a dipole, it is evident that **m** corresponds to the magnetic moment of the current loop. At distances greater than the dimensions of the loop, the magnetic field is that of a dipole at the center of the loop (Fig. 5.1b). The definition of **m** in terms of a current-carrying loop shows that magnetic moment has the units of current times area (A m^2).

5.2.5 Magnetization and the magnetic field inside a material

A true picture of magnetic behavior requires a quantum-mechanical analysis. Fortunately, a working understanding of the magnetic behavior of materials can be acquired without getting involved in the quantum-mechanical details. The simplified concept of atomic structure introduced by Ernest Rutherford in 1911 gives a readily understandable model for the magnetic behavior of materials. The motion of an electron around an atomic nucleus is treated like the orbital motion of a planet about the Sun. The orbiting charge forms an electrical current with which an *orbital magnetic moment* is associated. A planet also rotates about its axis; likewise each electron can be visualized as having a spin motion about an axis. The spinning electrical charge produces a *spin magnetic moment*. Each magnetic moment is directly related to the corresponding *angular momentum*. In quantum theory each type of angular momentum of an electron is quantized. Thus the spin and orbital magnetic moments are restricted to having discrete values. The spin magnetic moment is usually more important than the orbital moment in the rock-forming minerals (see Section 5.2.6).

A simplified picture of the magnetic moments inside a material is shown in Fig. 5.7. The magnetic moment **m** of each atom is associated with a current loop as illustrated in Fig. 5.1b and described in the previous section. The net magnetic moment of a volume V of the material depends on the degree of alignment of the individual atomic magnetic moments. It is the vector sum of all the atomic magnetic moments in the material. The magnetic moment per unit volume of the material is called its *magnetization*, denoted **M**:

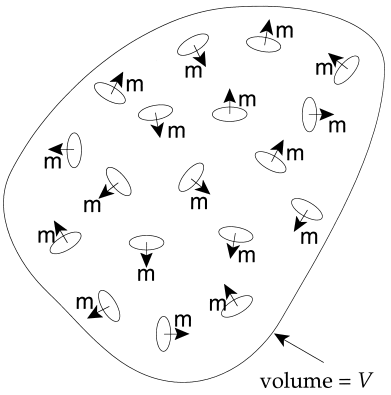

Fig. 5.7 Schematic representation of the magnetic moments inside a material; each magnetic moment **m** is associated with a current loop on an atomic scale.

$$\mathbf{M} = \sum \mathbf{m}_i / V \tag{5.15}$$

Magnetization has the dimensions of magnetic moment (A m^2) divided by volume (m^3), so that the SI units of **M** are A m^{-1}. The dimensions of **B** are N A^{-1} m^{-1} and those of μ_0 are N A^{-2}; consequently the dimensions of B/μ_0 are also A m^{-1}. In general, the magnetization **M** inside a magnetic material will not be exactly equal to B/μ_0; let the difference be **H**, so that

$$\mathbf{H} = \mathbf{B}/\mu_0 - \mathbf{M} \tag{5.16}$$

In the earlier c.g.s. system **H** was defined by the vector equation $\mathbf{H} = \mathbf{B} - 4\pi\mathbf{M}$, and the dimensions of **H** and **B** were the same. For this reason **H** became known as the *magnetizing field* (or **H**-field). It is a readily computed quantity that is useful in determining the value of the true magnetic field **B** in a medium. The fundamental difference between the **B**-field and the **H**-field can be understood by inspection of the configurations of their respective field lines. The field lines of **B** always form closed loops (Fig. 5.1). The field lines of **H** are discontinuous at surfaces where the magnetization **M** changes in strength or direction. Magnetic methods of geophysical exploration take advantage of surface effects that arise where the magnetization is interrupted.

Anomalous magnetic fields arise over geological structures that cause a magnetization contrast between adjacent rock types. Many magnetic anomalies can be analyzed by replacing the change in magnetization at a surface by an appropriate surface distribution of fictitious magnetic poles. The methodology, though based on a fundamentally false concept, is quite practical for modelling anomaly shapes and is often much simpler than a physically correct analysis in terms of current distributions. For example, in a uniformly magnetized rod, the N-poles of the elementary magnetic moments are considered to be exposed on one end of the rod, with a corresponding distribution of S-poles on the opposite end; inside the material the N-poles and S-poles cancel each other (Fig. 5.8a). The **H**-field inside the material arises from these pole distributions and

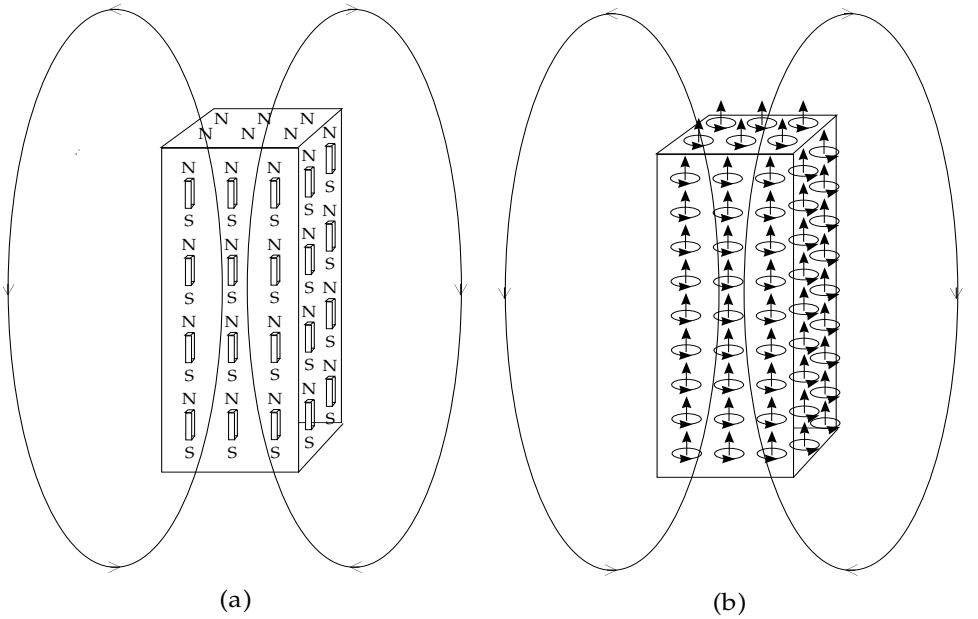

Fig. 5.8 The magnetization of a material may be envisaged as due to an alignment of (a) small dipoles or (b) equivalent current loops; even in a permanent magnet the physical source of the **B**-field of the material is a system of electrical currents on an atomic scale.

acts in the *opposite* direction to the magnetization **M**. Outside the magnet the **B**-field and **H**-field are parallel; the **H**-field is discontinuous at the ends of the magnet.

The same situation can be portrayed in terms of current loops. The physical source of every **B**-field is an electrical current, even in a permanent magnet (Fig. 5.8b). Atomic current loops give a continuous **B**-field that emerges from the magnet at one end, re-enters at the other end and is closed inside the magnet. The aligned magnetic moments of the elementary current loops cancel out inside the body of the magnet, but the currents in the loops adjacent to the sides of the magnet combine to form a surface "current" that maintains the magnetization **M**.

In a vacuum there is no magnetization ($\mathbf{M} = 0$); the vectors **B** and **H** are parallel and proportional ($\mathbf{B} = \mu_0\mathbf{H}$). Inside a magnetizable material the magnetic **B**-field has two sources. One is the external system of real currents that produce the magnetizing field **H**; the other is the set of internal atomic currents that cause the atomic magnetic moments whose net alignment is expressed as the magnetization **M**. In a general, anisotropic magnetic material **B**, **M** and **H** are not parallel. However, many magnetic materials are not strongly anisotropic and the elementary atomic magnetic moments align in a statistical fashion with the magnetizing field. In this case **M** and **H** are parallel and proportional to each other

$$\mathbf{M} = k\mathbf{H} \tag{5.17}$$

The proportionality factor k is a physical property of the material, called the *magnetic susceptibility*. It is a measure of the ease with which the material can be magnetized. Because **M** and **H** have the same units (A m^{-1}), k is a dimensionless quantity. The susceptibility of most materials is temperature dependent, and in some materials (ferromagnets and ferrites) k depends on **H** in a complicated fashion. In general, Eq. (5.16) can be rewritten

$$\mathbf{B} = \mu_0(\mathbf{H} + \mathbf{M}) = \mu_0\mathbf{H}(1 + k)$$
$$\mathbf{B} = \mu\mu_0\mathbf{H} \tag{5.18}$$

The quantity $\mu = (1 + k)$ is called the *magnetic permeability* of the material. The term "permeability" recalls the early nineteenth century association of magnetic powers with an invisible fluid. For example, the permeability of a material expresses the ability of the material to allow a fluid to pass through it. Likewise, the magnetic permeability is a measure of the ability of a material to convey a magnetic flux. Ferromagnetic metals have high permeabilities; in contrast, minerals and rocks have low susceptibilities and permeabilities $\mu \approx 1$.

5.2.6 The magnetic properties of materials

The magnetic behavior of a solid depends on the magnetic moments of the atoms or ions it contains. As discussed above, atomic and ionic magnetic moments are proportional to the quantized angular momenta associated with the orbital motion of electrons about the nucleus and with the spins of the electrons about their own axes of rotation. In quantum theory the *exclusion principle* of Wolfgang Pauli states that no two electrons in a given system can have the same set of quantum numbers. When applied to an atom or ion, Pauli's principle stipulates that each possible electron orbit can be occupied by up to two electrons with opposite spins. The orbits are arranged in shells around the nucleus. The magnetic moments of paired opposite spins cancel each other out. Consequently, the net angular momentum

and the net magnetic moment of a filled shell must be zero. The net magnetic moment of an atom or ion arises from incompletely filled shells that contain unpaired spins. The atoms or ions in a solid are not randomly distributed but occupy fixed positions in a regular lattice, which reflects the symmetry of the crystalline structure and which controls interactions between the ions. Hence, the different types of magnetic behavior observed in solids depend not only on the presence of ions with unpaired spins, but also on the lattice symmetry and cell size.

Three main classes of magnetic behavior can be distinguished on the basis of magnetic susceptibility: *diamagnetism*, *paramagnetism* and *ferromagnetism*. In diamagnetic materials the susceptibility is low and negative, i.e., a magnetization develops in the opposite direction to the applied field. Paramagnetic materials have low, positive susceptibilities. Ferromagnetic materials can be subdivided into three categories. True ferromagnetism is a cooperative phenomenon observed in metals like iron, nickel and cobalt, in which the lattice geometry and spacing allows the exchange of electrons between neighboring atoms. This gives rise to a *molecular field* by means of which the magnetic moments of adjacent atoms reinforce their mutual alignment parallel to a common direction. Ferromagnetic behavior is characterized by high positive susceptibilities and strong magnetic properties. The crystal structures of certain minerals permit an indirect cooperative interaction between atomic magnetic moments. This *indirect exchange* confers magnetic properties that are similar to ferromagnetism. The mineral may display *antiferromagnetism* or *ferrimagnetism*. The small group of ferrimagnetic minerals is geophysically important, especially in connection with the analysis of the Earth's paleomagnetic field.

5.2.6.1 Diamagnetism

All magnetic materials show a diamagnetic reaction in a magnetic field. The diamagnetism is often masked by stronger paramagnetic or ferromagnetic properties. It is characteristically observable in materials in which all electron spins are paired.

The Lorentz law (Eq. (5.10)) shows that a change in the **B**-field alters the force experienced by an orbiting electron. The plane of the electron orbit is compelled to precess around the field direction; the phenomenon is called *Larmor precession*. It represents an additional component of rotation and angular momentum. The sense of the rotation is opposite to that of the orbital rotation about the nucleus. Hence, the magnetic moment associated with the Larmor precession opposes the applied field. As a result a weak magnetization proportional to the field strength is induced in the opposite direction to the field. The magnetization vanishes when the applied magnetic field is removed. Diamagnetic susceptibility is reversible, weak and negative (Fig. 5.9a); it

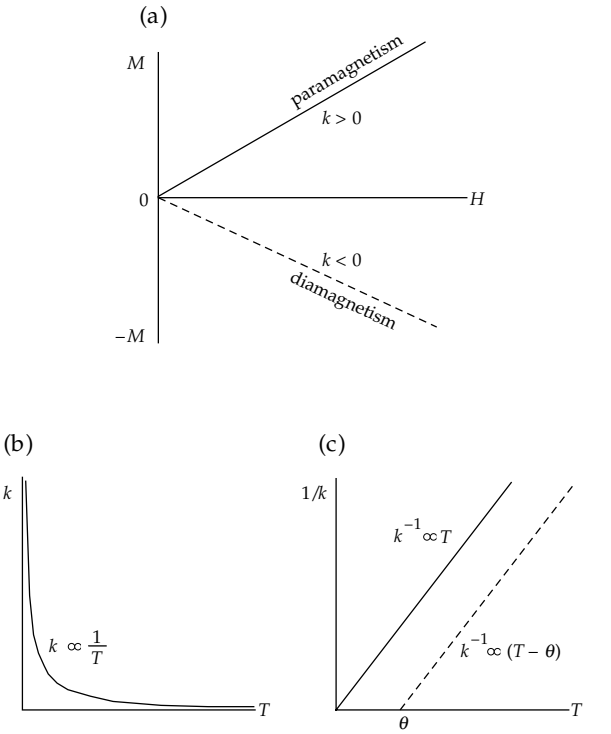

Fig. 5.9 (a) Variations of magnetization **M** with applied magnetic field **H** in paramagnetic and diamagnetic materials; (b) the variation of paramagnetic susceptibility with temperature, and (c) the linear plot of the inverse of paramagnetic susceptibility against temperature.

is independent of temperature. Many important rock-forming minerals belong to this class, amongst them quartz and calcite. They have susceptibilities around -10^{-6} in SI units.

5.2.6.2 Paramagnetism

Paramagnetism is a statistical phenomenon. When one or more electron spins is unpaired, the net magnetic moment of an atom or ion is no longer zero. The resultant magnetic moment can align with a magnetic field. The alignment is opposed by thermal energy which favors chaotic orientations of the spin magnetic moments. The magnetic energy is small compared to the thermal energy, and in the absence of a magnetic field the magnetic moments are oriented randomly. When a magnetic field is applied, the chaotic alignment of magnetic moments is biassed towards the field direction. A magnetization is induced proportional to the strength of the applied field and parallel to its direction. The susceptibility is reversible, small and positive (Fig. 5.9a). An important paramagnetic characteristic is that the susceptibility k varies inversely with temperature (Fig. 5.9b) as given by the *Curie law*

$$k = \frac{C}{T} \tag{5.19}$$

where the constant C is characteristic of the material. Thus, a plot of $1/k$ against temperature is a straight line (Fig. 5.9c). In solids and liquids mutual interactions

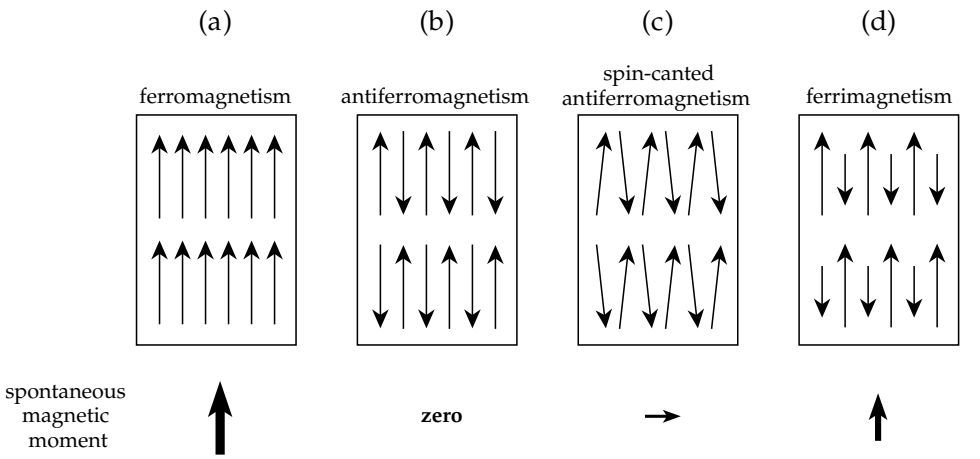

Fig. 5.10 Schematic representations of the alignments of atomic magnetic moments in (a) ferromagnetism, (b) antiferromagnetism, (c) spin-canted antiferromagnetism, and (d) ferrimagnetism.

between ions may be quite strong and paramagnetic behavior is only displayed when the thermal energy exceeds a threshold value. The temperature above which a solid is paramagnetic is called the *paramagnetic Curie temperature* or *Weiss constant* of the material, denoted by θ; it is close to zero kelvin in *paramagnetic* solids. At temperatures $T > \theta$ the paramagnetic susceptibility k is given by the *Curie–Weiss law*

$$k = \frac{C}{T - \theta} \tag{5.20}$$

For a solid the plot of $1/k$ against $(T - \theta)$ is a straight line (Fig. 5.9c). Many clay minerals and other rock-forming minerals (e.g., chlorite, amphibole, pyroxene, olivine) are paramagnetic at room temperature, with susceptibilities commonly around $10^{-5}-10^{-4}$ in SI units.

5.2.6.3 Ferromagnetism

In paramagnetic and diamagnetic materials the interactions between individual atomic magnetic moments are small and often negligible. However, in some metals (e.g., iron, nickel, cobalt) the atoms occupy lattice positions that are close enough to allow the exchange of electrons between neighboring atoms. The exchange is a quantum-mechanical effect that involves a large amount of energy, called the *exchange energy* of the metal. The exchange interaction produces a very strong *molecular field* within the metal, which aligns the atomic magnetic moments (Fig. 5.10a) exactly parallel and produces a *spontaneous magnetization* (M_s). The magnetic moments react in unison to a magnetic field, giving rise to a class of strong magnetic behavior known as *ferromagnetism*.

A rock sample may contain thousands of tiny ferromagnetic mineral grains. The magnetization loop of a rock sample shows the effects of *magnetic hysteresis* (Fig. 5.11). In strong fields the magnetization reaches a saturation value (equal to M_s), at which the individual magnetic moments are aligned with the applied field. If the magnetizing field is reduced to zero, a ferromagnetic material retains part of the induced magnetization. The residual

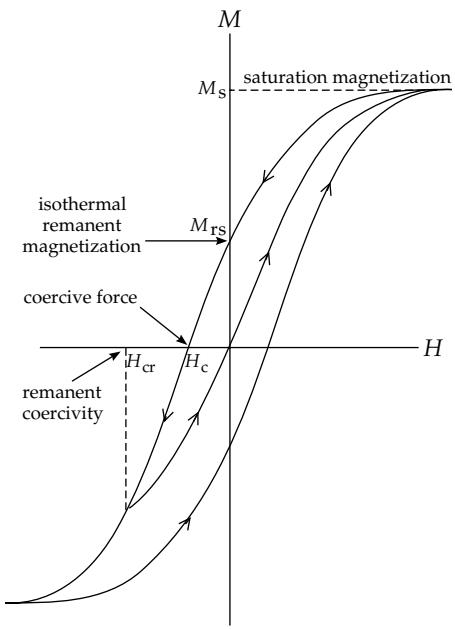

Fig. 5.11 The magnetization loop of an arbitrary ferromagnetic material.

magnetization is called the *remanence*, or *isothermal remanent magnetization* (IRM); if the sample is magnetized to saturation, the remanence is a saturation IRM (M_{rs}). For a given ferromagnetic mineral, the ratio M_{rs}/M_s depends on grain size. If a magnetic field is applied in the opposite direction to the IRM, it remagnetizes part of the material in the antiparallel direction. For a particular value H_c of the reverse field (called the *coercive force*) the induced reverse magnetization exactly cancels the original remanence and the net magnetization is zero. If the reverse field is removed at this stage, the residual remanence is smaller than the original IRM. By repeating the process in ever stronger reverse fields a back-field H_{cr} (called the *coercivity of remanence*) is found which gives a reverse remanence that exactly cancels the IRM, so that the residual remanence is zero. The ratio H_{cr}/H_c also depends on grain size. Rock-forming magnetic minerals often have natural remanences with very high coercive properties.

When a ferromagnetic material is heated, its spontaneous magnetization disappears at the *ferromagnetic Curie temperature* (T_c). At temperatures higher than the *paramagnetic Curie temperature* (θ) the susceptibility k becomes the paramagnetic susceptibility, so that $1/k$ is proportional to $(T - \theta)$ as given by the Curie–Weiss law (Eq. (5.20)). The paramagnetic Curie temperature for a ferromagnetic solid is several degrees higher than the ferromagnetic Curie temperature, T_c. The gradual transition from ferromagnetic to paramagnetic behavior is explained by persistence of the molecular field due to short-range magnetic order above T_c.

5.2.6.4 Antiferromagnetism

In oxide crystals the oxygen ions usually keep the metal ions far apart, so that direct exchange of electrons between the metal ions is not possible. However, in certain minerals, interaction between magnetic spins becomes possible by the exchange of electrons from one metal ion to another through the electron "cloud" of the oxygen ion. This *indirect exchange* (or *superexchange*) process results in antiparallel directions of adjacent atomic magnetic moments (Fig. 5.10b), giving two sublattices with equal and opposite intrinsic magnetic moments. As a result, the susceptibility of an antiferromagnetic crystal is weak and positive, and remanent magnetization is not possible. The antiferromagnetic alignment breaks down at the *Néel temperature*, above which paramagnetic behavior is shown. The Néel temperature T_N of many antiferromagnetic substances is lower than room temperature, at which they are paramagnetic. A common example of an antiferromagnetic mineral is ilmenite ($FeTiO_3$), which has a Néel temperature of 50 K.

5.2.6.5 Parasitic ferromagnetism

When an antiferromagnetic crystal contains defects, vacancies or impurities, some of the antiparallel spins are unpaired. A weak "defect moment" can result due to these lattice imperfections. Also if the spins are not exactly antiparallel but are inclined at a small angle, they do not cancel out completely and again a ferromagnetic type of magnetization can result (Fig. 5.10c). Materials that exhibit this form of *parasitic ferromagnetism* have the typical characteristics of a true ferromagnetic metal, including hysteresis, a spontaneous magnetization and a Curie temperature. An important geological example is the common iron mineral hematite (α-Fe_2O_3), in which both the spin-canted and defect moments contribute to the ferromagnetic properties. Hematite has a variable, weak spontaneous magnetization of about $2000\,A\,m^{-1}$, very high coercivity and a Curie temperature around 675 °C. The variable magnetic properties are due to variation in the relative importances of the defect and spin-canted moments.

5.2.6.6 Ferrimagnetism

The metallic ions in an antiferromagnet occupy the voids between the oxygen ions. In certain crystal structures, of which the most important geological example is the spinel structure, the sites of the metal ions differ from each other in the coordination of the surrounding oxygen ions. Tetrahedral sites have four oxygen ions as nearest neighbors and octahedral sites have six. The tetrahedal and octahedral sites form two sublattices. In a normal spinel the tetrahedral sites are occupied by divalent ions and the octahedral sites by Fe^{3+} ions. The most common iron oxide minerals have an *inverse spinel* structure. Each sublattice has an equal number of Fe^{3+} ions. The same number of divalent ions (e.g. Fe^{2+}) occupy other octahedral sites, while the corresponding number of tetrahedral sites is empty.

When the indirect exchange process involves antiparallel and unequal magnetizations of the sublattices (Fig. 5.10d), resulting in a net spontaneous magnetization, the phenomenon is called *ferrimagnetism*. Ferrimagnetic materials (called *ferrites*) exhibit magnetic hysteresis and retain a remanent magnetization when they are removed from a magnetizing field. Above a given temperature – sometimes called the ferrimagnetic Néel temperature but more commonly the Curie temperature – the long-range molecular order breaks down and the mineral behaves paramagnetically. The most important ferrimagnetic mineral is magnetite (Fe_3O_4), but maghemite, pyrrhotite and goethite are also significant contributors to the magnetic properties of rocks.

5.2.7 Magnetic anisotropy

Anisotropy is the directional dependency of a property. The magnetism of metals and crystals is determined by the strengths of the magnetic moments associated with atoms or ions, and the distances between neighbors. Here the symmetry of the lattice plays an important role, and so the magnetic properties of most ferromagnetic materials depend on direction. Magnetic anisotropy is an important factor in the dependence on grain size of the magnetic behavior of rocks and minerals. There are three important types: magnetocrystalline, magnetostatic and magnetostrictive anisotropies.

5.2.7.1 Magnetocrystalline anisotropy

The direction of the spontaneous magnetization (M_s) in a ferromagnetic metal is not arbitrary. The molecular field that produces M_s originates in the direct exchange of electron spins between neighboring atoms in a metal. The symmetry of the lattice structure of the metal affects the exchange process and gives rise to a *magnetocrystalline anisotropy energy*, which has a minimum value when M_s is parallel to a favored direction referred to as the *easy axis* (or *easy direction*) of magnetization. The simplest form of

magnetic anisotropy is uniaxial anisotropy, when a metal has only a single easy axis. For example, cobalt has a hexagonal structure and the easy direction is parallel to the *c*-axis at room temperature. Iron and nickel have cubic unit cells; at room temperature, the easy axes in iron are the edges of the cube, but the easy axes in nickel are the body diagonal directions.

Magnetocrystalline anisotropy is also exhibited by ferrites, including the geologically important ferrimagnetic minerals. The exchange process in a ferrite is indirect, but energetically preferred easy axes of magnetization arise that reflect the symmetry of the crystal structure. This gives rise to different forms of the anisotropy in hematite and magnetite.

Hematite has a rhombohedral or hexagonal structure and a *uniaxial anisotropy* with regard to the *c*-axis of symmetry. Oxygen ions form a close-packed hexagonal lattice in which two-thirds of the octahedral interstices are occupied by ferric (Fe^{3+}) ions. When the spontaneous magnetization makes an angle ϕ with the *c*-axis of the crystal, the uniaxial anisotropy energy density can be written to first order

$$E_a = K_u \sin^2\phi \tag{5.21}$$

K_u is called the uniaxial magnetocrystalline anisotropy constant. Its value in hematite is around -10^3 J m^{-3} at room temperature. The negative value of K_u in Eq. (5.21) means that E_a decreases as the angle ϕ increases, and is minimum when $\sin^2\phi$ is maximum, i.e., when ϕ is 90°. As a result, the spontaneous magnetization lies in the basal plane of the hematite crystal at room temperature.

Because of its inverse spinel structure, magnetite has *cubic anisotropy*. Let the direction of the spontaneous magnetization be given by direction cosines α_1, α_2 and α_3 relative to the edges of the cubic unit cell (Box 1.5). The magnetocrystalline anisotropy energy density is then given by

$$E_a = K_1(\alpha_1^2\alpha_2^2 + \alpha_2^2\alpha_3^2 + \alpha_3^2\alpha_1^2) + K_2\alpha_1^2\alpha_2^2\alpha_3^2 \tag{5.22}$$

The anisotropy constants K_1 and K_2 of magnetite are equal to -1.36×10^4 J m^{-3} and -0.44×10^4 J m^{-3}, respectively, at room temperature. Because these constants are negative, the anisotropy energy density E_a is minimum when the spontaneous magnetization is along a [111] body diagonal, which is the magnetocrystalline easy axis of magnetization at room temperature.

5.2.7.2 Magnetostatic (shape) anisotropy

In strongly magnetic materials the shape of the magnetized object causes a *magnetostatic anisotropy*. In rocks this effect is associated with the shapes of the individual grains of ferrimagnetic mineral in the rock, and to a lesser extent with the shape of the rock sample. The anisotropy is magnetostatic in origin and can be conveniently explained with the aid of the concept of magnetic poles.

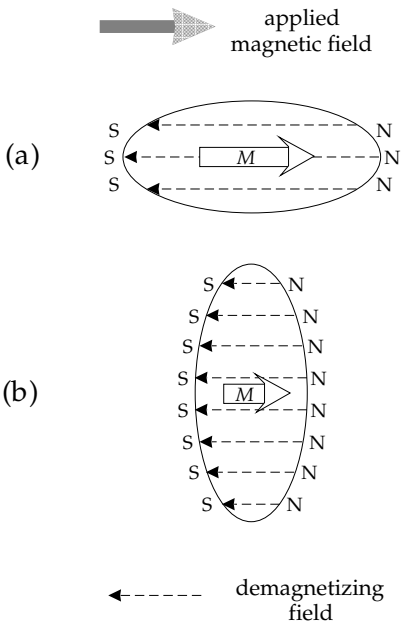

Fig. 5.12 The origin of shape anisotropy: the distributions of magnetic poles on surfaces that intersect the magnetization of a uniformly magnetized prolate ellipsoid produce internal demagnetizing fields; these are weak parallel to the long axis (a) and strong parallel to the short axis (b). As a result, the net magnetization is stronger parallel to the long axis than parallel to the short axis.

The spontaneous magnetization of a uniformly magnetized material can be pictured as giving rise to a distribution of poles on the free end surfaces (Fig. 5.12). As noted above, a property of the magnetic **B**-field is that its field lines form closed loops, whereas the **H**-field begins and ends on boundary surfaces, at which it is discontinuous. The field lines of the magnetic field **H** outside a magnet are parallel to the **B**-field and are directed from the surface distribution of N-poles to the distribution of S-poles. In the absence of an externally applied field the **H**-field inside the magnet is also directed from the distribution of N-poles on one end to the S-poles on the other end. It forms a *demagnetizing field* ($\mathbf{H}_d$) that opposes the magnetization. The strength of the demagnetizing field varies directly with the surface density of the magnetic pole distribution on the end surfaces of the magnet, and inversely with the distance between these surfaces. $\mathbf{H}_d$ thus depends on the shape of the magnet and the intensity of magnetization; it can be written

$$\mathbf{H}_d = -N\mathbf{M} \tag{5.23}$$

N is called the *demagnetizing factor*. It is a dimensionless constant determined by the shape of the magnetic grain. It can be computed for a geometrical shape, such as a triaxial ellipsoid. The demagnetizing factors N_1, N_2 and N_3 parallel to the symmetry axes of an ellipsoid satisfy the relationship

$$N_1 + N_2 + N_3 = 1 \tag{5.24}$$

The magnetostatic energy of the interaction of the grain magnetization with the demagnetizing field is called the

demagnetizing energy (E_d). For a grain with uniform magnetization M in a direction with demagnetizing factor N,

$$E_d = \frac{\mu_0}{2} N M^2 \tag{5.25}$$

Consider the shape anisotropy of a small grain shaped like a prolate ellipsoid. When the spontaneous magnetization M_s is along the long axis of the ellipsoid (Fig. 5.12a), the opposing pole distributions are further away from each other and their surface density is lower than when M_s is parallel to the short axis (Fig. 5.12b). The demagnetizing field and energy are smallest when M_s is parallel to the long axis, which is the energetically favored direction of magnetization. The demagnetizing energy is larger in any other direction, giving a *shape anisotropy*. If N_1 is the demagnetizing factor for the long axis and N_2 that for the short axis ($N_1 < N_2$), the difference in energy between the two directions of magnetization defines a magnetostatic anisotropy energy density given by

$$E_a = \frac{\mu_0}{2} (N_2 - N_1) M^2 \tag{5.26}$$

which is minimum when M_s is parallel to the longest dimension of the grain.

Shape-dependent magnetic anisotropy is important in minerals that have a high spontaneous magnetization. The more elongate the grain is, the higher the shape anisotropy will be. It is the predominant form of anisotropy in very fine grains of magnetite (and maghemite) if the longest axis exceeds the shortest axis by only about 20%.

5.2.7.3 Magnetostrictive anisotropy

The process of magnetizing some materials causes them to change shape. Within the crystal lattice the interaction energy between atomic magnetic moments depends on their separations (called the bond length) and on their orientations, i.e., on the direction of magnetization. If an applied field changes the orientations of the atomic magnetic moments so that the interaction energy is increased, the bond lengths adjust to reduce the total energy. This produces strains which result in a shape change of the ferromagnetic specimen. This phenomenon is called *magnetostriction*. A material which elongates in the direction of magnetization exhibits positive magnetostriction, while a material that shortens parallel to the magnetization shows negative magnetostriction. The maximum difference in magnetoelastic strain, which occurs between the demagnetized state and that of saturation magnetization, is called the *saturation magnetostriction*, denoted λ_s.

The inverse effect is also possible. For example, if pressure is applied to one face of a cubic crystal, it will shorten elastically along the direction of the applied stress and will expand in directions perpendicular to it. These strains alter the separations of atomic magnetic moments, thereby perturbing the effects that give rise to magnetocrystalline anisotropy. Thus the application of stress to a magnetic material can change its magnetization; the effect is called *piezomagnetism*. On a submicroscopic scale the stress field that surrounds a vacancy, defect or dislocation in the crystal structure can locally affect the orientations of ionic magnetic spins.

Magnetostriction is a further source of anisotropy in magnetic minerals. The magnetostrictive (or magnetoelastic) anisotropy energy density E_a depends on the amount and direction of the stress σ. If the saturation magnetization makes an angle θ to the stress, E_a is given for a uniaxial magnetic mineral by

$$E_a = \frac{3}{2} \lambda_s \sigma \cos^2\theta \tag{5.27}$$

This is the simplest expression for magnetostrictive energy. It assumes that the magnetostriction is isotropic, i.e., that it has the same value in all directions. This condition is fulfilled if the magnetocrystalline axes of the ferrimagnetic minerals in a rock are randomly distributed. The magnetoelastic energy of a cubic mineral is more complicated. Instead of a single magnetostriction constant λ_s, separate constants λ_{100} and λ_{111} are required for the saturation magnetostriction along the [100] and [111] directions, respectively, corresponding to the edge and body diagonal directions of the cubic unit cell.

In magnetite the magnetoelastic energy is more than an order of magnitude less than the magnetocrystalline energy at room temperature. Consequently, magnetostriction plays only a secondary role in determining the direction of magnetization of magnetite grains. However, in minerals that have high magnetostriction (e.g., titanomagnetites (see Section 5.3.2.1) with a compositional factor $x \approx 0.65$) the magnetoelastic energy may be significant in determining easy directions of magnetization, and the magnetization may be sensitive to modification by deformation.

5.3 ROCK MAGNETISM

5.3.1 The magnetic properties of rocks

A rock may be regarded as a heterogeneous assemblage of minerals. The matrix minerals are mainly silicates or carbonates, which are diamagnetic in character. Interspersed in this matrix is a lesser quantity of secondary minerals (such as the clay minerals) that have paramagnetic properties. The bulk of the constituent minerals in a rock contribute to the magnetic susceptibility but are incapable of any contribution to the remanent magnetic properties, which are due to a dilute dispersion of ferrimagnetic minerals (e.g., commonly less than 0.01% in a limestone). The variable concentrations of ferrimagnetic and matrix minerals result in a wide range of susceptibilities in rocks (Fig. 5.13).

The weak and variable concentration of ferrimagnetic minerals plays a key role in determining the magnetic properties of the rock that are significant geologically and geophysically. The most important factors influencing

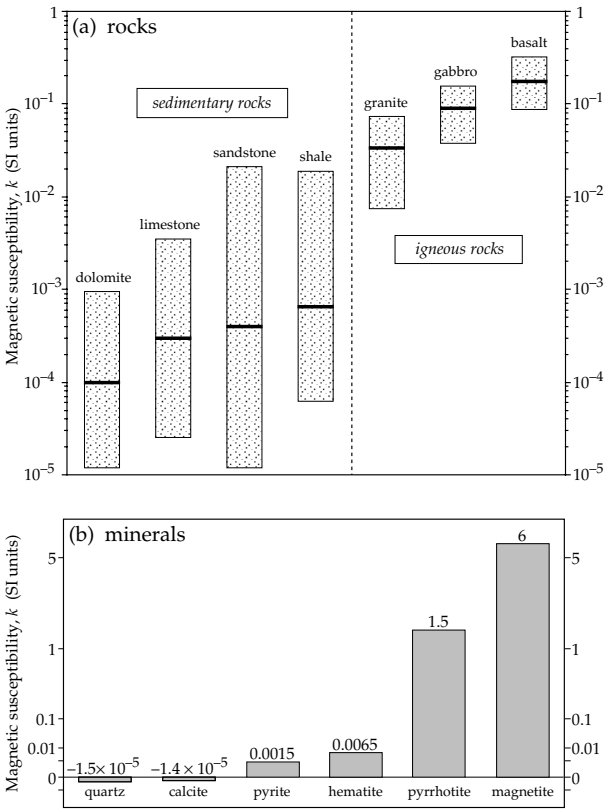

Fig. 5.13 (a) Median values and ranges of the magnetic susceptibility of some common rock types, and (b) the susceptibilities of some important minerals.

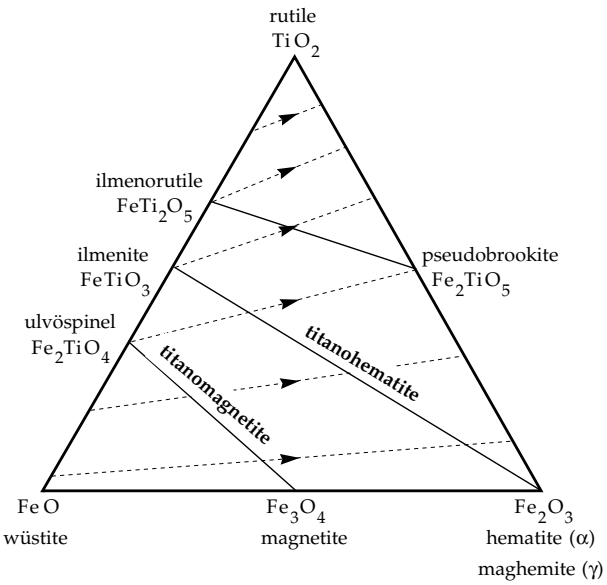

Fig. 5.14 Ternary compositional diagram of the iron–titanium oxide solid solution magnetic minerals (after McElhinny, 1973).

rock magnetism are the type of ferrimagnetic mineral, its grain size, and the manner in which it acquires a remanent magnetization.

5.3.2 The ternary oxide system of magnetic minerals

The most important magnetic minerals are iron–titanium oxides, which are naturally occurring ferrites. The mineral structure consists of a close-packed lattice of oxygen ions, in which some of the interstitial spaces are occupied by regular arrays of ferrous (Fe^{2+}) and ferric (Fe^{3+}) iron ions and titanium (Ti^{4+}) ions. The relative proportions of these three ions determine the ferrimagnetic properties of the mineral. The composition of an iron–titanium oxide mineral can be illustrated graphically on the ternary oxide diagram (Fig. 5.14), the corners of which represent the minerals rutile (TiO_2), wustite (FeO), and hematite (Fe_2O_3). The proportions of these three oxides in a mineral define a point on the ternary diagram. The vertical distance of the point above the $FeO–Fe_2O_3$ baseline reflects the amount of titanium in the lattice. Hematite is in a higher state of oxidation than wustite; hence the horizontal position along the $FeO–Fe_2O_3$ axis expresses the degree of oxidation.

The most important magnetic minerals belong to two solid-solution series: (a) the titanomagnetite, and (b) the titanohematite series. The minerals of a third series, pseudobrookite, are paramagnetic at room temperature. They are quite rare and are of minor importance in rock magnetism. The compositions of naturally occurring forms of titanomagnetite and titanohematite usually plot as points on the ternary diagram that are displaced from the ideal lines towards the $TiO_2–Fe_2O_3$ axis, which indicates that they are partly oxidized.

5.3.2.1 The titanomagnetite series

Titanomagnetite is the name of the family of iron oxide minerals described by the general formula $Fe_{3-x}Ti_xO_4$ ($0 \leq x \leq 1$). These minerals have an inverse spinel structure and exemplify a solid-solution series in which ionic replacement of two Fe^{3+} ions by one Fe^{2+} and one Ti^{4+} ion can take place. The compositional parameter x expresses the relative proportion of titanium in the unit cell. The end members of the solid-solution series are magnetite (Fe_3O_4), which is a typical strongly magnetic ferrite, and ulvöspinel (Fe_2TiO_4), which is antiferromagnetic at very low temperature but is paramagnetic at room temperature. An alternative form of the general formula is $xFe_2TiO_4(1-x)Fe_3O_4$. Written in this way, it is apparent that the compositional parameter x describes the molecular fraction of ulvöspinel. As the amount of titanium (x) increases, the cell size increases and the Curie temperature θ and spontaneous magnetization M_s of the titanomagnetite decrease (Fig. 5.15).

Magnetite is one of the most important ferrimagnetic minerals. It has a strong spontaneous magnetization ($M_s = 4.8 \times 10^5$ A m^{-1}) and a Curie temperature of 578 °C. Because of the high value of M_s, magnetite grains can have a strong shape anisotropy. The magnetic susceptibility is the strongest of any naturally occurring mineral

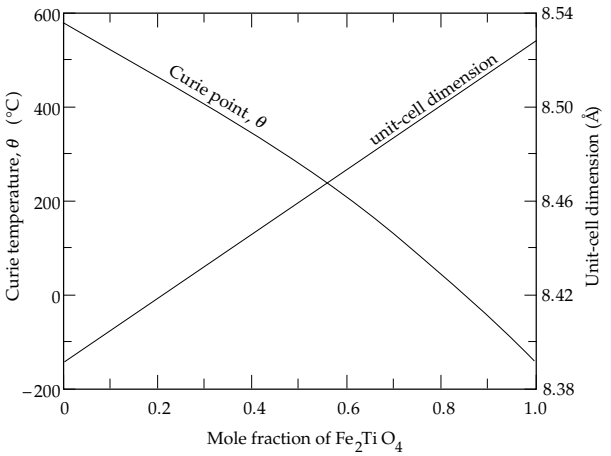

Fig. 5.15 Variations of Curie temperature and unit-cell size with composition in titanomagnetite (after Nagata, 1961).

($k \approx 1$–10 SI). For many sedimentary and igneous rocks the magnetic susceptibility is proportional to the magnetite content.

Maghemite (γ-Fe_2O_3) can be produced by low-temperature oxidation of magnetite. It is a strongly magnetic mineral ($M_s \approx 4.5 \times 10^5$ A m^{-1}). Experiments on maghemite doped with small amounts of foreign ions indicate that it has a Curie temperature of 675 °C. However, it is metastable and reverts to hematite (α-Fe_2O_3) when heated above 300–350 °C. The low-temperature oxidation of titanomagnetite leads to a "titanomaghemite" solid-solution series.

Titanomagnetite is responsible for the magnetic properties of oceanic basalts. The basaltic layer of the oceanic crust is the main origin of the marine magnetic anomalies that are of vital importance to modern plate tectonic theory. The magnetic properties of the 0.5 km thick basaltic layer are due to the presence of very fine grained titanomagnetite (or titanomaghemite, depending on the degree of ocean-floor weathering). The molecular fraction (x) of Fe_2TiO_4 in titanomagnetite in oceanic basalts is commonly around 0.6.

5.3.2.2 The titanohematite series

The minerals of the titanohematite solid-solution series are also variously referred to as "hemoilmenite," "hematite-ilmenite" or "ilmenohematite." They have the general formula $Fe_{2-x}Ti_xO_3$. The unit cell has rhombohedral symmetry. Ionic substitution is the same as for titanomagnetite, and the compositional parameter x has the same implications for the titanium content of the unit cell. The end members of the solid-solution series are hematite (Fe_2O_3) and ilmenite ($FeTiO_3$). The chemical formula can be written in the alternative form $xFeTiO_3 \cdot (1 - x)Fe_2O_3$, where x represents the molecular fraction of ilmenite. As in the case of titanomagnetite, the cell size increases and the Curie point decreases as the titanium content increases. The Curie point of hematite is 675 °C, while ilmenite is antiferromagnetic at low temperature and paramagnetic at room temperature. For titanium contents $0.5 < x < 0.95$ titanohematite is ferrimagnetic and for $x < 0.5$ it exhibits parasitic ferromagnetism.

The end member hematite (α-Fe_2O_3) is an extremely important magnetic mineral. Its magnetic properties arise from parasitic ferromagnetism due to the spin-canted magnetic moment and the possible defect moment of its otherwise antiferromagnetic lattice. Hematite has a weak spontaneous magnetization ($M_s \approx 2.2 \times 10^3$ A m^{-1}) and a strong uniaxial magnetocrystalline anisotropy ($K_u \approx 10^3$ J m^{-3}). Hematite is paleomagnetically important because of its common occurrence and its high magnetic and chemical stability. It often occurs as a secondary mineral, formed by oxidation of a precursor mineral, such as magnetite, or by precipitation from fluids passing through a rock.

5.3.3 Other ferrimagnetic minerals

Although the iron–titanium oxides are the dominant magnetic minerals, rocks frequently contain other minerals with ferromagnetic properties. Although pyrite (FeS_2) is a very common sulfide mineral, especially in sedimentary rocks, it is paramagnetic and therefore cannot carry a remanent magnetization. As a result it does not contribute directly to the paleomagnetic properties of rocks, but it may act as a source for the formation of goethite or secondary magnetite.

Pyrrhotite is a common sulfide mineral which can form authigenically or during diagenesis in sediments, and which can be ferrimagnetic in certain compositional ranges. It is non-stoichiometric (i.e., the numbers of anions and cations in the unit cell are unequal) and has the formula $Fe_{1-x}S$. The parameter x refers to the proportion of vacancies among the cation lattice sites and is limited to the range $0 < x < 0.14$. Pyrrhotite has a pseudo-hexagonal crystal structure and would be antiferromagnetic but for the presence of the cation vacancies. The Néel temperature at which the fundamental antiferromagnetism disappears is around 320 °C. Pyrrhotite with the formula Fe_7S_8 is ferrimagnetic with a Curie temperature close to the Néel temperature and a strong spontaneous magnetization of about 10^5 A m^{-1} at room temperature. The magnetocrystalline anisotropy restricts the easy axis of magnetization to the hexagonal basal plane at room temperature.

The iron oxyhydroxide goethite (FeOOH) is another common authigenic mineral in sediments. Like hematite, goethite is antiferromagnetic, but has a weak parasitic ferromagnetism. It has a very high coercivity (with maximum values in excess of 5 T) and a low Curie point around 100 °C or less. It is thermally unstable relative to hematite under most natural conditions, and decomposes on heating above about 350 °C. It is a common (and paleomagnetically undesirable) secondary mineral in limestones and other sedimentary rocks.

5.3.4 Identification of ferrimagnetic minerals

It is often difficult to identify the ferrimagnetic minerals in a rock, because their concentration is so low, especially in sedimentary rocks. If the rock is coarse grained, ferrimagnetic minerals may be identified optically among the opaque grains by studying polished sections in reflected light. However, in many rocks that are paleomagnetically important (e.g., basaltic lava, pelagic limestone) optical examination may be unable to resolve the very fine grain size of the ferrimagnetic mineral. The ferrimagnetic mineral fraction may then be identified by its properties of Curie temperature and coercivity.

The Curie temperature is measured using a form of balance in which a strong magnetic field gradient exerts a force on the sample that is proportional to its magnetization. The field (usually 0.4–1 T) is strong enough to saturate the magnetization of many minerals. The sample is heated and the change of magnetic force (i.e., sample magnetization) is observed with increasing temperature. When the Curie point is reached, the ferromagnetic behavior disappears; at higher temperatures the sample is paramagnetic. The Curie point is diagnostic of many minerals. For example, an extract of magnetic minerals from a pelagic limestone (Fig. 5.16) shows the presence of goethite (~100 °C Curie point, sample SR3A), magnetite (~570 °C Curie point, all samples) and hematite (~650 °C Curie point, sample SR11). Some Curie balances are sensitive enough to analyze whole rock samples, but this is generally only possible in strongly magnetized igneous rocks. For most rocks it is necessary to extract the ferrimagnetic minerals, or to concentrate them. The extraction is sometimes difficult, and often it is not certain that the extract is representative of the rock as a whole. This is also a drawback of optical methods, which only allow description of large grains.

To avoid the difficulties and uncertainties associated with making a special extract or concentrate of the ferrimagnetic fraction, alternative methods of ferrimagnetic mineral identification, based on bulk magnetic properties, are more widely used. One simple method makes use of the coercivities and Curie temperatures, as expressed in the thermal demagnetization of the isothermal remanent magnetization (see Section 5.3.6.4). Another method, useful for pure magnetite and hematite, takes advantage of the low-temperature variations of the magnetocrystalline anisotropy constants of these minerals.

5.3.5 Grain size dependence of ferrimagnetic properties

The ferromagnetic properties of metals and ferrites vary sensitively with grain size. Consider an assemblage of uniformly magnetized grains of a ferrimagnetic mineral characterized by a spontaneous magnetization M_s and uniform grain volume v. Let the spontaneous magnetization be oriented parallel to an easy direction of magnetization (crystalline or shape determined), defined by the anisotropy energy K_u per unit volume. The energy that keeps the

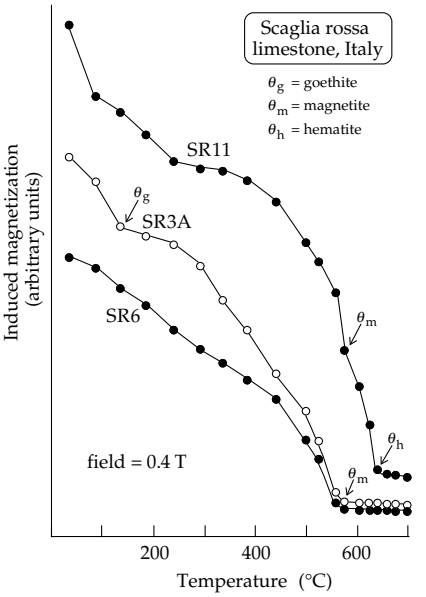

Fig. 5.16 Identification of the ferromagnetic minerals in a pelagic limestone by determination of their Curie temperatures in concentrated extracts (after Lowrie and Alvarez, 1975).

magnetization parallel to the easy direction is equal to vK_u. Thermal energy, proportional to the temperature, has the effect of disturbing this alignment. At temperature T the thermal energy of a grain is equal to kT, where k is Boltzmann's constant ($k = 1.381 \times 10^{-23}$ J K^{-1}). At any instant in time there is a chance that thermal energy will deflect the magnetic moment of a grain away from its easy direction. Progressively, the net magnetization of the material (the sum of all the magnetic moments of the numerous magnetic grains) will be randomized by the thermal energy, and the magnetization will be observed to decay. If the initial magnetization of the assemblage is M_{r0}, after time t it will decrease exponentially to $M_r(t)$, according to

$$M_r(t) = M_{r0} \exp\left(-\frac{t}{\tau}\right) \tag{5.28}$$

In this equation τ is known as the *relaxation time* of the grain (Box 5.1). If the relaxation time is long, the exponential decrease in Eq. (5.28) is slow and the magnetization is stable. The parameter τ depends on properties of the grain and is given by the equation

$$\tau = \frac{1}{\nu_0} \exp\left(\frac{vK_u}{kT}\right) \tag{5.29}$$

The constant ν_0 is related to the lattice vibrational frequency and has a very large value ($\approx 10^8 - 10^{10}$ s^{-1}). The value of K_u depends on whether the easy direction of the magnetic mineral is determined by the magnetocrystalline anisotropy or the magnetostatic (shape) anisotropy. For example, in hematite the magnetocrystalline anisotropy prevails because the spontaneous magnetization is very weak, and K_u is equal to the magnetocrystalline

Box 5.1: Magnetic relaxation

Relaxation behavior is characterized by the exponential return of a physical property with time from a state of elevated energy to a state of lower energy. The most familiar example is radioactive decay (Section 4.1.3.1), but the magnetizations of natural materials also exhibit relaxation behavior, as explained in Section 5.3.5.

In the absence of an external field, the easy direction of magnetization of a single domain magnetic grain with volume v and anisotropy energy K_u per unit volume is determined by the anisotropy energy vK_u (Section 5.2.7). The probability that the grain's thermal energy kT can overcome this energy barrier and allow the grain magnetization to change direction is determined by the Maxwell–Boltzmann distribution of energies, and is proportional to $\exp(-vK_u/kT)$. The probability per unit time, λ, of a magnetic moment changing to a different easy axis is given by the *Arrhenius equation* for a thermally activated process

$$\lambda = C\exp\left(-\frac{vK_u}{kT}\right) \quad (1)$$

The parameter C is called the frequency factor; here it is the lattice vibration frequency, v_o. At a particular temperature, all parameters on the right side of Eq. (1) are constant and so the probability λ per unit time of a magnetic moment changing to a different easy axis is constant.

Now suppose an assemblage of identical noninteracting single domain particles, of which N_1 are magnetized initially in one direction (state 1) and N_2 in the opposite direction (state 2). The net magnetization is proportional to $(N_1 - N_2)$. Assuming a constant probability λ per unit time, the number of particles dN_1 that change from state 1 to state 2 is proportional to the time interval dt and to the number of grains N_1 in state 1. It is given by

$$dN_1 = -\lambda N_1 dt \quad (2)$$

where the negative sign indicates a reduction in N_1. Similarly, the number changing in the opposite sense from state 2 to state 1 is

$$dN_2 = -\lambda N_2 dt \quad (3)$$

The net change in magnetization is therefore

$$dM = \mu dN_1 - \mu dN_2 = \mu d(N_1 - N_2) \quad (4)$$

$$dM = -\lambda\mu(N_1 - N_2)dt = -\lambda M dt \quad (5)$$

The solution of this differential equation is

$$M = M_0\exp(-\lambda t) = M_0\exp\left(-\frac{t}{\tau}\right) \quad (6)$$

where τ, the relaxation time, is the inverse of λ in Eq. (1):

$$\tau = \frac{1}{v_0}\exp\left(\frac{vK_u}{kT}\right) \quad (7)$$

Equations (6) and (7) are very important in paleomagnetism. The strong anisotropy of fine grained ferromagnetic minerals can result in very long relaxation times, and consequently the magnetizations of fine grained rocks can be extremely stable over geological lengths of time.

anisotropy. In grains of magnetite the value of K_u is equal to $((K_1/3) + (K_2/27))$, if magnetocrystalline anisotropy controls the magnetization (as in an equidimensional grain). If the magnetite grain is elongate with demagnetizing factors N_1 and N_2, shape anisotropy determines K_u, which is then equal to the energy density E_a given by Eq. (5.26).

This theory applies only to very small grains that are uniformly magnetized. Fine grained ferrimagnetic minerals are, however, very important in paleomagnetism and rock magnetism. The very finest grains, smaller than a critical size, exhibit an unstable type of magnetic behavior called *superparamagnetism*, with relaxation times typically less than 100 s. Above the critical size the uniformly magnetized grain is very stable and is called a single domain grain.

5.3.5.1 Superparamagnetism

In a ferromagnetic material the strong molecular fields keep the atomic spin magnetic moments uniformly aligned with each other, and the grain anisotropy requires this spontaneous magnetization to lie parallel to an "easy" direction. If the temperature is too high, thermal energy (kT) may exceed the anisotropy energy (vK_u) but still be too small to break up the spontaneous magnetization. The thermal energy causes the entire magnetic moment of the grain to fluctuate coherently in a manner similar to paramagnetism (the theory of which applies to individual atomic magnetic moments). The grain magnetization has no stable direction, and the behavior is said to be *superparamagnetic*. It is important to note that superparamagnetic grains themselves are immobile; only their uniform magnetization fluctuates relative to the grain. Whether the ferrimagnetic grain exists in a stable or superparamagnetic state depends on the grain size, the grain shape (if the origin of K_u is magnetostatic) and the temperature. If the grain volume v is very small, unstable magnetic behavior due to superparamagnetism becomes likely. Magnetite and hematite grains finer than about

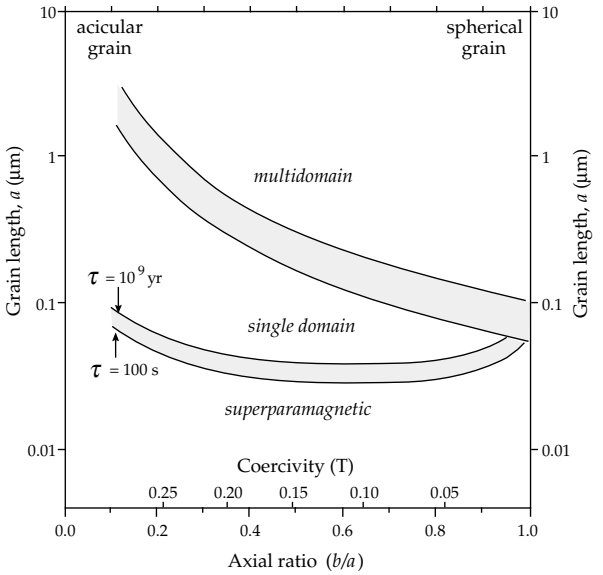

Fig. 5.17 Ranges of grain sizes and shapes for superparamagnetic, single domain and multidomain magnetic behavior in ellipsoidal magnetite grains (after Evans and McElhinny, 1969).

0.03 μm in diameter are superparamagnetic at room temperature.

5.3.5.2 Single domain particles

When the anisotropic magnetic energy (vK_u) of a grain is greater than the thermal energy (kT), the spontaneous magnetization direction favors one of the easy directions. The entire grain is uniformly magnetized as a *single domain*. This situation occurs in very fine grains of ferrimagnetic minerals.

In magnetite K_u is the magnetostatic energy related to the particle shape. The theoretical range of single domain sizes in magnetite is narrow, from about 0.03 to 0.1 μm in equant grains and up to about 1 μm in elongate grains (Fig. 5.17). In hematite K_u is the large magnetocrystalline anisotropy energy, and the range of single domain sizes is larger, from about 0.03 to 15 μm.

The magnetization of a single domain particle is very stable, because to change it requires rotating the entire uniform spontaneous magnetization of the grain against the grain anisotropy, which requires a very strong magnetic field. The magnetic field required to reverse the direction of magnetization of a single domain grain is called its *coercivity* B_c and is given by:

$$B_c = \frac{2K_u}{M_s} \tag{5.30}$$

The maximum coercivity of single domain magnetite is around 0.3 T for needle-shaped elongate grains. The magnetocrystalline anisotropy of hematite gives it higher maximum coercivities, in excess of 0.5 T. However, the magnetic properties of hematite are very variable and its maximum coercivity commonly exceeds 2 T. Because of their stable remanent magnetizations, single domain particles play a very important role in paleomagnetism.

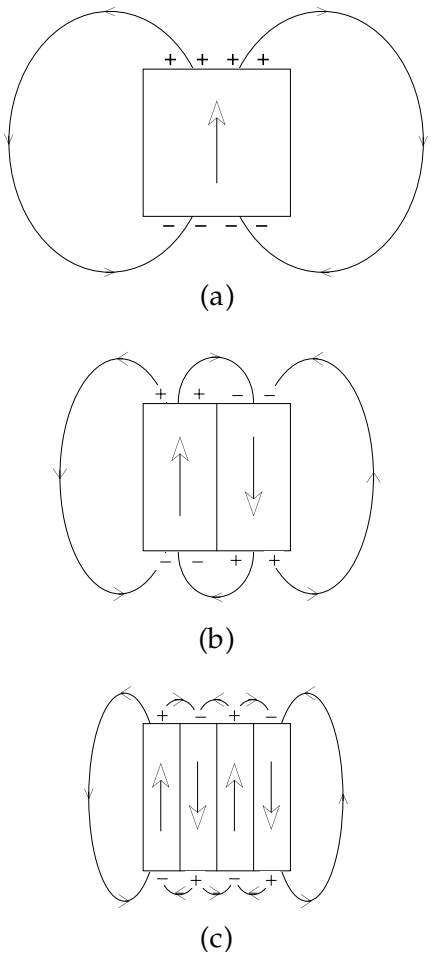

Fig. 5.18 Subdivision of (a) the uniform magnetization of a large grain into (b) two oppositely magnetized magnetic domains and (c) four alternately magnetized domains.

5.3.5.3 Multidomain particles

Single domain behavior is restricted to a limited range of grain sizes. When a grain is large enough, the magnetic energy associated with its magnetization becomes too large for the magnetization to remain uniform. This is because the demagnetizing field of a uniformly magnetized grain (Fig. 5.18a) interacts with the spontaneous magnetization and generates a magnetostatic (or self-demagnetizing) energy. To reduce this energy, the magnetization subdivides into smaller, uniformly magnetized units, called *Weiss domains* after P. Weiss, who theoretically predicted domain structure in 1907. In the simplest case the magnetization divides into two, oppositely magnetized domains (Fig. 5.18b). The net magnetization is reduced to zero, and the magnetostatic energy is reduced by about a half. Further subdivision (Fig. 5.18c) reduces the magnetostatic energy correspondingly. In a grain with n domains of alternately opposed spontaneous magnetizations the magnetostatic energy is reduced by $1/n$. The

domains are separated from one another by thin regions, about 0.1 μm thick, that are usually much thinner than the domains they divide. These regions are called *Bloch domain walls* in recognition of F. Bloch, who in 1932 proposed a theory for the structure of the domain wall on an atomic scale. Within the domain wall the magnetization undergoes small progressive changes in direction from each atom to its neighbor. The crystalline magnetic anisotropy of the material attempts to keep the atomic magnetic spins parallel to favored crystalline directions, while the exchange energy resists any change of direction from parallel alignment by the molecular field. The energy of these competing effects is expressed as a *domain wall energy* associated with each unit area of the wall.

The magnetization of a *multidomain* grain can be changed by moving the position of a domain wall, which causes some domains to increase in size and others to decrease. A large multidomain grain may contain many easily movable domain walls. Consequently, it is much easier to change the magnetization of a multidomain grain than of a single domain grain. As a result multidomain grains are less stable carriers of remanent magnetization than single domain grains.

The transition between single domain and multidomain behavior occurs when the reduction of magnetostatic energy is balanced by the energy associated with the domain wall that has been added. If magnetite grains are elongate, they can persist as single domain grains up to about 1 μm (Fig. 5.17). Magnetite grains larger than a few micrometers in diameter are probably multidomain. In equidimensional grains of magnetite the transition should occur in grains of about 0.05–0.1 μm diameter. However, at this point the grain is not physically large enough to contain a wall, which has a thickness of about 0.1 μm. Grains in the intermediate range of sizes, and those large enough to contain only a few walls, are said to carry a *pseudo-single domain* magnetization. True multidomain behavior in magnetite is observed when the grain size exceeds 15–20 μm.

In a pseudo-single domain grain that is large enough to contain only two domains, the domain wall separating them is not able to move freely. Its freedom of movement is restricted by interactions with the grain surface. A small grain in this size range has more stable magnetic properties than a multidomain particle but is not as stable as a true single domain grain. Magnetite grains between about 0.1 m and several micrometers in diameter have pseudo-single domain properties.

5.3.6 Remanent magnetizations in rocks

The small concentration of ferrimagnetic minerals in a rock gives it the properties of magnetic hysteresis. Most important of these is the ability to acquire a remanent magnetization (or *remanence*). The untreated remanence of a rock is called its *natural remanent magnetization* (NRM). It may be made up of several components acquired in different ways and at different times. The geologically important types of remanence are acquired at known times in the rock's history, such as at the time of its formation or subsequent alteration. The remanence of a rock can be very stable against change; the high coercivity (especially of the fine grains) of the ferrimagnetic mineral assures preservation of the magnetic signal during long geological epochs.

A remanence acquired at or close to the time of formation of the rock is called a *primary* magnetization; a remanence acquired at a later time is called a *secondary* magnetization. Examples of primary remanence are thermoremanent magnetization, which an igneous rock acquires during cooling, and the remanent magnetizations acquired by a sediment during or soon after deposition. Secondary remanences may be caused by chemical change of the rock during diagenesis or weathering, or by sampling and laboratory procedures.

5.3.6.1 Thermoremanent magnetization

The most important type of remanent magnetization in igneous (and high-grade metamorphic) rocks is *thermoremanent magnetization* (TRM). Igneous rocks solidify at temperatures well above 1000 °C. At this temperature the grains are solid and fixed in a rigid matrix. The grains of a ferrimagnetic mineral are well above their Curie temperature, which in magnetite is 578 °C and in hematite is 675 °C. There is no molecular field and the individual atomic magnetic moments are free to fluctuate chaotically; the magnetization is paramagnetic (Fig. 5.19).

As the rock cools, the temperature eventually passes below the Curie temperature of the ferrimagnetic grains and a spontaneous magnetization appears. In single domain grains the relaxation time of the grain magnetization is governed by Eq. (5.29), which can be modified by writing the anisotropy energy density K_u in terms of the spontaneous magnetization M_s and coercivity B_c of the grain. This gives the relaxation time as follows

$$\tau = \frac{1}{\nu_0} \exp\left(\frac{vM_sB_c}{2kT}\right) \tag{5.31}$$

At high temperature the thermal energy (kT) is larger than the magnetic energy ($vM_sB_c/2$) and the magnetization is unstable. Although the individual atomic magnetic moments are forced by the molecular field to act as coherent units, the grain magnetizations are superparamagnetic. As the rock cools further, the spontaneous magnetization and the magnetic anisotropy energy K_u of the grain increase. Eventually the temperature passes below a value at which the thermal energy, whose effect is to randomize the grain magnetic moments, is no longer greater than the magnetic anisotropy energy. The spontaneous magnetization then becomes "blocked" along an easy direction of magnetization of the grain. In the absence of an external magnetic field the grain

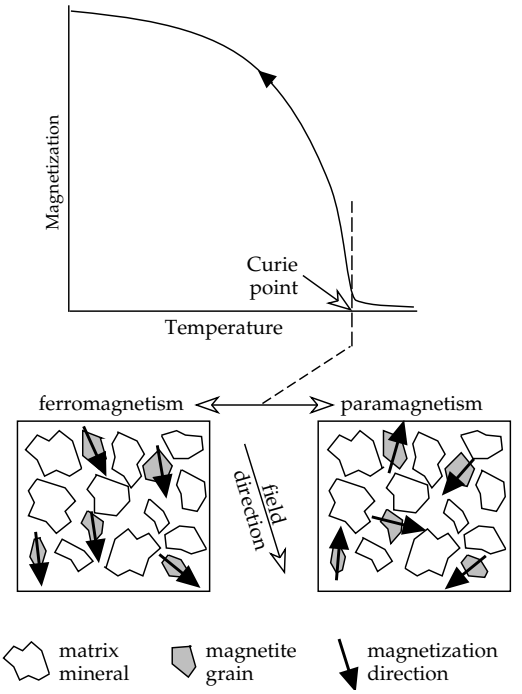

Fig. 5.19 On cooling through the Curie temperature the magnetic state of magnetite grains changes from paramagnetism to ferromagnetism. On cooling further the magnetizations in the magnetite grains become blocked along easy directions of magnetization close to the field direction. The resultant thermoremanent magnetization is parallel to the field direction.

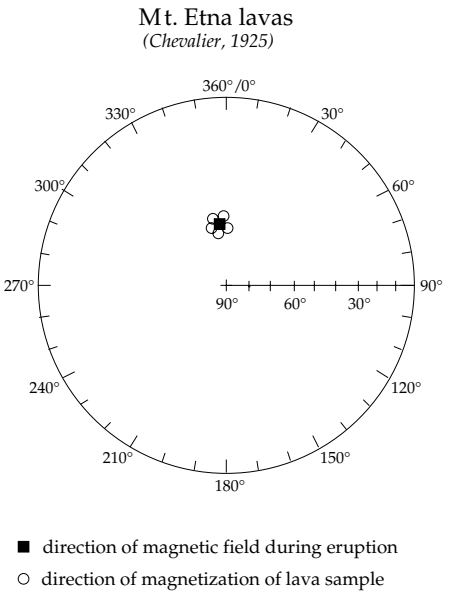

Fig. 5.20 Agreement of directions of thermoremanent magnetization in a basaltic lava flow on Mt. Etna (Sicily) with the direction of the geomagnetic field during eruption of the lava (based upon data from Chevallier, 1925).

magnetic moments will be randomly oriented (assuming the easy axes to be randomly distributed). If the grain cools below its *blocking temperature* in a magnetic field, the grain magnetic moment is "blocked" along the easy axis that is closest to the direction of the field at that time (Fig. 5.19). The alignment of grain magnetic moments with the field is neither perfect nor complete; it represents a statistical preference. This means that in an assemblage of grains more of the grains have their magnetic moments aligned close to the field direction than any other direction. The degree of alignment depends on the strength of the field.

It is important to note that the mineral grains themselves are immobile throughout the process of acquisition of TRM. Only the internal magnetizations of the grains can change direction and eventually become blocked. The blocking temperatures of TRM are dependent on the grain size, grain shape, spontaneous magnetization and magnetic anisotropy of the ferrimagnetic mineral. If the rock contains a wide range of grain sizes and perhaps more than a single magnetic mineral, there may be a broad spectrum of blocking temperatures. Maximum blocking temperatures may range as high as the Curie point, and the spectrum can extend to below ambient temperature. If the magnetic field is applied only while the rock is cooling through a limited temperature range, only grains with blocking temperatures in this range are activated, and a partial TRM (or pTRM) results.

TRM is a very stable magnetization which can exist unchanged for long intervals of geological time. The ability of TRM to record accurately the field direction is demonstrated by the results from a lava that erupted on Mt. Etna at a time for which a record of the magnetic field direction is available from observatory data. The directions of the TRM in the lava samples are the same as the direction of the ambient field (Fig. 5.20).

5.3.6.2 Sedimentary remanent magnetizations

The acquisition of *depositional remanent magnetization* (DRM) during deposition of a sediment takes place at constant temperature. Magnetic and mechanical forces compete to produce a physical alignment of detrital ferrimagnetic particles. During settling through still water these particles are oriented by the ambient magnetic field in the same way that it orients a compass needle. The particles become aligned statistically with the Earth's magnetic field (Fig. 5.21). The action of mechanical forces may at times spoil this alignment. Water currents cause hydromechanical forces that disturb the alignment during settling, giving rise to a *declination error*. On contact with the bottom of the sedimentary basin, the mechanical force of gravity rolls the particle into a stable attitude, causing an *inclination error*. The pressure of overlying sediment during deep burial results in compaction, which can produce further directional errors. The DRM is finally fixed in sedimentary rocks during diagenesis.

A modified form of *post-depositional remanence* (pDRM) is important in fine grained sediments. A water-logged slurry forms at the sediment–water interface. Fine grained magnetic minerals in the water-filled pore spaces in

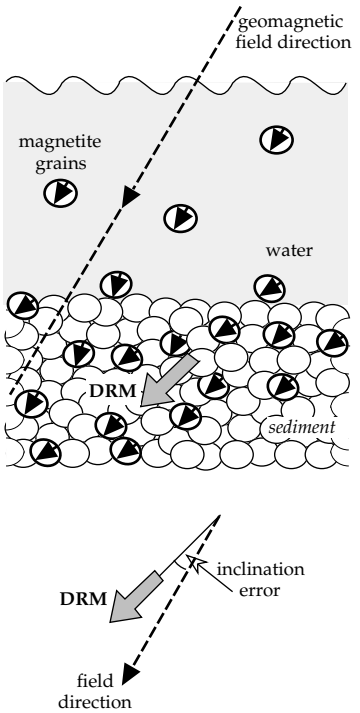

Fig. 5.21 Acquisition of depositional remanent magnetization (DRM) in a sediment; gravity causes an inclination error between the magnetization and field directions.

the sediment are partially in suspension and may be reoriented by the magnetic field, if they are free enough to move (Fig. 5.22a). The energy for this motion of the particles is obtained from the Brownian motion of the water molecules, which continuously and randomly collide with the particles in the pore spaces. Large particles are probably in contact with the surrounding grains and are unaffected by collisions with the water molecules. Very fine particles that are virtually floating in the pore spaces may acquire enough freedom from the Brownian agitation to align statistically with the Earth's magnetic field. Laboratory experiments have established that the direction of pDRM is an accurate record of the depositional field, without inclination error (Fig. 5.22b). The pDRM is acquired later than the actual time of sedimentation, and is fixed in the sediment during compaction and de-watering at a depth of ~10 cm. This may represent a lock-in time delay of 100 yr in lacustrine sediments or 10,000 yr in pelagic marine sediments, where it is no more important geologically than the errors involved in locating paleontological stage boundaries. The pDRM process is particularly effective in fine grained sediments containing strongly magnetic magnetite grains. For example, pDRM is the most important mechanism of primary magnetization in pelagic limestones. Compaction may cause a flattening of the inclination under some conditions.

Bioturbation may mix the sediment, typically to a depth of about 10 cm in pelagic sediments. This affects the positions of stratigraphic marker levels. First occurrence datum levels of fossils are carried deeper, and last occurrences are carried higher than the true stratigraphic levels. Agitation

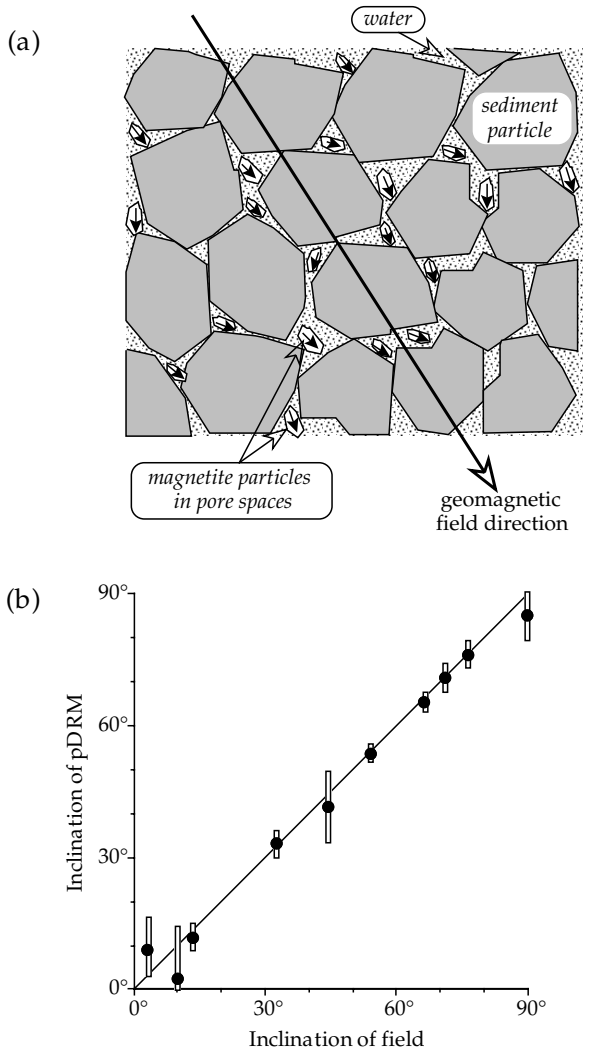

Fig. 5.22 (a) Post-depositional remanent magnetization (pDRM) is acquired by reorientation of ferromagnetic grains in the pore spaces of a deposited sediment. (b) Comparison of the pDRM inclination with the field inclination in a redeposited deep-sea sediment (after Irving and Major, 1964).

of bioturbated sediment by the burrowing organisms assists the Brownian motion of the magnetic particles. Under these conditions the pDRM is acquired at the base of the bioturbated zone.

5.3.6.3 Chemical remanent magnetization

Chemical remanent magnetization (CRM) is usually a secondary form of remanence in a rock. It occurs when the magnetic minerals in a rock suffer chemical alteration or when new minerals form authigenically. An example is the precipitation of hematite from a goethite precursor or from iron-saturated fluids that pass through the rock. The magnetic minerals may also experience diagenetic modification or oxidation by weathering, which usually happens on the grain surface and along cracks (Fig. 5.23). The growth of a new mineral (or the alteration of an existing one) involves changes in grain volume v, spontaneous

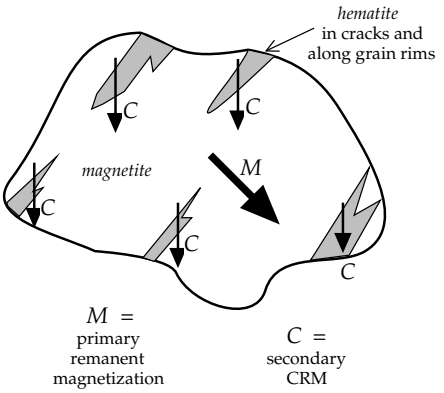

Fig. 5.23 Acquisition of chemical remanent magnetization (CRM) accompanies the diagenetic modification or oxidation by weathering of magnetic minerals; this often happens on the grain surface and along cracks.

magnetization M_s and coercivity B_c. The chemical change affects the relaxation time of the grain magnetization, according to Eq. (5.31). The grains eventually grow through a critical volume, at which the grain magnetization becomes blocked. The new CRM is acquired in the direction of the ambient field during the chemical change, and so it is younger than the host rock. It has stable magnetic properties similar to TRM. A common example is the formation of hematite during diagenesis or weathering. Hematite that originates in this way typically carries a secondary remanent magnetization.

5.3.6.4 Isothermal remanent magnetization

Isothermal remanent magnetization (IRM) is induced in a rock sample by placing it in a magnetic field at constant temperature. For example, rock samples are exposed to the magnetic fields of the sampling equipment and to other magnetic fields during transport to the laboratory. A common technique of rock magnetic analysis consists of deliberately inducing IRM via a known magnetic field produced in a large coil or between the poles of an electromagnet. The magnetic moments within each grain are partially aligned by the applied field. The degree of alignment depends on the field strength and on the resistance of the magnetic mineral to being magnetized, loosely referred to as its coercivity. After removing the sample from the applied field an IRM remains in the rock (see Fig. 5.11). If the rock sample is placed in progressively stronger fields the IRM increases to a maximum value called the saturation IRM, which is determined by the type and concentration of the magnetic mineral. The shape of the progressive acquisition curve and the field needed to reach saturation IRM depend on the coercivities of the magnetic minerals in the rock (Fig. 5.24).

The maximum coercivities of the most common ferromagnetic minerals in rocks are fairly well known (Table 5.1). These minerals also have distinctive maximum blocking temperatures (Section 5.3.6.1). The combination of these properties provides a method of identification of the predominant magnetic minerals in rocks. Starting with the strongest field available, IRM is imparted in successively smaller fields, chosen to remagnetize different coercivity fractions, along two or three orthogonal directions. The compound IRM is then subjected to progressive thermal demagnetization. The demagnetization characteristics of

Table 5.1 *Maximum coercivities and blocking temperatures for some common ferromagnetic minerals*

Ferromagnetic mineral	Maximum coercivity [T]	Maximum blocking temperature [°C]
Magnetite	0.3	575
Maghemite	0.3	≈350
Titanomagnetite ($Fe_{3-x}Ti_xO_4$):		
$x = 0.3$	0.2	350
$x = 0.6$	0.1	150
Pyrrhotite	0.5–1	325
Hematite	1.5–5	675
Goethite	> 5	80–120

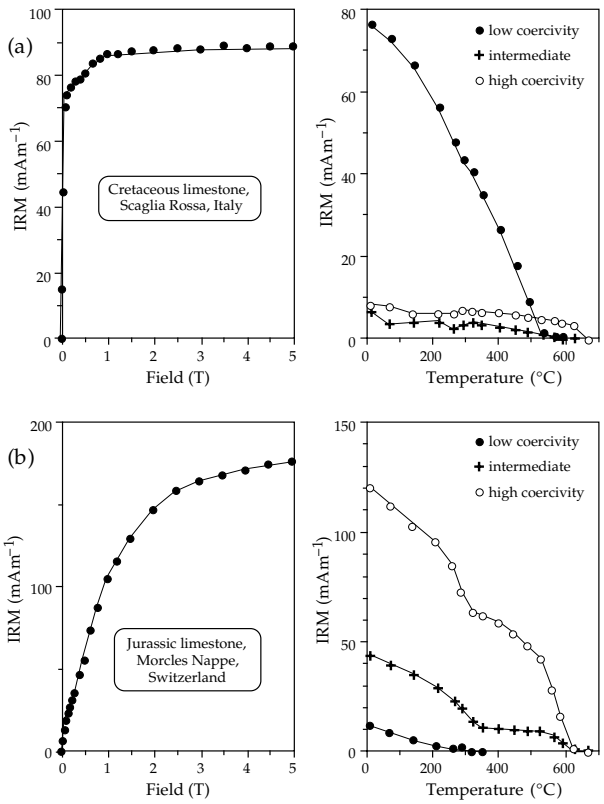

Fig. 5.24 Examples of the identification of magnetic minerals by acquisition and subsequent thermal demagnetization of IRM. Hematite is present in both (a) and (b), because saturation IRM requires fields > 1 T and thermal demagnetization of the hard fraction persists to T ≈ 675 °C. In (a) the soft fraction that demagnetizes at T ≈ 575 °C is magnetite, while in (b) no magnetite is indicated but pyrrhotite is present in all three fractions, shown by thermal unblocking at T ≈ 300–330 °C (after Lowrie, 1990).

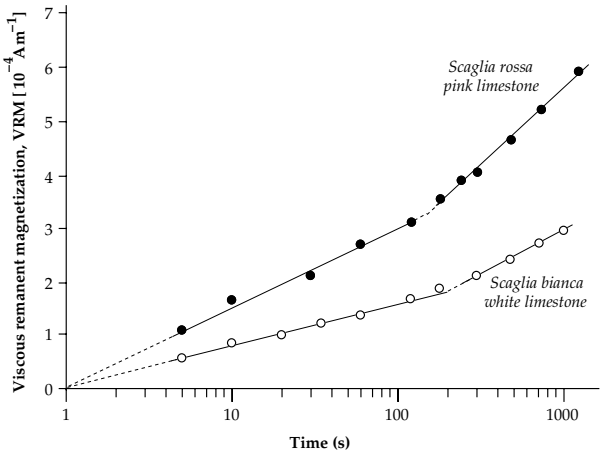

Fig. 5.25 Viscous remanent magnetization (VRM) in pelagic limestone samples, showing logarithmic growth with increasing time (after Lowrie and Heller, 1982).

the different coercivity fractions help to identify the magnetic mineralogy (Fig. 5.24).

5.3.6.5 Other remanent magnetizations

If a rock containing magnetic minerals with unstable magnetic moments experiences a magnetic field, there is a finite probability that some magnetic moments opposite to the field may switch direction to be parallel to the field. As time goes on, the number of magnetic moments in the direction of the field increases and the magnetization grows logarithmically with time (Fig. 5.25). The time-dependent remanence acquired in this way is called a *viscous remanent magnetization* (VRM). The VRM also decreases logarithmically when the field is removed or changed and is often identifiable during laboratory analysis as an unstable time-dependent change in remanence. The direction of a VRM is often parallel to the present-day field direction, which can be useful in its identification. However, it is always a secondary remanence and it can mask the presence of geologically interesting stable components. Techniques of progressive demagnetization have been designed to remove VRM and IRM, effectively "cleaning" the remanence of a rock of undesirable components.

An important form of remanent magnetization can be produced in a rock sample by placing it in a coil that carries an alternating magnetic field, whose amplitude is then slowly reduced to zero. In the absence of another field, this procedure randomizes the orientations of grain magnetic moments with coercivities less than the peak field. If, however, the rock sample is exposed to a small constant magnetic field while the amplitude of the alternating magnetic field is decreasing to zero, the magnetic moments are not randomized. Their distribution is biassed with a statistical preference for the direction of the constant field. This produces an *anhysteretic remanent magnetization* (ARM) in the sample. The intensity of ARM increases with the amplitude of the alternating field, and also with the strength of the constant bias field. ARM may be produced deliberately, as described, and it is commonly observed as a spurious effect during progressive alternating field demagnetization of rock samples when the shielding from external fields is imperfect (Section 5.6.3.2).

Stress and the associated strains of magnetostriction combine to produce magnetoelastic energy (see Section 5.2.7.3). This acts as a source of magnetic anisotropy that can modify the easy directions of magnetization in some magnetic minerals. As a result, stress caused by tectonic deformation or by defects in the crystal structure of constituent minerals may influence the direction of magnetization in a rock. The effect of high hydrostatic pressure, such as might be encountered at depth in the Earth's crust, is to deflect the magnetizations of individual grains away from existing easy axes, which leads to a net demagnetization of the rock. On the other hand, the effect of non-hydrostatic stress in the presence of a magnetic field is to produce a *piezoremanent magnetization* (PRM) that is added to, or may replace, any pre-existing remanent magnetization. The modification of rock magnetization by deformational stress, whether elastic or plastic, can overprint the original magnetization in rocks that have been deeply buried, or subjected to high stress and temperature during deformation.

A related type of magnetization has been observed in terrestrial and lunar rocks that have been shocked by meteoritic impact. The event causes very high local stress of short duration, and gives rise to a *shock remanent magnetization* (SRM) by a similar mechanism to PRM. The collision of a meteorite with another planetary body imposes a characteristic shock texture on the impacted rocks, so that SRM and PRM are not exactly equivalent. Moreover, much of the energy of the collision is released as heat, which can modify and reduce the SRM over a much longer time than the brief duration of the impact. However, SRM may have played a role in the origin of anomalous crustal magnetizations on the Moon, Mars and other extraterrestrial bodies that have suffered extensive meteoritic bombardment.

5.3.7 Environmental magnetism

Since the mid-1980s rock magnetic properties have found important new applications in environmental research, where they can serve as tracers for pollution or as indicators of past climates. Heavy metals from industrial processes enter the environment, contaminating both the ground surface and the water in lakes, rivers and the groundwater. Magnetic minerals such as magnetite and hematite accompany more toxic elements in the emissions. Magnetic susceptibility surveys can provide a rapid method of determining the geographic dispersal and relative concentration of the heavy metal pollution. Motor-vehicle exhaust emissions also pollute the environment by loading it with heavy metals as well as sub-micrometer sized particles of soot, a fraction of which consists of nanoparticle sized magnetic minerals. Rock magnetic parameters and investigative techniques provide ways of

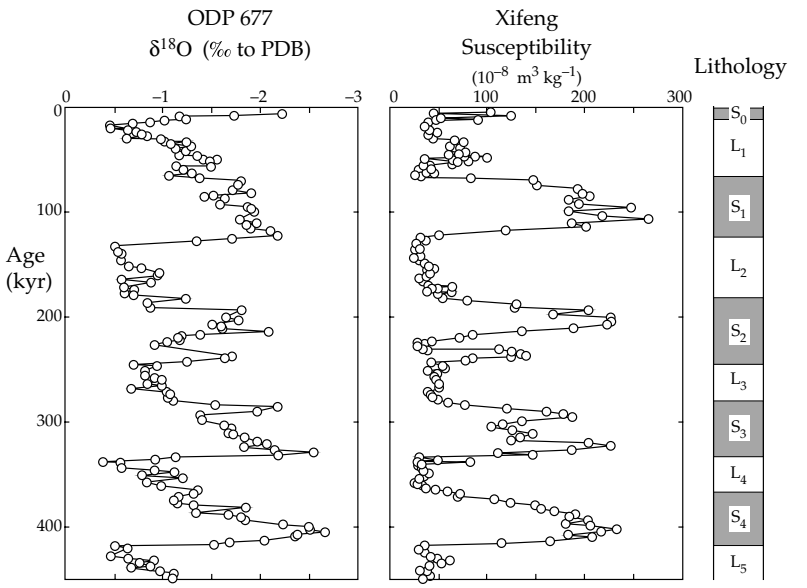

Fig. 5.26 Comparison of the magnetic susceptibility variation in a section of loess and paleosols at Xifeng, China, with the oxygen isotope record in marine sediments cored at ODP site 677 (after Evans and Heller, 2003).

characterizing these particles and of describing their regional distribution and concentration.

The magnetic grain fraction in a sediment or soil usually consists of hematite, magnetite, maghemite or an iron sulfide. The magnetic mineral composition may be modified by the climatic conditions at or after deposition. These affect magnetic properties of the sediment that depend on grain size and mineral composition, such as magnetic susceptibility, coercivity and the various remanent magnetizations. These magnetic parameters can act as proxies for paleoclimatic change. Numerous studies have been devoted to understanding the processes involved and their application. The following example illustrates the potential of magnetic methods for analyzing a paleoclimatic problem.

Great thicknesses of loess sediments up to 100 m in thickness occur in Central China. The loess are very fine grained (10–50 μm size) wind-blown sediments that are deposited in cold, dry conditions. Alternating with the beds of loess are layers of *paleosol*, the name given to fossil soils. These form by conversion of the loess to soils (a process called *pedogenesis*), which takes place during interglacial periods of warmer, humid conditions. In turn, later loess deposits bury the soils. The alternation of loess and paleosol is therefore a record of past climatic variations. The magnetic susceptibility correlates with the lithology of the loess–paleosol sequences. In the loess beds the susceptibility measures around 25 SI units, but in the paleosol layers the values exceed 200 SI units (Fig. 5.26). Rock magnetic analysis showed that the dominant magnetic mineral in both lithologies is magnetite. The higher susceptibility of the paleosols is thus due to higher concentrations of magnetite. The susceptibility variation correlates very well with the oxygen isotope stratigraphy measured in deep-sea sediments at site 677 of the Ocean Drilling Program (ODP). The oxygen isotope ratio (see Box 5.2) is a record of climatic variation, with the most negative values corresponding to warmer temperature, and it has been dated by comparison to magnetostratigraphy in marine sediments (Section 5.7.2). The correlation in Fig. 5.26 provides a way of dating the loess–paleosol sequence and shows that the paleosols were formed under warmer conditions than the loess. Possibly the change to a warmer, humid climate encouraged the *in situ* formation of a new phase of magnetite in the paleosols, with a consequent increase in susceptibility.

The new phase of magnetite in the paleosols originates by a chemical process. However, magnetite can be produced by the action of bacteria in sediments deposited in lakes and in the sea. This is referred to as a *biogenic* process and the bacteria that can produce magnetite are called *magnetotactic bacteria*. The magnetite forms as tiny crystallites called *magnetosomes*, less than 0.1 μm in size and thus of single domain type, which occur as chains of particles enclosed in a membrane. The most common magnetosome mineral is magnetite, but greigite, an iron sulfide with structure similar to magnetite, has also been found. The chain-like assembly imparts a dipole magnetic moment to the bacteria. This is evidently an evolutionary feature, which helps the bacteria to survive. If the sediment is disturbed, the magnetic moment of the bacteria enables them to move along the Earth's magnetic field lines. The dipping field lines guide them back down into the sediment where they find nutrition needed for their survival. It was long believed that magnetite in deep-sea sediments was mainly of detrital origin, washed in from the continents and ocean ridges, but it is now clear that a large portion must be biomagnetic.

Magnetite of biogenic origin has been identified in many unusual settings. For example, submicroscopic magnetite occurs in the brains of dolphins and birds; whether it plays a role in their guidance during migration is unclear. Magnetite of nanometer size has been located in the human brain, where it may be related to neurological disorders such as epilepsy, Alzheimer's disease and Parkinson's disease. It also occurs in other human organs. The magnetic properties

Box 5.2: Oxygen isotope ratio

The element oxygen has two important stable isotopes. These are a "light" isotope ^{16}O, with 8 protons and 8 neutrons in its nucleus, and a "heavy" isotope ^{18}O, with 8 protons and 10 neutrons. Mass spectrometers are capable of determining accurately the masses of these isotopes, and so the mass ratio $^{18}O/^{16}O$ can be measured in quite small samples. In order to describe the deviation of the $^{18}O/^{16}O$ ratio in a given sample from a standard value, a useful parameter, $\delta^{18}O$, is defined as follows:

$$\delta^{18}O = 1000 \times \left(\frac{(^{18}O/^{16}O)_{sample} - (^{18}O/^{16}O)_{standard}}{(^{18}O/^{16}O)_{standard}} \right)$$

The standard value is taken to be the $^{18}O/^{16}O$ ratio in the modern oceans at depths in the 200–500 m range, or alternatively the ratio in a fossil belemnite known as PDB. The factor 1000 causes $\delta^{18}O$ values to be expressed in parts per thousand. The global climate at present is relatively warmer than in the past, so $^{18}O/^{16}O$ ratios measured in ancient samples tend to be smaller than the standard value and give negative $\delta^{18}O$ values.

The $^{18}O/^{16}O$ ratio in water is dependent on temperature, as evident in the plot of $\delta^{18}O$ in the annual precipitation against the mean temperature at a global set of sites (Fig. B5.2). Two factors determine this correlation: cool air holds less moisture than warm air, and the "heavy" isotope ^{18}O condenses more easily than the "light" isotope ^{16}O. From an air mass that moves polewards, precipitation in warmer regions is relatively rich in ^{18}O whereas in colder regions it is enriched in ^{16}O.

The situation is reversed in the oceans. During global warm periods, polar ice sheets melt, adding fresh water enriched in ^{16}O to the oceans. As a result, low (i.e., large negative) $\delta^{18}O$ values in the oceans indicate intervals of global warming. In contrast, during glacial intervals water is transferred from the oceans to the ice sheets

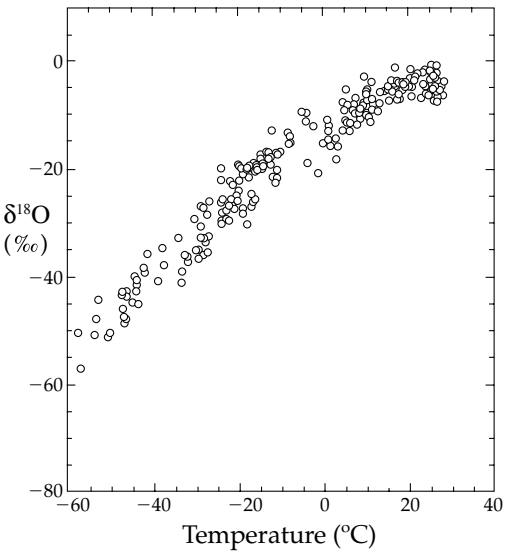

Fig. B5.2 Observed correlation between $\partial^{18}O$ in precipitation and temperature for the present-day climate (after Jouzel *et al.*, 1994).

primarily as ^{16}O, so the remaining ocean water is enriched in ^{18}O, which increases the $\delta^{18}O$ value. Thus, high (i.e., small negative or even positive) $\delta^{18}O$ values in oceanic water and sediments indicate cool intervals. Conversely, the same conditions result in the opposite relationships between global temperature and $\delta^{18}O$ values measured in polar ice.

Paleoclimatology uses the $\delta^{18}O$ parameter as a guide to past climates, as illustrated by the use of the record in sediment cores from the Ocean Drilling Project to interpret the paleoclimate that affected Chinese loess–paleosol profiles (Fig. 5.26). Samples can be used from a variety of sources: polar ice cores, ocean sediments, and fossil shells. In the last case, biological and chemical processes disturb the simple relationship with temperature, but this can be taken into account and corrected.

of the magnetite, its source and the mechanism of its formation in human tissue are exciting fields of modern research.

5.4 GEOMAGNETISM

5.4.1 Introduction

The magnetic field of the Earth is a vector, that is, it has both magnitude and direction. The magnitude, or intensity F, of the field is measured in the same units as other **B**-fields, namely in *tesla* (see Eq. (5.10)). However, a tesla is an extremely strong magnetic field, such as one would observe between the poles of a powerful electromagnet. The Earth's magnetic field is much weaker; its maximum intensity is reached near to the magnetic poles, where it amounts to about 6×10^{-5} T. Modern instruments for measuring magnetic fields (called magnetometers) have a sensitivity of about 10^{-9} T; this unit is called a nanotesla (nT) and has been adopted in geophysics as the practical unit for expressing the intensity of geomagnetic field intensity. There is a practical reason for adopting this unit. Most geomagnetic surveys carried out until the 1970s used the now abandoned c.g.s. system of units, in which the **B**-field was measured in *gauss*, equivalent to 10^{-4} T. The practical unit of geophysical exploration was then 10^{-5} gauss, called a *gamma* (γ). Thus, the former unit (γ) is conveniently equal to 10^{-9} T, which is the new unit (nT).

The magnetic vector can be expressed as Cartesian components parallel to any three orthogonal axes. The *geomagnetic elements* are taken to be components parallel to the geographic north and east directions and the vertically downward direction (Fig. 5.27). Alternatively, the

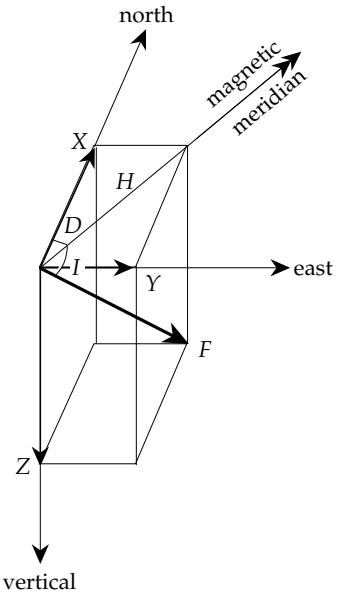

Fig. 5.27 Definition of the geomagnetic elements. The geomagnetic field can be described by north (*X*), east (*Y*) and vertically downward (*Z*) Cartesian components, or by the angles of declination (*D*) and inclination (*I*) together with the total field intensity (*F*).

geomagnetic elements can be expressed in spherical polar coordinates. The magnitude of the magnetic vector is given by the field strength F; its direction is specified by two angles. The *declination* D is the angle between the magnetic meridian and the geographic meridian; the *inclination* I is the angle at which the magnetic vector dips below the horizontal (Fig. 5.27). The Cartesian (X, Y, Z) and spherical polar (F, D, I) sets of geomagnetic elements are related to each other as follows:

$$X = F\cos I\cos D \qquad Y = F\cos I\sin D \qquad Z = F\sin I$$

$$F^2 = X^2 + Y^2 + Z^2$$

$$D = \arctan\left(\frac{Y}{X}\right) \qquad I = \arctan\left(\frac{Z}{\sqrt{X^2 + Y^2}}\right) \tag{5.32}$$

5.4.2 Separation of the magnetic fields of external and internal origin

The magnetic field B and its potential W at any point can be expressed in terms of the spherical polar coordinates (r, θ, ϕ) of the point of observation. Gauss expressed the potential of the geomagnetic field as an infinite series of terms involving these coordinates. Essentially, his method divides the field into separate components that decrease at different rates with increasing distance from the center of the Earth. The detailed analysis is complicated and beyond the scope of this text. The magnitude of the potential is given by

$$W = R\sum_{n=1}^{n=\infty}\left(A_n r^n + \frac{B_n}{r^{n+1}}\right)\sum_{l=0}^{l=n} Y_n^l(\theta,\phi) \tag{5.33}$$

where R is the Earth's radius.

This is a rather formidable expression, but fortunately the most useful terms are quite simple. The summation signs indicate that the total potential is made up of an infinite number of terms with different values of n and l. We will only pay attention here to the few terms for which $n = 1$. The expression in parentheses describes the variation of the potential with distance r. For each value of n there will be different dependences (e.g., on r, r^2, r^3, r^{-2}, r^{-3}, etc.). The function $Y_n^l(\theta,\phi)$ describes the variation of the potential when r is constant, i.e., on the surface of a sphere. It is called a *spherical harmonic function*, because it has the same value when θ or ϕ is increased by an integral multiple of 2π (Box 2.3). For observations made on the spherical surface of the Earth, the constants A_n describe parts of the potential that arise from magnetic field sources outside the Earth, which are called the *geomagnetic field of external origin*. The constants B_n describe contributions to the magnetic potential from sources inside the Earth. This part is called the *geomagnetic field of internal origin*.

The potential itself is not measured directly. The geomagnetic elements X, Y and Z (Fig. 5.27) are recorded at magnetic observatories. Ideally these should be distributed uniformly over the Earth's surface but in fact they are predominantly in the northern hemisphere. The geomagnetic field components are directional derivatives of the magnetic potential and depend on the same coefficients A_n and B_n. Observations of magnetic field elements at a large number of measurement stations with a world-wide distribution allows the relative importance of A_n and B_n to be assessed. From the sparse data-set available in 1838 Gauss was able to show that the coefficients A_n are very much smaller than B_n. He concluded that the field of external origin was insignificant and that the field of internal origin was predominantly that of a dipole.

5.4.3 The magnetic field of external origin

The magnetic field of the Earth in space has been measured from satellites and spacecraft. The external field has a quite complicated appearance (Fig. 5.28). It is strongly affected by the *solar wind*, a stream of electrically charged particles (consisting mainly of electrons, protons and helium nuclei) that is constantly emitted by the Sun. The solar wind is a *plasma*. This is the physical term for an ionized gas of low particle density made up of nearly equal concentrations of oppositely charged ions. At the distance of the Earth from the Sun (1 AU) the density of the solar wind is about 7 ions per cm^3, and it produces a magnetic field of about 6 nT. The solar wind interacts with the magnetic field of the Earth to form a region called the *magnetosphere*. At distances greater than a few Earth radii the interaction greatly alters the magnetic field from that of a simple dipole.

The velocity of the solar wind relative to the Earth is about 450 km s^{-1}. At a great distance (about 15 Earth radii) from the Earth, on the day side, the supersonic solar wind

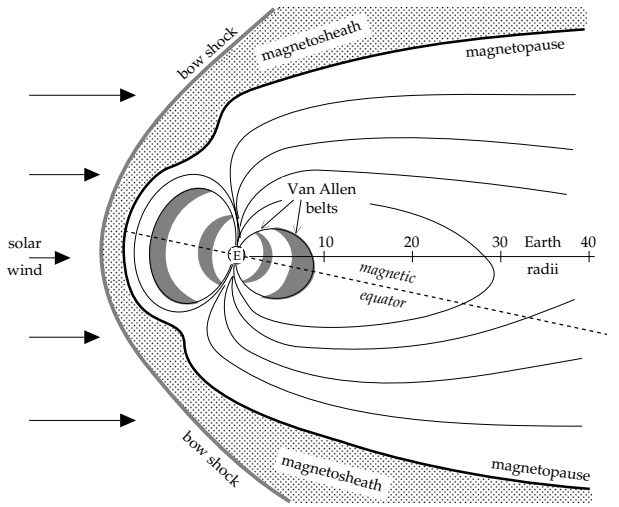

Fig. 5.28 Schematic cross-section through the magnetosphere, showing various regions of interaction of the Earth's magnetic field with the solar wind.

collides with the thin upper atmosphere. This produces an effect similar to the build-up of a shock wave in front of a supersonic aircraft. The shock front is called the *bow-shock* region (Fig. 5.28); it marks the outer boundary of the magnetosphere. Within the bow-shock region the solar wind is slowed down and heated up. After passing through the shock front the solar wind is diverted around the Earth in a region of turbulent motion called the *magnetosheath*. The moving charged particles of the solar wind constitute electrical currents. They produce an *interplanetary magnetic field*, which reinforces and compresses the geomagnetic field on the day side and weakens and stretches it out on the night side of the Earth. This results in a geomagnetic tail, or *magnetotail*, which extends to great distances "downwind" from the Earth. The Moon's distance from the Earth is about 60 Earth radii and so its monthly orbit about the Earth brings it in and out of the magnetotail on each circuit. The transition between the deformed magnetic field and the magnetosheath is called the *magnetopause*.

5.4.3.1 The Van Allen radiation belts

Charged particles that penetrate the magnetopause are trapped by the geomagnetic field lines and form the *Van Allen radiation belts*. These constitute two doughnut-shaped regions coaxial with the geomagnetic axis (Fig. 5.29). The inner belt contains mainly protons, the outer belt energetic electrons. Within each belt the charged particles move in helical fashion around the geomagnetic field lines (Fig. 5.30). The pitch of the spiraling motion gets smaller as the particle comes ever closer to the Earth and the field intensity increases; eventually it reaches zero and reverses sense. This compels the particles to shuttle rapidly from one polar region to the other along the field lines. The inner Van Allen belt starts about 1000 km above the Earth's surface and extends to an altitude of about 3000 km (Fig. 5.29); the outer belt occupies a doughnut shaped region at distances between about 3 and 4 Earth radii (20,000–30,000 km) from the center of the Earth.

5.4.3.2 The ionosphere

The effects described above illustrate how the Earth's magnetic field acts as a shield against much of the extra-terrestrial radiation. The atmosphere acts as a protective blanket against the remainder. Most of the very short-wavelength fraction of the solar radiation that penetrates the atmosphere does not reach the Earth's surface. Energetic γ- and x-rays and ultraviolet radiation cause ionization of the molecules of nitrogen and oxygen in the thin upper atmosphere at altitudes between about 50 km and 1500 km, forming an ionized region called the *ionosphere*. It is formed of five layers, labelled the D, E, F_1, F_2 and G layers from the base to the top. Each layer can reflect radio waves. The thicknesses and ionizations of the layers change during the course of a day; all but one or two layers on the night side of the Earth disappear while they thicken and strengthen on the day side (Fig. 5.31). A radio transmitter on the day side can bounce signals off the ionosphere that then travel around the world by multiple reflections between the ground surface and the ionosphere. Consequently, radio reception of distant stations from far across the globe is best during the local night hours. The D layer is closest to the Earth at an altitude of about 80–100 km. It was first discovered in 1902, before the nature of the ionosphere was known, because of its ability to reflect long-wavelength radio waves, and is named the *Kennelly–Heaviside layer* in honor of its discoverers. The E layer is used by short-wave amateur radio enthusiasts. The F layers are the most intensely ionized.

5.4.3.3 Diurnal variation and magnetic storms

The ionized molecules in the ionosphere release swarms of electrons that form powerful, horizontal, ring-like electrical currents. These act as sources of external magnetic fields that are detected at the surface of the Earth. The ionization is most intense on the day side of the Earth, where extra layers develop. The Sun also causes atmospheric tides in the ionosphere, partly due to gravitational attraction but mainly because the side facing the Sun is heated up during the day. The motions of the charged particles through the Earth's magnetic field produce an electrical field, according to Lorentz's law (Eq. (5.10)), which drives electrical currents in the ionosphere. In particular, the horizontal component of particle velocity interacts with the vertical component of the geomagnetic field to produce horizontal electrical current loops in the ionosphere. These currents cause a magnetic field at the Earth's surface. As the Earth rotates beneath the ionosphere the observed intensity of the geomagnetic field fluctuates with a range of amplitude of about 10–30 nT at the Earth's surface and a period of one day (Fig. 5.32a). This

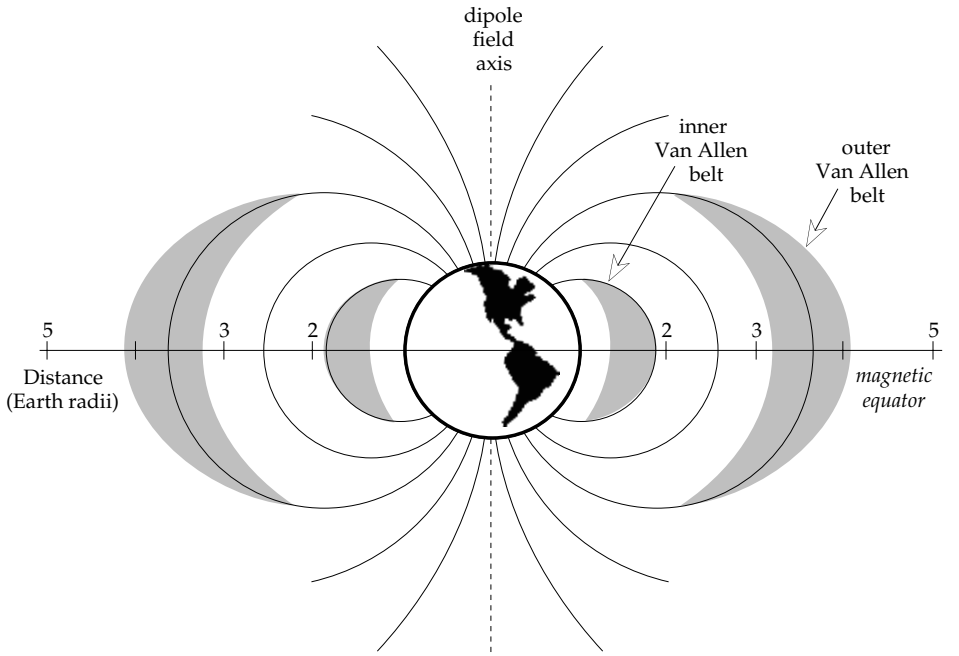

Fig. 5.29 Schematic representation of the inner and outer Van Allen belts of charged particles trapped by the magnetic field of the Earth.

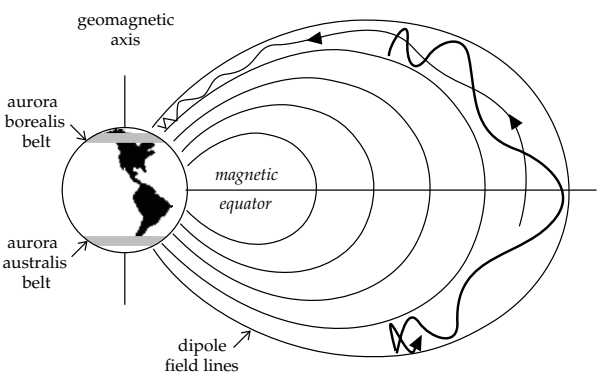

Fig. 5.30 Charged particles from the solar wind are constrained to move in a helical fashion about the geomagnetic field lines (after Vestine, 1962).

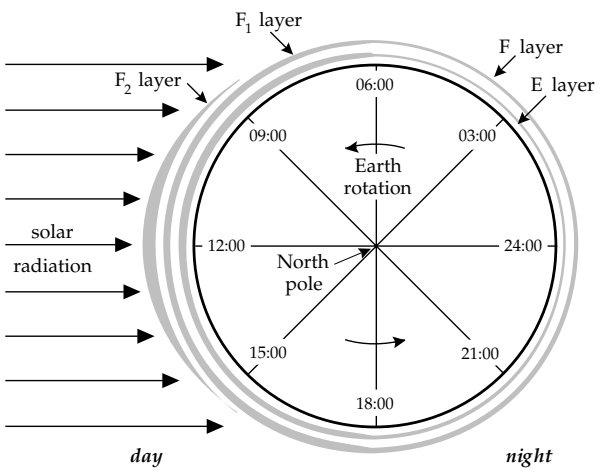

Fig. 5.31 Cross-section through the Earth showing the layered structure of the ionosphere (after Strahler, 1962).

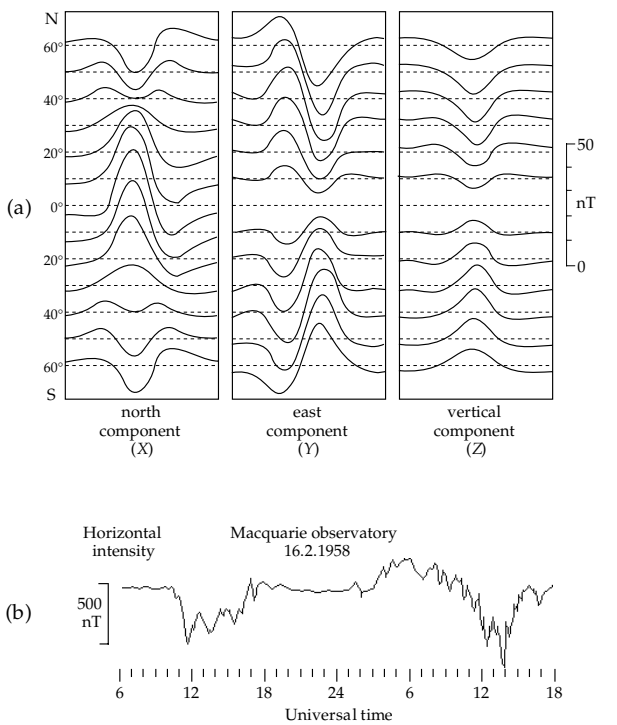

Fig. 5.32 (a) The time-dependent daily (or diurnal) variation of the components of geomagnetic field intensity at different latitudes (after Chapman and Bartels, 1940), and (b) the variation of horizontal field intensity during a magnetic storm (after Ondoh and Maeda, 1962).

time-dependent change of geomagnetic field intensity is called the *diurnal* (or *daily*) *variation*.

The magnitude of the diurnal variation depends on the latitude at which it is observed. Because it greatly exceeds the accuracy with which magnetic fields are measured during surveys, the diurnal variation must be compensated by correcting field measurements accordingly. The intensity

of the effect depends on the degree of ionization of the ionosphere and is therefore determined by the state of solar activity. As described in Section 5.4.7.1, the solar activity is not constant. On days when the activity of the Sun is especially low, the diurnal variation is said to be of solar quiet (S_q) type. On normal days, or when the solar activity is high, the S_q variation is overlaid by a solar disturbance (S_D) variation. Solar activity changes periodically with the 11-yr cycle of sunspots and solar flares. The enhanced emission of radiation associated with these solar phenomena increases the ionospheric currents. These give rise to rapidly varying, anomalously strong magnetic fields (called *magnetic storms*) with amplitudes of up to 1000 nT at the Earth's surface (Fig. 5.32b). The ionospheric disturbance also disrupts short-wave to long-wave radio transmissions. Magnetic surveying must be suspended temporarily while a magnetic storm is in progress, which can last for hours or days, depending on the duration of the solar activity.

5.4.4 The magnetic field of internal origin

To understand how geophysicists describe the geomagnetic field of internal origin mathematically we return to Eq. (5.33). First, we follow Gauss and omit the coefficients A_n of the external field. The spherical harmonic functions $Y_n^m(\theta,\phi)$ that describe the variation of potential on a spherical surface are then written in expanded form (Box 2.3). The potential W of the field of internal origin becomes

$$W = R\sum_{n=1}^{n=\infty}\sum_{m=0}^{m=n}\left(\frac{R}{r}\right)^{n+1}(g_n^m\cos m\phi + h_n^m\sin m\phi)P_n^m(\cos\theta) \qquad (5.34)$$

Here, R is the Earth's radius, as before, and $P_n^m(\cos\theta)$ are called Schmidt polynomials, which are related to the associated Legendre polynomials (Box 2.2).

Equation (5.34) is a *multipole* expression of the geomagnetic potential. It relates the potential of the measured field to the potentials of particular combinations of magnetic poles (Box 5.3). The constants g_n^m and h_n^m in the geomagnetic potential are called the Gauss (or Gauss–Schmidt) coefficients of order n and degree m. Inspection of Eq. (5.34) shows that they have the same dimensions (nT) as the **B**-field. Their values are computed from analysis of measurements of the geomagnetic field.

Data from several sources are integrated in modern analyses of the Earth's magnetic field. Until the dawn of the satellite era, continuous records at magnetic observatories were the principal sources of geomagnetic data. Average values of the geomagnetic elements were determined, from which optimum values for the Gauss coefficients could be derived. Currently, about 200 permanent observatories make continuous measurements of the field. However, satellites orbiting the Earth in low near-polar orbits now provide most of the high-quality data used to model the field. The Polar Orbiting Geophysical Observatory (POGO), launched in 1965, was the first to deliver field measurements, but the greatest advance came with the Magnetic Field Satellite (MAGSAT), which delivered high-quality data during a six-month mission in 1979–1980. In 1979, a Danish satellite, ØRSTED, was placed in an elliptical, low-polar orbit, with altitude between 650 km and 865 km. It carried a vector magnetometer and a total field magnetometer, each with a sensitivity of 0.5 nT; the mission was dedicated to a survey of the geomagnetic field. The German satellite CHAMP (see also Section 2.4.6.4), was launched in 2000 in a lower, near-circular orbit on a planned five-year mission. In addition to measuring the gravity field, this satellite was also equipped to make scalar and vector measurements of the magnetic field. The low orbit and improved instrumentation were designed to provide magnetic measurements with high resolution.

In principle, an infinite number of Gauss coefficients would be needed to define the field completely. The coefficients of order and degree 8 and higher are very small and the calculation of Gauss coefficients must usually be truncated. A global model of the field is provided by the International Geomagnetic Reference Field (IGRF), which is based on coefficients up to $n = 10$, although analyses of higher order have been made. It is updated at regular intervals. The IGRF also gives the rate of change of each of the Gauss coefficients (its *secular variation*), which permits correction of the current values between update years.

The Gauss coefficients get smaller with increasing order n; this decrease provides a way of estimating the origin of the internal field. The analysis involves a technique called *power spectral analysis*. The distance across a feature of the magnetic field (for example, a region where the field is stronger than average) is called the wavelength of the feature. As in the case of gravity anomalies, deep-seated magnetic sources produce broad (long-wavelength) magnetic anomalies, while shallow sources result in narrow (short-wavelength) anomalies. Spectral analysis consists of calculating the power (alternatively called the energy density) associated with each "frequency" in the signal. This is obtained by computing the sum of the squares of all coefficients with the same order. In the case of the geomagnetic field, the spectral analysis is based on the values of the Gauss coefficients. The spatial frequency of any part of the observed field is contained in the order n of the coefficients. Low-order terms (those with small values of n) correspond to long-wavelength features, high-order terms are related to short-wavelength features.

Measurements of the geomagnetic field from the MAGSAT Earth-orbiting satellite at a mean altitude of 420 km above the Earth's surface have been analyzed to yield Gauss coefficients to order $n = 66$, special techniques being invoked for orders $n > 29$. A plot of the energy density associated with each order n of the geomagnetic field shows three distinct segments (Fig. 5.33). The high-frequency terms of order $n > 40$ are uncertain and the terms with $n > 50$ are in the "noise level" of the analysis

Box 5.3: Multipole representation of the geomagnetic field

Each term in Eq. (5.34) is the potential of the magnetic field due to a particular combination of magnetic poles. For example, Eq. (5.34) contains three terms for which $n = 1$. Each corresponds to a dipole field. One dipole is parallel to the axis of rotation of the Earth and the other two are at right angles to each other in the equatorial plane. The five terms with $n = 2$ describe a geometrically more complex field, known as a quadrupole field. Just as a dipole field results when two single poles are brought infinitesimally close to each other (see Section 5.2.3), a quadrupole field results when two opposing coaxial dipoles are brought infinitesimally close end-to-end. As its name implies, the quadrupole field derives from four magnetic poles of which two are "north" poles and two are "south" poles. The terms with $n = 3$ describe an octupole field which is characterized by eight (2^3) poles. The terms with $n = N$ describe a field that arises from a configuration of 2^N poles.

The configurations of axial dipole, quadrupole and octupole fields relative to a reference sphere are illustrated in Fig. B5.3.1 for the case where the order m of the Gauss coefficients is zero. If $m = 0$ in Eq. (5.34), the potential does not vary around a circle of "latitude" defined by a chosen combination of θ and r. This kind of field is said to have *zonal symmetry*. Any cross-section that contains the axis of symmetry is representative for the symmetry. Fig. B5.3.1 shows axial cross-sections of the simplest field line geometries corresponding to (a) dipole, (b) quadrupole and (c) octupole fields; each field is rotationally symmetrical about the axis of the configuration. The corresponding *zonal spherical harmonics* are illustrated symbolically by shading the alternate zones in which magnetic field lines leave or return to the surface of a sphere.

The dipole field is horizontal at the equator. In the southern hemisphere the field lines leave the reference sphere; in the northern hemisphere they return to it. In the northern hemisphere the field of an axial quadrupole is horizontal at latitude 35.3°N. North of this latitude the field lines of the quadrupole leave the reference sphere. An equivalent circle of latitude is located in the southern hemisphere at 35.3°S; south of this latitude the quadrupole field lines also leave the Earth. The field lines re-enter the Earth in the band of latitudes between those where the field is horizontal. The symmetry of the quadrupole field is described by these three *zones* around the axis. The axial octupole field exhibits zonal symmetry with four zones; two zones in which the field leaves the Earth alternate with two zones in which it re-enters it.

Terms in the potential expansion for which the degree m of the Gauss coefficients is equal to the order n (e.g., g_1^1, h_1^1, g_2^2, h_2^2) are called *sectorial harmonics*. Their symmetry relative to the Earth's axis is characterized by an even number of sectors around the equator in which the field lines alternately leave and re-enter the Earth (Fig. B5.3.2).

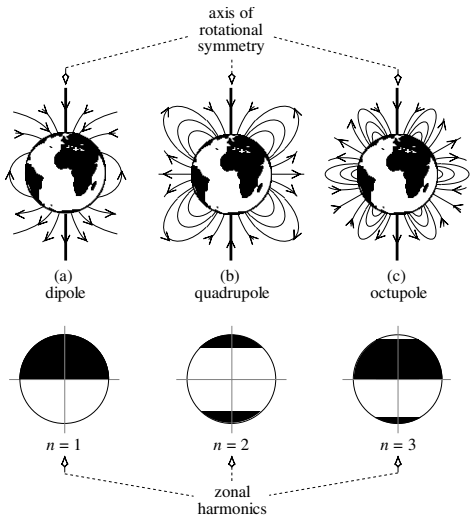

Fig.B5.3.1 Axial cross-sections showing the field line geometries of (a) dipole, (b) quadrupole and (c) octupole fields; each field is rotationally symmetrical about the axis of the configuration. The corresponding zonal spherical harmonics are illustrated symbolically by shading the alternate zones in which magnetic field lines leave or return to the surface of a sphere.

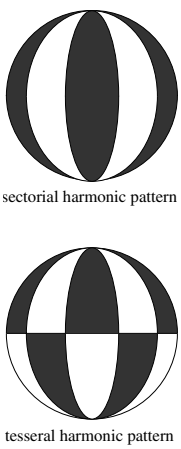

Fig.B5.3.2 Symmetry relative to the axis of rotation of sectorial and tesseral spherical harmonic functions.

The potential terms for which $m \neq n$ (e.g., g_2^1, h_2^1, g_3^2, h_3^1) are known as *tesseral harmonics*. Their pattern of symmetry is defined by the intersections of circles of latitude and longitude, which outline alternating domains in which the field lines leave and re-enter the Earth, respectively.

Multipole representation allows the very complex geometry of the total field to be broken down into contributions from a number of fields with simple geometries.

By superposing many terms corresponding to these simple geometries a field of great complexity can be generated. It must be kept in mind that this is not a physical expression of the magnetic field, because magnetic poles do not exist. It is a convenient technique for describing the field mathematically.

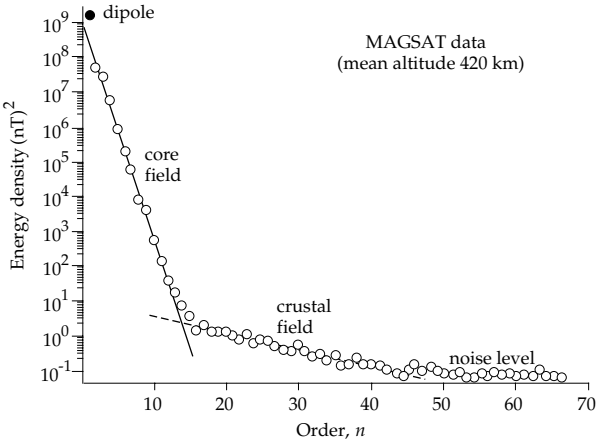

Fig. 5.33 The energy density spectrum derived from measurements of the geomagnetic field made by the MAGSAT Earth-orbiting satellite (after Cain, 1989).

and cannot be attributed any geophysical importance. The terms $15 \leq n \leq 40$ are due to short-wavelength magnetic anomalies associated with the magnetization of the Earth's crust. The terms $n \leq 14$ dominate the Earth's magnetic field and are due to much deeper sources in the fluid core.

5.4.4.1 The dipole field

The most important part of the Earth's magnetic field at the surface of the Earth is the dipole field, given by the Gauss coefficients for which $n = 1$. If we write only the first term of Eq. (5.34) we get the potential

$$W = \frac{R^3 g_1^0 \cos\theta}{r^2} \tag{5.35}$$

Note that the spatial variation of this potential depends on $(\cos\theta/r^2)$ in the same way as the potential of a dipole, which was found (Eq. (5.8)) to be

$$W = \frac{\mu_0 m \cos\theta}{4\pi r^2} \tag{5.36}$$

Comparison of the coefficients of $(\cos\theta/r^2)$ in Eq. (5.35) and Eq. (5.36) gives the dipole moment of the Earth's axial dipole in terms of the first Gauss coefficient:

$$m = \frac{4\pi}{\mu_0} R^3 g_1^0 \tag{5.37}$$

The term g_1^0 is the strongest component of the field. It describes a magnetic dipole at the center of the Earth and aligned with the Earth's rotation axis. This is called the *geocentric axial magnetic dipole*.

The magnetic field **B** of a dipole is symmetrical about the axis of the dipole. At any point at distance r from the center of a dipole with moment m on a radius that makes an angle θ to the dipole axis the field of the dipole has a radial component B_r and a tangential component B_θ, which can be obtained by differentiating the potential with respect to r and θ, respectively:

$$B_r = -\frac{\partial W}{\partial r} = \frac{\mu_0}{4\pi}\frac{2m\cos\theta}{r^3} \tag{5.38}$$

$$B_\theta = -\frac{1}{r}\frac{\partial W}{\partial \theta} = \frac{\mu_0}{4\pi}\frac{m\sin\theta}{r^3} \tag{5.39}$$

Note that B_r vanishes at the equator ($\theta = 90°$) and the field is horizontal; comparing Eqs. (5.37) and (5.39) we get that the horizontal equatorial field B_θ is equal to g_1^0. At a point (r, θ) on the surface of a uniformly magnetized sphere the magnetic field line is inclined to the surface at an angle I, which is given by

$$\tan I = \frac{B_r}{B_\theta} = 2\cot\theta = 2\tan\lambda \tag{5.40}$$

The angle I is called the *inclination* of the field, and θ is the angular distance (or *polar angle*) of the point of observation from the magnetic axis. The polar angle is the complement of the magnetic latitude, λ (i.e., $\theta = 90° - \lambda$). Equation (5.40) has an important application in paleomagnetism, as will be seen later.

The terms g_1^1 and h_1^1 are the next strongest in the potential expansion. They describe contributions to the potential from additional dipoles with their axes in the equatorial plane. The total dipole moment of the Earth is then obtained from the vector sum of all three components:

$$m = \frac{4\pi}{\mu_0} R^3 \sqrt{(g_1^0)^2 + (g_1^1)^2 + (h_1^1)^2} \tag{5.41}$$

The analysis of the geomagnetic field for the year 2005 gave the following values for the dipole coefficients: $g_1^0 = -29{,}556.8$ nT; $g_1^1 = -1671.8$ nT; $h_1^1 = 5080.0$ nT. The strength of the Earth's dipole magnetic moment obtained by inserting these values in Eq. (5.41) is $m = 7.7674 \times 10^{22}$ A m^2. Note that the sign of g_1^0 is negative. This means that the axial dipole points opposite to the direction of rotation. Taken together, the three dipole components describe a geocentric dipole inclined at about 11.2° to the Earth's rotation axis. This tilted geocentric dipole accounts for more than 90% of the geomagnetic field at the Earth's surface. Its axis cuts the surface at the north and south *geomagnetic poles*. For epoch 2005 the respective poles were located at 79.7°N, 71.8°W (i.e., 288.2°E) and 79.7°S, 108.2°E. The geomagnetic poles are antipodal (i.e., exactly opposite) to each other.

The *magnetic poles* of the Earth are defined as the locations where the inclination of the magnetic field is $\pm 90°$ (i.e., where the field is vertically upward or downward). An *isoclinal* map (showing constant inclination values) for the year 1980 shows that the location of the north magnetic pole was at 77.3°N, 258.2°E while the south magnetic pole was at 65.6°S, 139.4°E (Fig. 5.34a). These poles are not exactly opposite one another. The discrepancy between the magnetic poles and the geomagnetic poles arises because the terrestrial magnetic field is somewhat more complex than that of a perfect dipole. The intensity of the geomagnetic field is generally stronger in high latitudes than near the equator (Fig. 5.34b). The intensity is

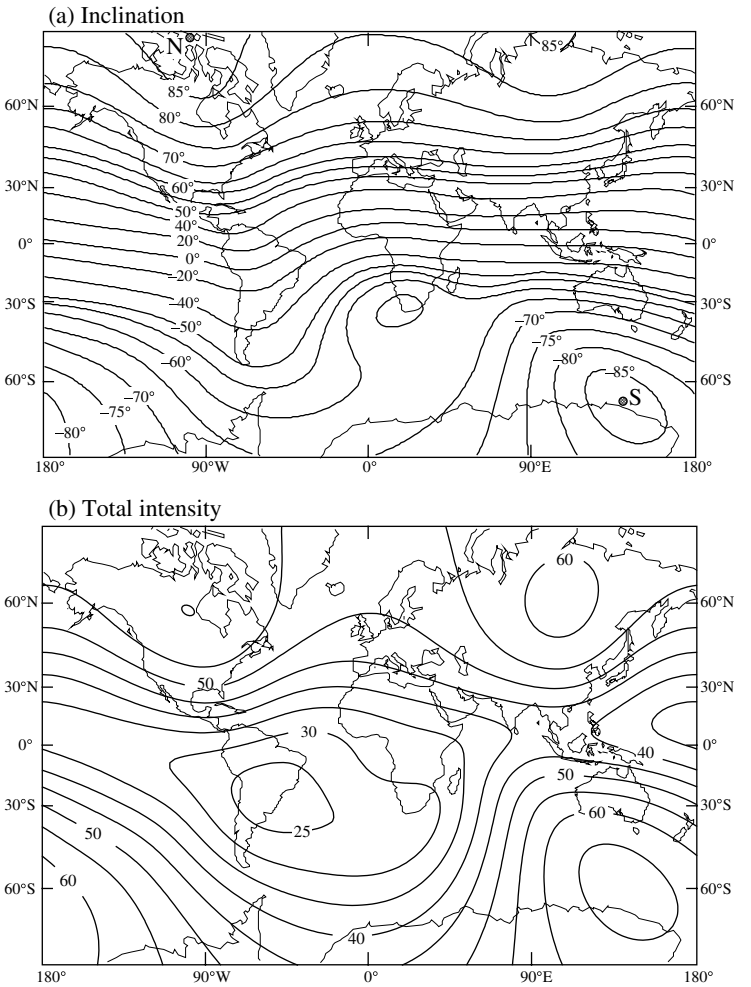

Fig. 5.34 (a) The isoclinal map of the geomagnetic field for the year 1980 AD (after Merrill and McElhinny, 1983), and (b) the total intensity of the International Geomagnetic Reference Field (in μT) for 2000 (source: http://geomag.nasa.gov).

especially low over the South Atlantic, where it is about 20 μT weaker than expected. The cause of this "South Atlantic magnetic anomaly" is not understood. Because the geomagnetic field shields the Earth from cosmic radiation and charged particles of the solar wind, this protection is less effective over the South Atlantic. Orbiting satellites note increased impacts of extra-terrestrial particles over this region. The feature poses hazards for astronauts in low-orbiting spacecraft and also for pilots and passengers in high-altitude aircraft that pass through the region. The enhanced particle flux can interfere with their on-board computers, communications and guidance systems.

5.4.4.2 The non-dipole field

The part of the field of internal origin (about 5% of the total field), obtained by subtracting the field of the inclined geocentric dipole from the total field, is collectively called the *non-dipole field*. A map of the non-dipole field consists of a system of irregularly sized, long-wavelength magnetic anomalies (Fig. 5.35). To describe this field requires all the terms in the potential expansion of order $n \geq 2$ in Eq. (5.34).

The distribution of positive and negative non-dipole field anomalies suggests an alternative representation of the non-dipole field to the multipole portrayal. The positive and negative anomalies have been modelled by inward or outward oriented radial dipoles in the core at about one-quarter the Earth's radius. Each dipole is presumed to be caused by a toroidal current loop parallel to the surface of the core. A single centered axial dipole and eight auxiliary radial dipoles are adequate to represent the field observed at the Earth's surface. The secular variation at a site (Section 5.4.5.2) is explained by this model as the passage of one of the auxiliary dipoles under the site. This model may be a little closer to physical reality but it is more unwieldy to handle. The multipole representation is the most convenient way of modelling the geomagnetic potential for mathematical analysis.

5.4.5 Secular variation

At any particular place on the Earth the geomagnetic field is not constant in time. When the Gauss coefficients of the internal field are compared from one epoch to another, slow but significant changes in their values are observed. The slow changes of the field only become appreciable

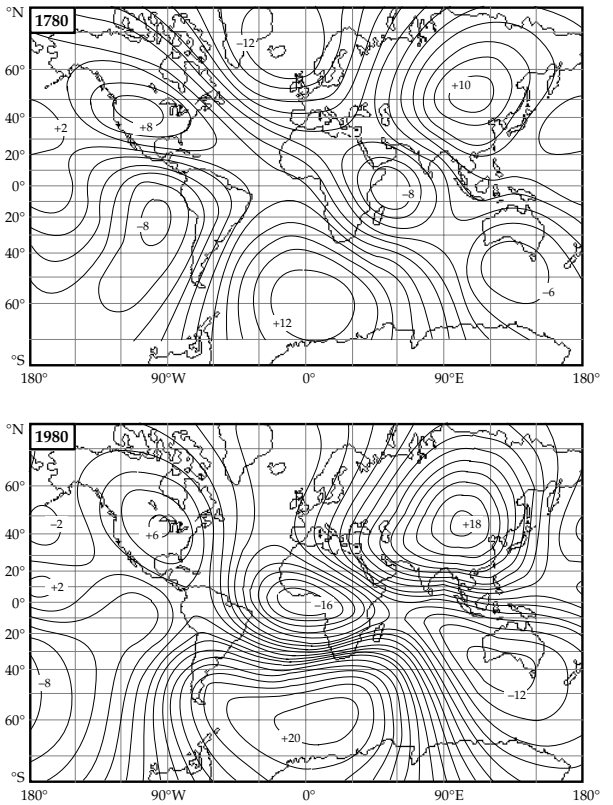

Fig. 5.35 The vertical component of the non-dipole magnetic field for the years 1780 AD (after Yukutake and Tachinaka, 1968) and 1980 AD (after Barton, 1989).

over decades or centuries of observation and so they are called *secular variations* (from the Latin word *saeculum* for a long age). They are manifest as variations of both the dipole and non-dipole components of the field.

5.4.5.1 Secular variation of the dipole field

The dipole field exhibits secular variations of intensity and direction. Calculations of the Gauss coefficients for different historical epochs show a near-linear decay of the strength of the dipole moment at a rate of about 3.2% per century between about 1550 AD and 1900 AD. At the start of the twentieth century the decay became even faster and has averaged about 5.8% per century during the last 80 yr (Fig. 5.36a). If it continues at the same almost linear rate, the field intensity would reach zero in about another 2000 yr. The cause of the quite rapid decay in intensity is not known; it may simply be part of a longer term fluctuation. However, another possibility is that the dipole moment may be decreasing preparatory to the next reversal of geomagnetic field polarity.

The position of the dipole axis also shows secular variation. The changes can be traced by plotting the colatitude (the angle between the dipole axis and the rotation axis) and longitude of the geomagnetic pole as a function of time. Data are only sufficiently abundant for spherical harmonic analysis since the early nineteenth

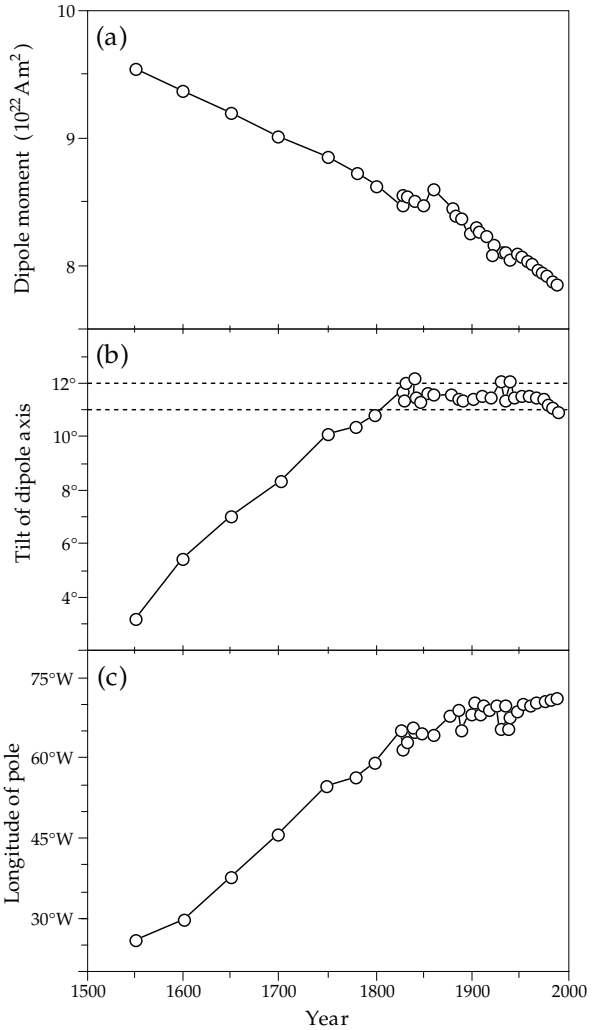

Fig. 5.36 Secular variations of the tilted geomagnetic centered dipole from 1550 AD to 1900 AD. (a) Decrease of dipole moment; (b) slow changes of the tilt of the dipole axis relative to the rotation axis, and (c) longitude variation indicating westward drift of the geomagnetic poles (after Barton, 1989).

century. Less reliable data, enlarged by archeomagnetic results (see Section 5.6.2.1), allow estimates of the secular variation of the dipole axis since the middle of the sixteenth century. The earlier data suggest that in the sixteenth century the dipole axis was tilted at only about 3° to the rotation axis; a gradual increase in tilt took place between the sixteenth and nineteenth centuries. During the last 200 yr the dipole axis has maintained an almost constant tilt of about 11–12° to the rotation axis (Fig. 5.36b).

For the past 400 yr the longitude of the geomagnetic pole has drifted steadily westward (Fig. 5.36c). Before the nineteenth century the pole moved westward at about $0.14°\,yr^{-1}$; this corresponds to a pseudo-period of 2600 yr for a complete circle about the geographic pole. However, since the early nineteenth century the westward motion of the pole has been slower, at an average rate of $0.044°\,yr^{-1}$, which corresponds to a pseudo-period of 8200 yr.

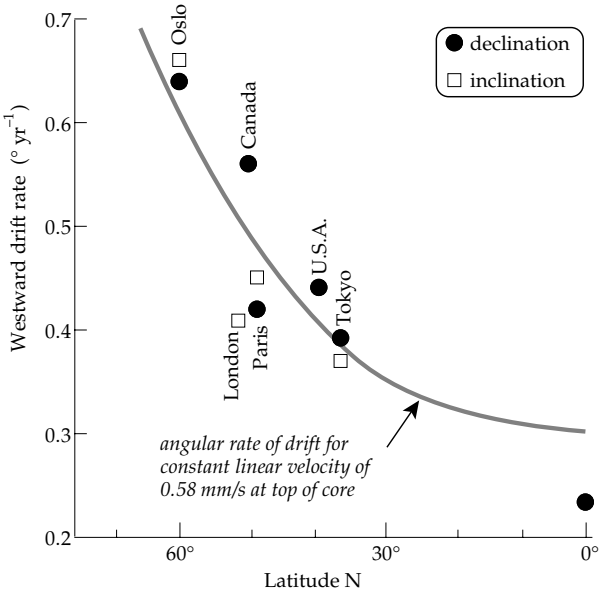

Fig. 5.37 The variation with latitude of average westward drift rates estimated from inclination and declination observations at geomagnetic observatories in the northern hemisphere. The curve gives the angular rotation rate at the surface of the core for a linear velocity of 0.058 cm s^{-1} (after Yukutake, 1967).

5.4.5.2 Secular variation of the non-dipole field

Comparison of maps of the non-dipole field for different epochs (Fig. 5.35) show two types of secular variation. Some anomalies (e.g., over Mongolia, the South Atlantic and North America) appear to be stationary but they change in intensity. Other anomalies (e.g., over Africa) slowly change position with time. The secular variation of the non-dipole field therefore consists of a standing part and a drifting part.

Although some foci may have a north–south component of motion, the most striking feature of the secular variation of the recent non-dipole field is a slow westward drift. This is superposed on the westward drift of the dipole, but can be separated readily by spherical harmonic analysis. The rate of drift of the non-dipole field can be estimated from longitudinal changes in selected features plotted for different epochs. The mean rate of westward drift of the non-dipole field in the first half of the last century has been estimated to be 0.18° yr^{-1}, corresponding to a period of about 2000 yr. However, some foci drift at up to about 0.7° yr^{-1}, much faster than the average rate. Results from several geomagnetic observatories show that the rate of drift is dependent on latitude (Fig. 5.37).

Westward drift is an important factor in theories of the origin of the geomagnetic field. It is considered to be a manifestation of rotation of the outer layers of the core relative to the lower mantle. Theoretical models of the geomagnetic field (discussed in the next section) presume conservation of angular momentum of the fluid core. To maintain the angular momentum of a particle of fluid that moves radially inwards (decreasing the distance from the rotational axis) its angular rate of rotation must speed up. This results in a layered structure for the radial profile of angular rate of rotation relative to the mantle (Fig. 5.38). The outer layers of the core probably rotate more slowly than the solid mantle, imparting a westward drift to features of the magnetic field rooted in the fluid motion.

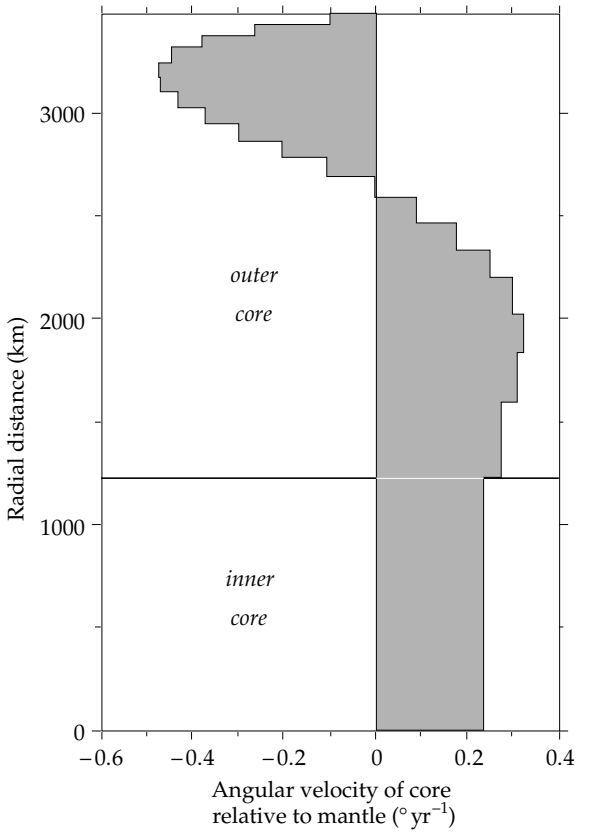

Fig. 5.38 Interpreted velocity distribution (relative to the mantle) for a multi-layered core model in which the change of angular momentum of each layer due to convectional fluid motion is balanced by electromagnetic forces (after Watanabe and Yukutake, 1975).

5.4.6 Origin of the internal field

Analysis of the Gauss coefficients and the wavelengths of features of the non-dipole field indicate that the main field is produced in the fluid outer core of the Earth. The composition of the fluid core has been estimated from seismic and geochemical data. The major constituent is liquid iron, with smaller amounts of other less dense elements. Geochemical analyses of iron meteorites suggest that the core composition may have a few percent of nickel, while shock-wave experiments require 6–10% of non-metallic light elements such as silica, sulfur or oxygen. The solid inner core is inferred from seismic and shock-wave data to consist of almost pure iron.

For the generation of the magnetic field the important parameters of the core are its temperature, viscosity and electrical conductivity. Temperature is known very poorly inside the Earth, but probably exceeds 3000 °C in

the liquid core. The electrical conductivity of iron at 20 °C is $10^7\ \Omega^{-1}\,m^{-1}$ and decreases with increasing temperature. At the high temperatures and pressures in the core the electrical conductivity is estimated to be around $(3–5)\times10^5\ \Omega^{-1}\ m^{-1}$, which corresponds to a good electrical conductor. For comparison, the conductivity of carbon (used for many electrical contacts) is $3\times10^4\ \Omega^{-1}m^{-1}$ at 20 °C.

5.4.6.1 Magnetostatic and electromagnetic models

As observed by Gilbert in 1600, the dipole field of the Earth resembles that of a uniformly magnetized sphere. However, permanent magnetization is an inadequate explanation for the geomagnetic dipole. The mean magnetization of the Earth would need to be many times greater than that of the most strongly magnetic crustal rocks. The Curie point of the most important minerals at atmospheric pressure is less than 700 °C, which is reached at depths of about 25 km so that only a thin outer crustal shell could be permanently magnetized. The necessary magnetization of this shell is even greater than values observed in crustal rocks. Moreover, a magnetostatic origin cannot account for the temporal changes observed in the internal field, such as its secular variation.

The main magnetic field of the Earth is thought to be produced by electrical currents in the conductive core. Although the core is a good conductor, an electrical current system in the core continually loses energy through ohmic dissipation. The lost electrical energy is converted to heat and contributes to the thermal balance of the core. The equations of electromagnetism applied to the core show that an electrical current in the core would decay to zero in around 10,000–20,000 yr unless it is sustained. Paleomagnetic evidence in the form of coherently magnetized rocks supports the existence of a geomagnetic field since Precambrian time, i.e. for about 3 000 Myr. This implies that it must be continuously maintained or regenerated. The driving action for the main field is called the *dynamo process*, by analogy to the production of electrical power in a conductor that rotates in a magnetic field.

5.4.6.2 The geomagnetic dynamo

When a charged particle moves through a magnetic field, it experiences a deflecting electrical field (called the Lorentz field) proportional to the magnetic flux density B and the particle velocity v, and acting in the direction normal to both B and v. The Lorentz field acts as an additional source of electrical current in the core. Its strength is dependent on the velocity of motion of the conducting fluid relative to the magnetic field lines. When this term is included in the Maxwell electromagnetic equations, a *magnetohydrodynamic* equation relating the magnetic field $\mathbf{B}$ to the fluid flow $\mathbf{v}$ and conductivity σ in the core is obtained. It is written

$$\frac{\partial \mathbf{B}}{\partial t} = \frac{1}{\mu_0 \sigma}\nabla^2\mathbf{B} + \nabla\times(\mathbf{v}\times\mathbf{B}) \tag{5.42}$$

This vector equation, although complicated, has immediate consequences. The left side gives the rate of change of magnetic flux in the core; it is determined by two terms on the right side. The first is inversely dependent on the electrical conductivity, and determines the decay of the field in the absence of a driving potential; the better the conductor, the smaller is this *diffusion term*. The second, *dynamo term*, depends on the Lorentz electrical field, which is determined by the velocity field of the fluid motions in the core. The conductivity of the outer core ($(3–5)\times10^5\ \Omega^{-1}\,m^{-1}$) is high and for a fluid velocity of about $1\,mm\,s^{-1}$ the dynamo term greatly exceeds the diffusion term. Under these conditions, the lines of magnetic flux in the core are dragged along by the fluid flow. This concept is called the *frozen-flux theorem*, and it is fundamental to dynamo theory. The diffusion term is only zero if the electrical conductivity is infinite. There is probably some diffusion of the field through the fluid, because it is not a perfect conductor. However, the frozen-flux theorem appears to approximate well the conditions in the fluid outer core.

The derivation of a solution of the dynamo theory is difficult. In addition to Maxwell's equations with the addition of a term for the Lorentz field, the Navier–Stokes equation for the fluid flow, Poisson's equation for the gravitational potential and the generalized equation of heat transfer must be simultaneously satisfied. The fluid flow consists of a radial component and a rotational component. The energy for the radial flow comes from two sources. The slow cooling of the Earth produces a temperature gradient in the core, which results in thermally driven convection in the iron-rich fluid of the outer core. This is augmented by latent heat released at the boundary between the inner and outer cores as the inner core solidifies. The solidification of the pure iron inner core depletes the fluid of the outer core of its heaviest component. The remaining lighter elements rise through the liquid outer core, causing a buoyancy-driven convection.

The rotational component of the fluid flow is the result of a radial velocity gradient in the liquid core, with inner layers rotating faster than outer layers (Fig. 5.38). The relative rotation of the conducting fluid drags magnetic field lines around the rotational axis to form ring-like, *toroidal* configurations. The toroidal field lines are parallel to the flow and therefore to the surface of the core. This means that the toroidal fields are confined to the core and cannot be measured; their strengths and configurations must be estimated from models. Their interactions with the upwelling and descending branches of convective currents create electrical current systems that produce poloidal magnetic fields. These, in their turn, escape from the core and can be measured at the surface of the Earth. The fluid motions are subject to the effects of Coriolis forces, which prove to be strong enough to dominate the resultant flow patterns.

5.4.6.3 Computer simulation of the geodynamo

Important advances in understanding the geomagnetic dynamo (or *geodynamo*) have been made by simulating the related core processes with supercomputers. In 1995, G. A. Glatzmaier and P. H. Roberts presented a numerical model for the generation of a magnetic field assuming a hot convective fluid outer core surrounding a solid inner core, with rotation rate akin to that of the Earth. The heat flow, electrical conductivity and other material properties were made as similar as possible to those of the Earth's core. The simulated dynamo had dominantly dipole character and intensity similar to the Earth's, and it exhibited a westward drift of the non-dipole field comparable to that measured at the Earth's surface. It also reversed polarity spontaneously, with long periods of constant polarity between short polarity transitions, as is the case for the history of geomagnetic reversals in the last 160 Myr (Section 5.7). During a polarity reversal, the field intensity decreased by an order of magnitude, as is also observed in paleomagnetic studies (see Fig. 5.71).

The simulations showed that the ability to reverse polarity was increased when the heat flow across the core–mantle boundary was non-uniform, as in the Earth, showing that thermal conditions in the lower mantle influence the formation of the magnetic field in the fluid core. The solid inner core evidently plays an important role in the reversal process. Magnetic fields in the outer core can change quickly, accompanying convection, and may act to initiate reversals. However, magnetic fields in the solid inner core change more slowly by diffusion and thus the inner core may act to stabilize the field against reversals. A reversal occurs occasionally, on a longer time scale than the core processes.

A prediction of this model is that the magnetic field couples the inner core to the eastward flowing fluid above it, so that the inner core rotates slightly faster than the mantle and crust (Fig. 5.38). There is seismic evidence that this indeed occurs. The solid inner core is seismically anisotropic, with cylindrical symmetry about an axis close to the rotation axis. The axis of symmetry rotates at a rate about 1° faster than that of the mantle and crust.

5.4.7 Magnetic fields of the Sun, Moon and planets

Our knowledge of the magnetic fields of the Sun and planets derives from two types of observation. Indirect observations utilize spectroscopic effects. All atoms emit energy related to the orbital and spin motions. The energy is quantized so that the atom possesses a characteristic spectrum of energy levels. The lowest of these is called the ground state. When an atom happens to have been excited to a higher energy level, it is unstable and eventually returns to the ground state. In the process the energy corresponding to the difference between the elevated and ground states is emitted as light. For example atomic hydrogen gas in the Sun and galaxies emits radiation at 1420 MHz, with corresponding wavelength of 21 cm. This frequency is in the microwave range and can be detected by radio telescopes. If the hydrogen gas is in motion the frequency is shifted by the Doppler effect, from which the velocity of the motion can be deduced.

In the presence of a magnetic field a spectral line can split into several lines. This "hyperfine splitting" is called the *Zeeman effect*. When a hydrogen atom is in the ground state its hyperfine structure has only one line. However, if the atom is in a magnetic field, it acquires additional energy from the interactions between the atom and the magnetic field and hence it can exist in several energy states. As a result the spectral lines of energy emitted by the atom are split into closely spaced lines, representing transitions between the different energy states. The energy differences between these states are dependent on the strength of the magnetic field, which can be estimated from the observations.

Direct observations of extra-terrestrial magnetic fields have been carried out since the 1960s by space probes. Magnetometers mounted in these spacecraft have recorded directly the intensity of the interplanetary magnetic field as well as the magnetic fields around several planets. The manned Apollo missions to the Moon resulted in a large amount of data obtained from the orbiting spacecraft. The materials collected on the Moon's surface and brought back to Earth by the astronauts have provided valuable information about lunar magnetic properties.

5.4.7.1 Magnetic field of the Sun

The Sun has nearly 99.9% of the mass of the solar system. About 99% of this mass is concentrated in a massive central core that reaches out to about 80% of the Sun's radius. The remainder of the Sun consists of an outer conducting shell, which contains only 1% of the Sun's mass but has a thickness equivalent to about 20% of the solar radius. Thermonuclear conversion of hydrogen into helium in the dense core produces temperatures of the order of 15,000,000 K. The visible solar disk is called the *photosphere*. Its diameter is about 2,240,000 km (about 175 times the diameter of the Earth) and its surface temperature is about 6000 K. The lower solar atmosphere is called the *chromosphere*; the outer atmosphere is called the *corona*. The chromosphere includes spike-like emissions of hydrogen gas called solar prominences that sometimes can reach far out into the corona.

The heat from the core is radiated out to the outer conducting shell, where it sets up convection currents. Some of these convection currents are small scale (about 1000 km across) and last only a few minutes; others are larger scale (30,000 km across) and persist for about a (terrestrial) day. The convection is affected by the Sun's rotation and is turbulent.

The rotation of the Sun has been estimated spectroscopically by measuring the Doppler shift of spectral

lines. Independent estimates come from observing the motion of solar features like sunspots, etc. The rotational axis is tilted slightly at 7° to the pole to the ecliptic. Near the Sun's equator the rotational period is about 25 Earth days; the polar regions rotate more slowly with a period of 35–40 days. The Sun's core may rotate more rapidly than the outer regions. Turbulent convection and velocity shear in the outer conducting shell are conducive to a dynamo origin for the Sun's magnetic field. The surface field is dipolar in higher latitudes but has a more complicated pattern in equatorial latitudes.

Temperatures in the outer solar atmosphere (corona) are very high, around 1,000,000 K. The constituent particles achieve velocities in excess of the escape velocity of the Sun's gravitational field. The supersonic stream of mainly protons (H^+ ions), electrons and α-particles (He^{2+} ions) escaping from the Sun forms the solar wind. The flow of electric charge produces an interplanetary magnetic field (IMF) of varying intensity. At the distance of the Earth from the Sun the IMF measures about 6 nT.

Sunspots have been observed since the invention of the telescope (ca. 1610 AD). A sunspot is a dark fleck on the surface of the Sun, measuring roughly 1000 to 100,000 km in diameter. It has a lower temperature than the surrounding photosphere and represents a strong disturbance extending far into the Sun's interior. Sunspots last for several days or weeks and move with the Sun's rotation, providing a means of estimating the rotational speed. The frequency of sunspots changes cyclically with a period of 11 years.

Intense magnetic fields are associated with the sunspots. These often occur in unequally sized pairs of opposite polarity. The predominating magnetic polarity of sunspots changes from one period of maximum sunspot activity to the next, implying that the period is in fact 22 years. The magnetic field of each sunspot is toroidal. It can be imagined to resemble a vortex, or tornado, in which the magnetic field lines leave the solar surface in one sunspot and return to it in the other member of the pair. The polarity of the Sun's dipole field also reverses with the change of polarity of the sunspots, indicating that the features are related.

Associated with the sunspots and their strong magnetic fields are emissions of hydrogen gas, called *solar flares*. The charged particles ejected in the flares contribute to the solar wind, which consequently transfers the sunspot cyclicity to fluctuations in the Earth's magnetic field of external origin and to ancillary terrestrial phenomena such as magnetic storms, brilliant auroras and interference with radio transmissions.

5.4.7.2 Lunar magnetism

Classical hypotheses for the origin of the Moon – rotational fission, capture or binary accretion – have been superseded by the Giant Impact hypothesis. According to this model, the Earth experienced a catastrophic collision with a Mars-sized protoplanet early in its development. Some debris from the collision remained in orbit around the Earth, where it re-accumulated as the Moon about 4.5 Ga ago. This origin accounts for why the Earth and Moon have the same oxygen isotope composition. At the time of the Giant Impact the Earth's mantle and core had already differentiated and dense iron had settled into the core. This may also have taken place in the impactor so the Moon formed from the iron-depleted rocky mantles of the impacting bodies. The Moon has only a small core, whereas if it had originated like the other planets its core would be proportionately larger.

The early Moon was probably covered by an ocean of molten magma at least a hundred kilometers thick, the relicts of which are now the major constituents of the lunar highlands. After cooling and solidification, the lunar surface was bombarded by planetesimals and meteoroids until about 4 Ga ago. The huge craters left by the impacts were later filled by molten basalt to form the lunar maria. Rock samples recovered from the maria in the manned Apollo missions have been dated radiometrically at 3.1–3.9 Ga. The volcanism may have continued after this time but probably ceased about 2.5 Ga ago. Since then the lunar surface has been pulverized by the constant bombardment by meteorites, micrometeorites and elementary particles of the solar wind and cosmic radiation. Except for the lunar highlands the surface is now covered by a layer of shocked debris several meters thick called the lunar *regolith*.

Our knowledge of lunar magnetism derives from magnetic field measurements made from orbiting spacecraft, magnetometers set up on the Moon and rock samples collected from the lunar surface and brought back to Earth. Measurements of the lunar surface field from orbiting spacecraft have been made by on-board magnetometers and by the electron reflection method, the principle of which is basically the same as used to explain the origin of the Van Allen belts in the Earth's magnetosphere (see Section 5.4.3.1). Electrons rain abundantly upon the lunar surface, in part from the solar wind and in part from the charges trapped in the Earth's magnetotail, which is crossed by the monthly orbit of the Moon about the Earth. In the absence of a lunar magnetic field the electrons would be absorbed by the lunar surface. As in the Earth's magnetosphere, an electron incident on the Moon is forced by the Lorentz force to spiral about a magnetic field line (see Fig. 5.30). As the electron approaches the lunar surface the magnetic field strength increases and the pitch of the helix decreases to zero. At the point of closest approach (also called the *mirroring point*) the electron motion is completely rotational about the field line. The electron path then spirals with increasing pitch back along the field line, away from the Moon. The effectiveness of the electron reflection is directional; for a given electron velocity there is a critical angle of incidence below which reflection ceases. By counting the number of electrons with a known energy that are reflected past a

Table 5.2 *Magnetic characteristics of the planets (data source: Van Allen and Bagenal, 1999)*

Planet	Mean orbital radius [AU]	Mean radius of planet [km]	Period of rotation [days]	Magnetic dipole moment [m_E]	Equivalent equatorial magnetic field [nT]	Dipole tilt to rotation axis [°]
Mercury	0.3830	2,440	58.81	0.0007	300	14
Venus	0.7234	6,052	243.7(R)	< 0.0004	< 3	—
Earth	1	6,371	1	1	30,500	10.8
Moon	0.00257	1,738	27.32	—	—	—
Mars	1.520	3,390	1.0275	< 0.0002	< 30	—
Jupiter	5.202	69,910	0.414	20,000	428,000	9.6
Saturn	9.576	58,230	0.444	600	22,000	< 1
Uranus	19.19	25,362	0.720(R)	50	23,000	58.6
Neptune	30.05	24,625	0.671	25	14,000	47

satellite in known directions, the surface field B_s can be estimated from the field B_0 measured at the altitude of the satellite.

The lunar magnetic field was surveyed extensively in 1998 by the *Lunar Prospector* orbiting spacecraft. The measurements show that the Moon currently has no detectable dipole moment. It has only a very weak non-dipolar magnetic field due to local magnetization of crustal rocks. Estimates of surface anomalies suggest that the largest are of the order of 100 nT. From records of meteoritic impacts and moonquakes made by seismometers left on the Moon for several years it has been inferred that, if the Moon has a core (necessary for a lunar dynamo), it must be smaller than 400–500 km in radius, representing less than 2% of the Moon's volume and 1–3% of its mass. In contrast, the Earth's core occupies about 16% of the planet's volume and has about 33% of its mass. Lunar Prospector detected magnetic field changes due to electrical currents induced in the Moon as it traversed the stretched out tail of Earth's magnetosphere. They suggest an even smaller, iron-rich metallic core, with radius 340 ± 90 km (Hood *et al.*, 1999).

Although the Moon now has no global dipole magnetic field, samples of lunar rocks recovered in the manned Apollo missions possessed quite strong natural remanent magnetizations. Rock magnetic studies on Apollo samples with radiometric ages of ~3.6–3.9 Ga suggest that they were magnetized in fields of the order of 10–100 μT (0.1–1 gauss), much stronger than present fields on the Moon. As yet, the ancient lunar magnetic field is not well understood. The interior of the Moon may have acquired a primordial remanent magnetization in the external field of the Sun or Earth. In turn this may have provided the fields for acquisition of the observed crustal magnetizations. The small lunar metallic core is currently solid, and the core heat flux is too low to have powered an internal dynamo at the time of formation of the Apollo samples. However, models suggest that a thin layer of the Moon's mantle adjacent to the core may have first blanketed the core, then later provided enough radioactive heating to assist dynamo activity that persisted for a limited period during a "magnetic era" about 0.5–1.0 Ga after the Moon was formed (Stegman *et al.*, 2003).

5.4.7.3 Extra-terrestrial magnetic exploration

Jupiter and Saturn, like the Earth, have magnetic fields that are strong enough to trap charged particles. The motions of these charged particles generate electromagnetic radiation which is detectable as radio waves far from the planet. The magnetic field of Jupiter was first detected in this way. Moreover, the radio emissions are modulated by the rotation of the planet. Analysis of the periodicity of their modulated radio emissions provides the best estimates of the rotational rates of Jupiter and Saturn.

Most data concerning the magnetic fields of the planets (Table 5.2) have been obtained with flux-gate magnetometers (see Section 5.5.2.1) installed in passing or orbiting spacecraft. When the spacecraft traverses the magnetosphere of a planet, the magnetometer registers the passage through the bow shock and magnetopause (Fig. 5.39). A bow shock results from the supersonic collision of the solar wind with the atmosphere of a planet, just as it does for the Earth (see Fig. 5.28). Counters of energetic particles register a sudden increase in frequency and the magnetometer shows a change in magnetic field strength during passage through the bow shock into the magnetosheath. When the spacecraft leaves the magnetosheath and crosses the magnetopause it enters the region that is shielded from the solar wind by the magnetic field of the planet. The magnetopause is where the kinetic energy of the plasma is equal to the potential energy of the planetary magnetic field. The existence of a bow shock may be regarded as evidence for a planetary atmosphere, while the magnetopause is evidence that the planet has a magnetic field.

5.4.7.4 The magnetic fields of the planets

Mercury was visited by the *Mariner 10* spacecraft, which made three passes of the planet in 1974 and 1975. The

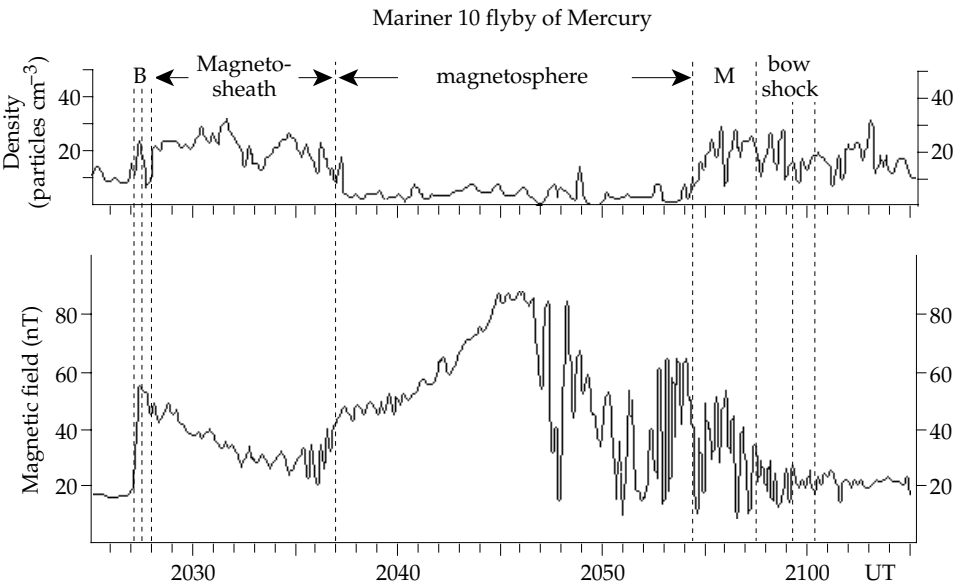

Fig. 5.39 Changes with time of particle density and magnetic field along the path of the Mariner 10 spacecraft during its flight past the planet Mercury (data from Ogilvie *et al.*, 1977).

on-board magnetometer detected a bow shock and a magnetopause (Fig. 5.39), which imply that the planet has a magnetic field. On the first encounter a magnetic field of about 100 nT was measured at an altitude of 700 km (radial distance of 3100 km), which was the point of closest approach. In estimating the magnetic field of the planet compensation must be made for the magnetic field of the solar wind. Different models have given estimates of the strength of the dipole moment in the range $(2–7)\times10^{-4}$ of the Earth's magnetic moment ($m_E \approx 7.7674\times10^{22}$ A m^2 in 2005), which would give a surface equatorial magnetic field of about 100–400 nT. The source of the magnetic field is uncertain. It is possible, but unlikely, that Mercury has a global magnetic moment due to crustal remanent magnetization; it would be difficult to explain the uniformity and duration of the external field needed to produce this. Mercury is believed to have a large iron core with a radius of about 1800 km, proportionately larger than Earth's. Probably part of this core is molten, so it is possible that Mercury has a small active internal dynamo. This would however be unlike Earth's. It might be of thermoelectric origin, or it could be due to dynamo processes in a thin shell-like liquid outer core surrounding a solid inner core.

Venus was investigated by several American and Russian spacecraft in the 1960s. The instruments on *Mariner 5* in 1967 clearly detected a bow shock from the collision of the solar wind with the planetary atmosphere. Magnetometer data from later spacecraft found no evidence for a planetary magnetic field. If a magnetopause exists, it must lie very close to the planet and may wrap around it. Data from the *Pioneer* Venus orbiter in 1978 set an upper limit of $10^{-5}\,m_E$ for a planetary dipole moment, which would give a surface equatorial field of less than 1 nT. The absence of a detectable magnetic field was not expected. As shown by Eq. (5.37) the dipole magnetic moment is proportional to the equatorial field times the cube of the planetary radius. The strength of a dynamo field is expected to be proportional to the core radius and to the rotation rate. These considerations give a scaling law whereby the dipole magnetic moment of a planet is proportional to its rotation rate and the fourth power of the core radius. The rotation of the planet is very slow compared to that of the Earth; one sidereal day on Venus lasts 243 Earth days, but the size of the planet is close to that of the Earth. It was therefore expected that Venus might have an internal dynamo with a dipole moment about 0.2% that of the Earth and an equatorial surface field of about 86 nT. It seems likely that the slow rotation does not provide enough energy for an active dynamo.

Mars was expected to have a magnetic moment between that of Earth and Mercury, because of its size and rotation rate. *Mariner 4* in 1965 was the first American spacecraft carrying magnetometers to visit Mars; it detected a bow shock but no conclusive evidence for a magnetopause. In September 1997, the *Mars Global Surveyor* spacecraft entered orbit around the planet. Since 1999 it has mapped the Martian magnetic field from an almost circular orbit about 400 ± 30 km above the planet's surface. The survey measurements have nearly uniform global coverage and show that there is no significant global magnetic field at present. This does not exclude the possible existence of a dynamo-generated global field in the planet's distant past. The measured magnetic field consists of large regional magnetic anomalies, which are attributed to remanent magnetization of the Martian crust. At the survey altitude the crustal magnetic anomalies have amplitudes up to 220 nT, an order of magnitude larger than the crustal anomalies of Earth at that altitude, which attests to the presence of strongly magnetic minerals in the Martian crust. The crustal magnetic field shows some features with circular geometry, some of which may be related to impact processes. However, the most striking anomalies are prominent

east–west trending linear features over a region in the planet's southern hemisphere. These sub-parallel lineations are attributed to alternating bands of strongly magnetized crust. It is tempting to interpret their origin in the same way as the generation of oceanic magnetic lineations on Earth by a plate tectonic process in the presence of a reversing field. However, as yet the origin of the magnetic anomalies on Mars is not understood.

Jupiter has been known since 1955 to possess a strong magnetic field, because of the polarized radio emissions associated with it. The spacecraft *Pioneer 10* and *11* in 1973–4 and *Voyager 1* and *2* in 1979 established that the planet has a bow shock and magnetopause. From 1995 to 2003 the spacecraft *Galileo* made extensive surveys of Jupiter's magnetosphere. The huge magnetosphere encounters the solar wind about 5,000,000 km "upwind" from the planet; its magnetotail may extend all the way to Saturn. Two reasons account for the great size of the magnetosphere compared to that of Earth. First, the solar wind pressure on the Jovian atmosphere is weaker due to the greater distance from the Sun; secondly, Jupiter's magnetic field is much stronger than that of the Earth. The dipole moment is almost $20{,}000m_E$ which gives a powerful equatorial magnetic field of more than 400,000 nT at Jupiter's surface. The quadrupole and octupole parts of the non-dipole magnetic field have been found to be proportionately much larger relative to the dipole field than on Earth. The dipole axis is tilted at 9.7° to the rotation axis, and is also displaced from it by 10% of Jupiter's equatorial radius. The magnetic field of Jupiter results from an active dynamo in the metallic hydrogen core of the planet. The core is probably very large, with a radius up to 75% of the planet's radius. This would explain the high harmonic content of the magnetic field near the planet.

Saturn was reached by *Pioneer 11* in 1979 and the *Voyager 1* and *2* spacecraft in 1980 and 1981, respectively. The on-board magnetometers detected a bow shock and a magnetopause. In 2004 the *Cassini–Huygens* spacecraft entered into orbit around Saturn. In 2005 the Huygens lander descended to the surface of Saturn's largest moon *Titan* while Cassini continued to orbit and measure the parent planet's properties. Saturn's dipole magnetic moment is smaller than expected, but is estimated to be around $500m_E$. This gives an equatorial field of 55,000 nT, almost double that of Earth. The magnetic field has a purer dipole character (i.e., the non-dipole components are weaker) than the fields of Jupiter or Earth. The simplest explanation for this is that the field is generated by an active dynamo in a conducting core that is smaller relative to the size of the planet. The axis of the dipole magnetic field lies only about 1° away from the rotation axis, in contrast to 11.4° on Earth and 9.7° on Jupiter.

Uranus is unusual in that its spin axis has an obliquity of 97.9°. This means that the rotation axis lies very close to the ecliptic plane, and the orbital planes of its satellites are almost orthogonal to the ecliptic plane. Uranus was visited by *Voyager 2* in January 1986. The spacecraft encountered a bow shock and magnetopause and subsequently entered the magnetosphere of the planet, which extends for 18 planetary radii (460,000 km) towards the Sun. Uranus has a dipole moment about 50 times stronger than Earth's, giving a surface field of 24,000 nT, comparable to that on Earth. Intriguingly, the axis of the dipole field has a large tilt of about 60° to the rotation axis; there is no explanation for this tilt. Another oddity is that the magnetic field is not centered on the center of the planet, but is displaced by 30% of the planet's radius along the tilted rotation axis. The quadrupole component of the field is relatively large compared to the dipole. It is therefore supposed that the magnetic field of Uranus is generated at shallow depths within the planet.

Neptune, visited by *Voyager 2* in 1989, has a magnetic field with similar characteristics to that of Uranus. It is tilted at 49° to the rotation axis and is offset from the planetary center by 55% of Neptune's radius. As in the case of Uranus, the magnetic field has a large quadrupole term compared to the dipole and thus probably originates in the outer layers of the planet, rather than in the deep interior.

It is not yet known whether **Pluto** has a magnetic field. The planet is probably too small to have a magnetic field sustained by dynamo action.

There is reasonable confidence that Mercury, Earth, Jupiter, Saturn, and Uranus have active planetary dynamos today. The magnetic data for Mars and Neptune are inconclusive. All available data indicate that Venus and the Moon do not have active dynamos now, but possibly each might have had one earlier in its history.

5.5 MAGNETIC SURVEYING

5.5.1 The magnetization of the Earth's crust

The high-order terms in the energy density spectrum of the geomagnetic field (Fig. 5.33) are related to the magnetization of crustal rocks. Magnetic investigations can therefore yield important data about geological structures. By analogy with gravity anomalies we define a magnetic anomaly as the difference between the measured (and suitably corrected) magnetic field of the Earth and that which would be expected from the International Geomagnetic Reference Field (Section 5.4.4). The magnetic anomaly results from the contrast in magnetization when rocks with different magnetic properties are adjacent to each other, as, for example, when a strongly magnetic basaltic dike intrudes a less magnetic host rock. The stray magnetic fields surrounding the dike disturb the geomagnetic field locally and can be measured with sensitive instruments called magnetometers.

As discussed in Section 5.3.1, each grain of mineral in a rock can be classified as having diamagnetic, paramagnetic or ferromagnetic properties. When the rock is in a magnetic field, the alignment of magnetic moments by the field produces an induced magnetization ($\mathbf{M}_i$)

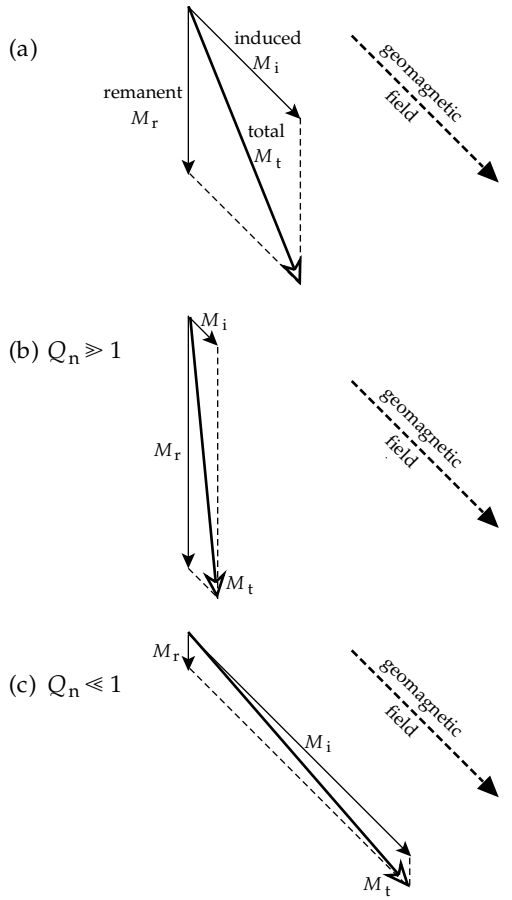

Fig. 5.40 The remanent (M_r), induced (M_i), and total (M_t) magnetizations in a rock. (a) For an arbitrary case M_t lies between M_i and M_r, (b) for a very large Königsberger ratio ($Q_n \gg 1$) M_t is close to M_r, and (c) for a very small Königsberger ratio ($Q_n \ll 1$) M_t is almost the same as M_i.

proportional to the field, the proportionality constant being the magnetic susceptibility, which can have a wide range of values in rocks (see Fig. 5.13). The geomagnetic field is able to produce a correspondingly wide range of induced magnetizations in ordinary crustal rocks. The direction of the induced magnetization is parallel to the Earth's magnetic field in the rock.

Each rock usually contains a tiny quantity of ferromagnetic minerals. As we have seen, these grains can become magnetized permanently during the formation of the rock or by a later mechanism. The remanent magnetization ($\mathbf{M}_r$) of the rock is not related to the present-day geomagnetic field, but is related to the Earth's magnetic field in the geological past. Its direction is usually different from that of the present-day field. As a result the directions of $\mathbf{M}_r$ and $\mathbf{M}_i$ are generally not parallel. The direction of $\mathbf{M}_i$ is the same as that of the present field but the direction of $\mathbf{M}_r$ is often not known unless it can be measured in rock samples.

The total magnetization of a rock is the sum of the remanent and induced magnetizations. As these have different directions they must be combined as vectors (Fig. 5.40a). The direction of the resultant magnetization of the rock is not parallel to the geomagnetic field. If the intensities of $\mathbf{M}_r$ and $\mathbf{M}_i$ are similar, it is difficult to interpret the total magnetization. Fortunately, in many important situations $\mathbf{M}_r$ and $\mathbf{M}_i$ are sufficiently different to permit some simplifying assumptions. The relative importance of the remanent and induced parts of the magnetization is expressed in the *Königsberger ratio* (Q_n), defined as the ratio of the intensity of the remanent magnetization to that of the induced magnetization (i.e., $Q_n = M_r/M_i$).

Two situations are of particular interest. The first is when Q_n is very large (i.e., $Q_n \gg 1$). In this case (Fig. 5.40b), the total magnetization is dominated by the remanent component and its direction is essentially parallel to $\mathbf{M}_r$. Oceanic basalts, formed by extrusion and rapid underwater cooling at oceanic ridges, are an example of rocks with high Q_n ratios. Due to the rapid quenching of the molten lava, titanomagnetite grains form with skeletal structures and very fine grain sizes. The oceanic basalts carry a strong thermoremanent magnetization and often have Q_n values of 100 or greater. This facilitates the interpretation of oceanic magnetic anomalies, because in many cases the induced component can be neglected and the crustal magnetization can be interpreted as if it were entirely remanent.

The other important situation is when Q_n is very small (i.e., $Q_n \ll 1$). This requires the remanent magnetization to be negligible in comparison to the induced magnetization. For example, coarse grained magnetite grains carry multidomain magnetizations (Section 5.3.5.3). The domain walls are easily moved around by a magnetic field. The susceptibility is high and the Earth's magnetic field can induce a strong magnetization. Any remanent magnetization is usually weak, because it has been subdivided into antiparallel domains. These two factors yield a low value for Q_n. Magnetic investigations of continental crustal rocks for commercial exploitation (e.g., in ancient shield areas) can often be interpreted as cases with $Q_n \ll 1$. The magnetization can then be assumed to be entirely induced (Fig. 5.40c) and oriented parallel to the direction of the present-day geomagnetic field at the measurement site, which is usually known. This makes it easier to design a model to interpret the feature responsible for the magnetic anomaly.

5.5.2 Magnetometers

The instrument used to measure magnetic fields is called a magnetometer. Until the 1940s magnetometers were mechanical instruments that balanced the torque of the magnetic field on a finely balanced compass needle against a restoring force provided by gravity or by the torsion in a suspension fiber. The balance types were cumbersome, delicate and slow to operate. For optimum sensitivity they were designed to measure changes in a selected component of the magnetic field, most commonly the vertical field. This type of magnetometer has now been superseded by more sensitive, robust electronic instruments. The most important of these are the flux-gate, proton-precession and optically pumped magnetometers.

5.5.2.1 The flux-gate magnetometer

Some special nickel–iron alloys have very high magnetic susceptibility and very low remanent magnetization. Common examples are *Permalloy* (78.5% Ni, 21.5% Fe) and *Mumetal* (77% Ni, 16% Fe, 5% Cu, 2% Cr). The preparation of these alloys involves annealing at very high temperature (1100–1200 °C) to remove lattice defects around which internal stress could produce magnetostrictive energy. After this treatment the coercivity of the alloy is very low (i.e., its magnetization can be changed by a very weak field) and its susceptibility is so high that the Earth's field can induce a magnetization in it that is a considerable proportion of the saturation value.

The sensor of a flux-gate magnetometer consists of two parallel strips of the special alloy (Fig. 5.41a). They are wound in opposite directions with primary energizing coils. When a current flows in the primary coils, the parallel strips become magnetized in opposite directions. A secondary coil wound about the primary pair detects the change in magnetic flux in the cores (Fig. 5.41b), which is zero as soon as the cores saturate. While the primary current is rising or falling, the magnetic flux in each strip changes and a voltage is induced in the secondary coil. If there is no external magnetic field, the signals due to the changing flux are equal and opposite and no output signal is recorded. When the axis of the sensor is aligned with the Earth's magnetic field, the latter is added to the primary field in one strip and subtracted from it in the other. The phases of the magnetic flux in the alloy strips are now different; one saturates before the other. The flux changes in the two alloy strips are no longer equal and opposite. An output voltage is produced in the secondary coil that is proportional to the strength of the component of the Earth's magnetic field along the axis of the sensor.

The flux-gate magnetometer is a *vector magnetometer*, because it measures the strength of the magnetic field in a particular direction, namely along the axis of the sensor. This requires that the sensor be accurately oriented along the direction of the field component to be measured. For total field measurements three sensors are employed. These are fixed at right angles to each other and connected with a feedback system which rotates the entire unit so that two of the sensors detect zero field. The magnetic field to be measured is then aligned with the axis of the third sensor.

The flux-gate magnetometer does not yield absolute field values. The output is a voltage, which must be calibrated in terms of magnetic field. However, the instrument provides a continuous record of field strength. Its sensitivity of about 1 nT makes it capable of measuring most magnetic anomalies of geophysical interest. It is robust and adaptable to being mounted in an airplane, or towed behind it. The instrument was developed during World War II as a submarine detector. After the war it was used extensively in airborne magnetic surveying.

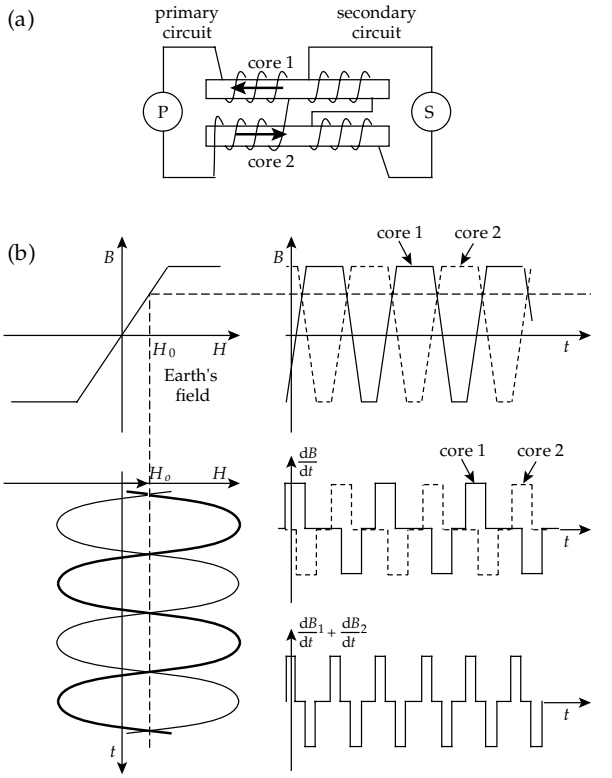

Fig. 5.41 Simplified principle of the flux-gate magnetometer. (a) Primary and secondary electrical circuits include coils wrapped around parallel strips of *Mumetal* in opposite and similar senses, respectively. (b) The output signal in a magnetic field is proportional to the net rate of change of magnetic flux in the *Mumetal* strips (after Militzer *et al.*, 1984).

5.5.2.2 The proton-precession magnetometer

Since World War II sensitive magnetometers have been designed around quantum-mechanical properties. The proton-precession magnetometer depends on the fact that the nucleus of the hydrogen atom, a proton, has a magnetic moment proportional to the angular momentum of its spin. Because the angular momentum is quantized, the proton magnetic moment can only have specified values, which are multiples of a fundamental unit called the nuclear magneton. The situation is analogous to the quantization of magnetic moment associated with electron spin, for which the fundamental unit is the Bohr magneton. The ratio of the magnetic moment to the spin angular momentum is called the *gyromagnetic ratio* (γ_p) of the proton. It is an accurately known fundamental constant with the value $\gamma_p = 2.675\,13 \times 10^8\ s^{-1}\ T^{-1}$.

The proton-precession magnetometer is simple and robust in design. The sensor of the instrument consists of a flask containing a proton-rich liquid, such as water. Around the flask are wound a magnetizing solenoid and a detector coil (Fig. 5.42); some designs use the same solenoid alternately for magnetizing and detection. When the current in the magnetizing solenoid is switched on, it creates a magnetic field of the order of 10 mT, which is about 200 times stronger than the Earth's field. The

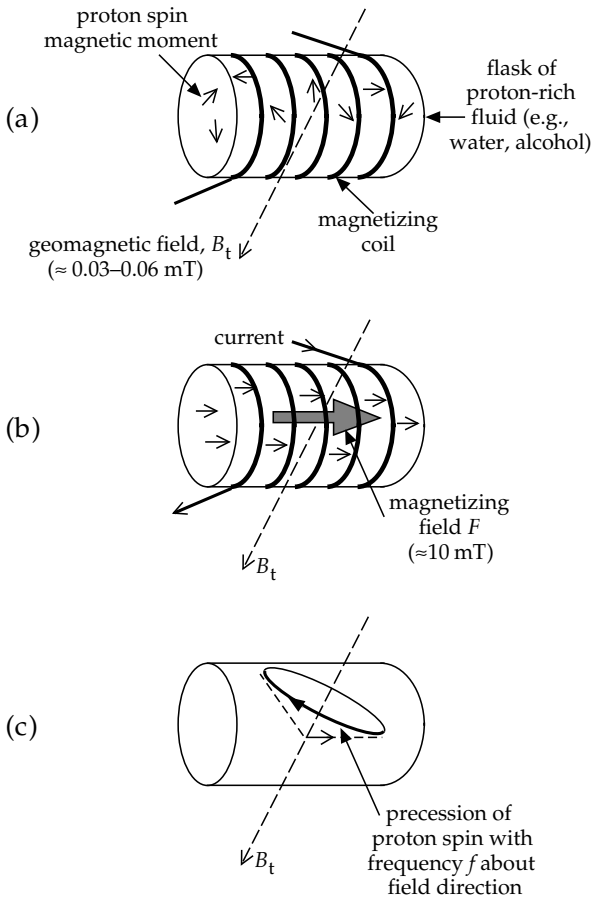

Fig. 5.42 (a) The elements of a proton-precession magnetometer. (b) Current in the magnetizing coil produces a strong field F that aligns the magnetic moments ("spins") of the protons. (c) When the field F is switched off, the proton spins precess about the geomagnetic field B_t, inducing an alternating current in the coil with the Larmor precessional frequency f.

magnetizing field aligns the magnetic moments of the protons along the axis of the solenoid, which is oriented approximately east–west at right angles to the Earth's field. After the magnetizing field is interrupted, the magnetic moments of the proton spins react to the couple exerted on them by the Earth's magnetic field. Like a child's top spinning in the field of gravity, the proton magnetic moments precess about the direction of the ambient magnetic field. They do so at a rate known as the *Larmor precessional frequency*. The motion of the magnetic moments induces a signal in the detector coil. The induced signal is amplified electronically and the precessional frequency is accurately measured by counting cycles for a few seconds. The strength B_t of the measured magnetic field is directly proportional to the *frequency* of the signal (f), and is given by

$$B_t = \frac{2\pi}{\gamma_p} f \tag{5.43}$$

The intensity of the Earth's magnetic field is in the range 30,000–60,000 nT. The corresponding precessional frequency is approximately 1250–2500 Hz, which is in the audio-frequency range. Accurate measurement of the signal frequency gives an instrumental sensitivity of about 1 nT, but requires a few seconds of observation. Although it gives an absolute value of the field, the proton-precession magnetometer does not give a continuous record. Its portability and simplicity give it advantages for field use.

The flux-gate and proton-precession magnetometers are widely used in magnetic surveying. The two instruments have comparable sensitivities of 0.1–1 nT. In contrast to the flux-gate instrument, which measures the component of the field along its axis, the proton-precession magnetometer cannot measure field components; it is a total-field magnetometer. The total field $\mathbf{B}_t$ is the vector sum of the Earth's magnetic field $\mathbf{B}_E$ and the stray magnetic field $\Delta\mathbf{B}$ of, say, an orebody. Generally, $\Delta B \ll B_E$, so that the direction of the total field does not deviate far from the Earth's field. In some applications it is often adequate to regard the measured total field anomaly as the projection of $\Delta\mathbf{B}$ along the Earth's field direction.

5.5.2.3 The absorption-cell magnetometer

The absorption-cell magnetometer is also referred to as the alkali-vapor or optically pumped magnetometer. The principle of its operation is based on the quantum-mechanical model of the atom. According to their quantum numbers the electrons of an atom occupy concentric shells about the nucleus with different energy levels. The lowest energy level of an electron is its ground state. The magnetic moment associated with the spin of an electron can be either parallel or antiparallel to an external magnetic field. The energy of the electron is different in each case. This results in the ground state splitting into two sublevels with slightly different energies. The energy difference is proportional to the strength of the magnetic field. The splitting of energy levels in the presence of a magnetic field is called the *Zeeman effect*.

Absorption-cell magnetometers utilize the Zeeman effect in vapors of alkali elements such as rubidium or cesium, which have only a single valence electron in the outermost energy shell. Consider the schematic representation of an alkali-vapor magnetometer in Fig. 5.43. A polarized light-beam is passed through an absorption cell containing rubidium or cesium vapor and falls on a photoelectric cell, which measures the intensity of the light-beam. In the presence of a magnetic field the ground state of the rubidium or cesium is split into two sublevels, G_1 and G_2. If the exact amount of energy is added to the vapor, the electrons may be raised from their ground state to a higher-energy level, H. Suppose that we irradiate the cell with light from which we have filtered out the spectral line corresponding to the energy needed for the transition G_2H. The energy for the transition G_1H has not been removed, so the electrons in ground state G_1 will receive energy that excites them to level H, whereas those in ground state G_2 will remain in this state. The energy for these transitions comes from the incident light-beam, which is absorbed in the cell. In due

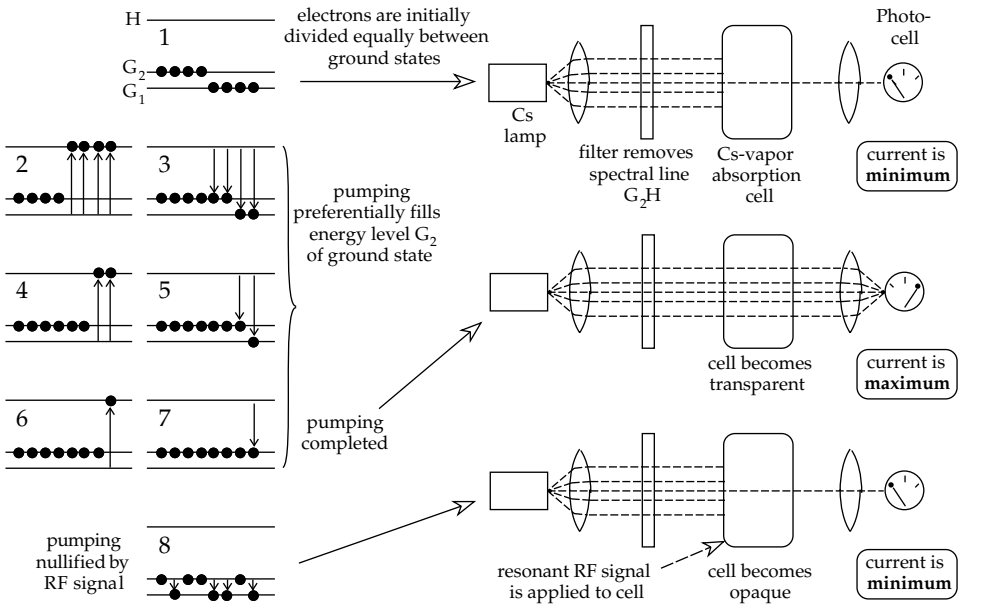

Fig. 5.43 The principle of operation of the optically pumped magnetometer (after Telford *et al.*, 1990).

course, the excited electrons will fall back to one of the more stable ground states. If an electron in excited state H falls back to sublevel G_1 it will be re-excited into level H; but if it falls back to sublevel G_2 it will remain there. In time, this process – called "optical pumping" – will empty sublevel G_1 and fill level G_2. At this stage no more energy can be absorbed from the polarized light-beam and the absorption cell becomes transparent. If we now supply electromagnetic energy to the system in the form of a radio-frequency signal with just the right amount of energy to permit transitions between the populated G_2 and unpopulated G_1 ground sublevels, the balance will be disturbed. The optical pumping will start up again and will continue until the electrons have been expelled from the G_1 level. During this time energy is absorbed from the light-beam and it ceases to be transparent.

In the rubidium-vapor and cesium-vapor magnetometers a polarized light-beam is shone at approximately 45° to the magnetic field direction. In the presence of the Earth's magnetic field the electrons precess about the field direction at the Larmor precessional frequency. At one part of the precessional cycle an electron spin is almost parallel to the field direction, and one half-cycle later it is nearly antiparallel. The varying absorption causes a fluctuation of intensity of the light-beam at the Larmor frequency. This is detected by the photocell and converted to an alternating current. By means of a feedback circuit the signal is supplied to a coil around the container of rubidium gas and a radio-frequency resonant circuit is created. The ambient geomagnetic field B_t that causes the splitting of the ground state is proportional to the Larmor frequency, and is given by

$$B_t = \frac{2\pi}{\gamma_e} f \tag{5.44}$$

Here, γ_e is the gyromagnetic ratio of the electron, which is known with an accuracy of about 1 part in 10^7. It is about 1800 times larger than γ_p, the gyromagnetic ratio of the proton. The precessional frequency is correspondingly higher and easier to measure precisely. The sensitivity of an optically pumped magnetometer is very high, about 0.01 nT, which is an order of magnitude more sensitive than the flux-gate or proton-precession magnetometer.

5.5.3 Magnetic surveying

The purpose of magnetic surveying is to identify and describe regions of the Earth's crust that have unusual (anomalous) magnetizations. In the realm of applied geophysics the anomalous magnetizations might be associated with local mineralization that is potentially of commercial interest, or they could be due to subsurface structures that have a bearing on the location of oil deposits. In global geophysics, magnetic surveying over oceanic ridges provided vital clues that led to the theory of plate tectonics and revealed the polarity history of the Earth's magnetic field since the Early Jurassic.

Magnetic surveying consists of (1) measuring the terrestrial magnetic field at predetermined points, (2) correcting the measurements for known changes, and (3) comparing the resultant value of the field with the expected value at each measurement station. The expected value of the field at any place is taken to be that of the International Geomagnetic Reference Field (IGRF), described in Section 5.4.4. The difference between the observed and expected values is a *magnetic anomaly*.

5.5.3.1 Measurement methods

The surveying of magnetic anomalies can be carried out on land, at sea and in the air. In a simple land survey an operator might use a portable magnetometer to measure the field at the surface of the Earth at selected points that

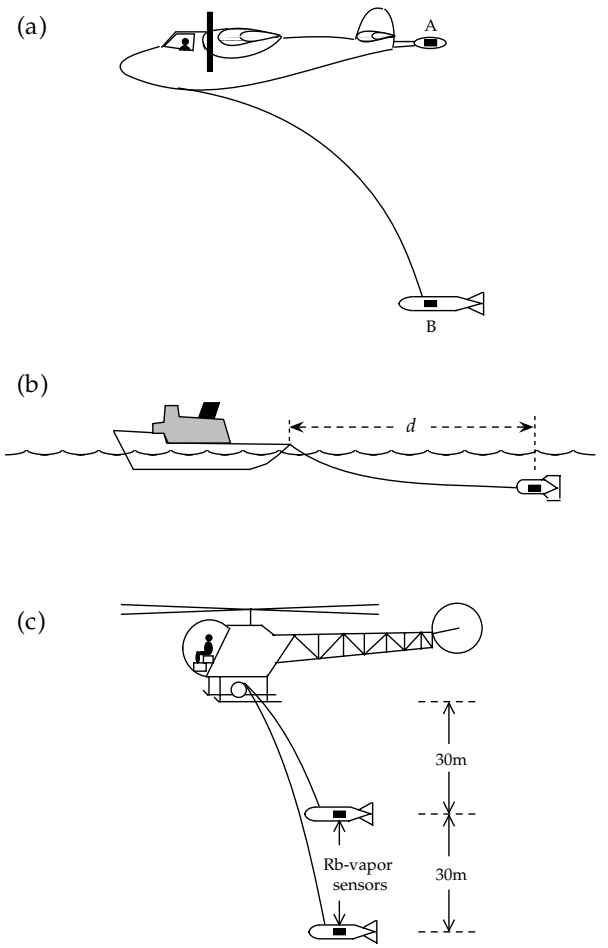

Fig. 5.44 (a) In airborne magnetic surveying the magnetometer may be mounted rigidly on the airplane at the end of a boom (A), or towed in an aerodynamic housing behind the plane (B). (b) In marine studies the magnetometer must be towed some distance *d* behind the ship to escape its magnetic field. (c) A pair of sensitive magnetometers in the same vertical plane act as a magnetic gradiometer (after Slack *et al.*, 1967).

form a grid over a suspected geological structure. This method is slow but it yields a detailed pattern of the magnetic field anomaly over the structure, because the measurements are made close to the source of the anomaly.

In practice, the surveying of magnetic anomalies is most efficiently carried out from an aircraft. The magnetometer must be removed as far as possible from the magnetic environment of the aircraft. This may be achieved by mounting the instrument on a fixed boom, A, several meters long (Fig. 5.44a). Alternatively, the device may be towed behind the aircraft in an aerodynamic housing, B, at the end of a cable 30–150 m long. The "bird" containing the magnetometer then flies behind and below the aircraft. The flight environment is comparatively stable. Airborne magnetometers generally have higher sensitivity (≈0.01 nT) than those used in ground-based surveying (sensitivity ≈1 nT). This compensates for the loss in resolution due to the increased distance between the magnetometer and the source of the anomaly. Airborne magnetic surveying is an economical way to reconnoitre a large territory in a short time. It has become a routine part of the initial phases of the geophysical exploration of an uncharted territory.

The magnetic field over the oceans may also be surveyed from the air. However, most of the marine magnetic record has been obtained by shipborne surveying. In the marine application a proton-precession magnetometer mounted in a waterproof "fish" is towed behind the ship at the end of a long cable (Fig. 5.44b). Considering that most research vessels consist of several hundred to several thousand tons of steel, the ship causes a large magnetic disturbance. For example, a research ship of about 1000 tons deadweight causes an anomaly of about 10 nT at a distance of 150 m. To minimize the disturbance of the ship the tow-cable must be about 100–300 m in length. At this distance the "fish" in fact "swims" well below the water surface. Its depth is dependent on the length of the tow-cable and the speed of the ship. At a typical survey speed of 10 km h^{-1} its operational depth is about 10–20 m.

5.5.3.2 Magnetic gradiometers

The magnetic gradiometer consists of a pair of alkali-vapor magnetometers maintained at a fixed distance from each other. In ground-based surveying the instruments are mounted at opposite ends of a rigid vertical bar. In airborne usage two magnetometers are flown at a vertical spacing of about 30 m (Fig. 5.44c). The difference in outputs of the two instruments is recorded. If no anomalous body is present, both magnetometers register the Earth's field equally strongly and the difference in output signals is zero. If a magnetic contrast is present in the subsurface rocks, the magnetometer closest to the structure will detect a stronger signal than the more remote instrument, and there will be a difference in the combined output signals.

The gradiometer emphasizes anomalies from local shallow sources at the expense of large-scale regional variation due to deep-seated sources. Moreover, because the gradiometer registers the *difference* in signals from the individual magnetometers, there is no need to compensate the measurements for diurnal variation, which affects each individual magnetometer equally. Proton-precession magnetometers are most commonly used in ground-based magnetic gradiometers, while optically pumped magnetometers are favored in airborne gradiometers.

5.5.3.3 The survey pattern

In a systematic regional airborne (or marine) magnetic survey the measurements are usually made according to a predetermined pattern. In surveys made with fixed-wing aircraft the survey is usually flown at a constant flight elevation above sea-level (Fig. 5.45a). This is the procedure favored for regional or national surveys, or for the investigation of areas with dramatic topographic relief. The survey focuses on the depth to the magnetic basement, which often underlies less magnetic sedimentary surface

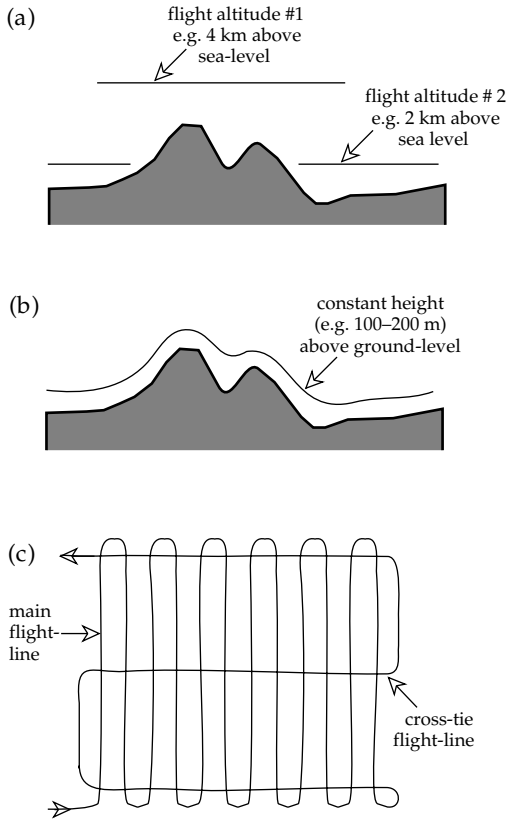

Fig. 5.45 In airborne magnetic surveying the flight-lines may be flown at (a) constant altitude above sea-level, or (b) constant height above ground-level. The flight pattern (c) includes parallel measurement lines and orthogonal cross-tie lines.

rocks at considerable depth. In regions that are flat or that do not have dramatic topography, it may be possible to fly a survey at low altitude, as close as possible to the magnetic sources. This method would be suitable over ancient shield areas, where the goal of the survey is to detect local mineralizations with potential commercial value. If a helicopter is being employed, the distance from the magnetic sources may be kept as small as possible by flying at a constant height above the ground surface (Fig. 5.45b).

The usual method is to survey a region along parallel flight-lines (Fig. 5.45c), which may be spaced anywhere from 100 m to a few kilometers apart, depending on the flight elevation used, the intensity of coverage, and the quality of detail desired. The orientation of the flight-lines is selected to be more or less normal to the trend of suspected or known subsurface features. Additional tie-lines are flown at right angles to the main pattern. Their separation is about 5–6 times that of the main flight-lines. The repeatability of the measurements at the intersections of the tie-lines and the main flight-lines provides a check on the reliability of the survey. If the differences (called closure errors) are large, an area may need to be re-surveyed. Alternatively, the differences may be distributed mathematically among all the observations until the closure errors are minimum.

5.5.4 Reduction of magnetic field measurements

In comparison to the reduction of gravity data, magnetic survey data require very few corrections. One effect that must be compensated is the variation in intensity of the geomagnetic field at the Earth's surface during the course of a day. As explained in more detail in Section 5.4.3.3 this *diurnal variation* is due to the part of the Earth's magnetic field that originates in the ionosphere. At any point on the Earth's surface the external field varies during the day as the Earth rotates beneath different parts of the ionosphere. The effect is much greater than the precision with which the field can be measured. The diurnal variation may be corrected by installing a constantly recording magnetometer at a fixed base station within the survey area. Alternatively, the records from a geomagnetic observatory may be used, provided it is not too far from the survey area. The time is noted at which each field measurement is made during the actual survey and the appropriate correction is made from the control record.

The variations of magnetic field with *altitude*, *latitude* and *longitude* are dominated by the vertical and horizontal variations of the dipole field. The total intensity B_t of the field is obtained by computing the resultant of the radial component B_r (Eq. (5.38)) and the tangential component B_θ (Eq. (5.39)):

$$B_t = \sqrt{B_r^2 + B_\theta^2} = \frac{\mu_0 m}{4\pi} \frac{\sqrt{1 + 3\cos^2\theta}}{r^3} \tag{5.45}$$

The *altitude* correction is given by the vertical gradient of the magnetic field, obtained by differentiating the intensity B_t with respect to radius, r. This gives

$$\frac{\partial B_t}{\partial r} = -3\frac{\mu_0 m}{4\pi} \frac{\sqrt{1 + 3\cos^2\theta}}{r^4} = -\frac{3}{r} B_t \tag{5.46}$$

The vertical gradient of the field is found by substituting $r = R = 6371$ km and an appropriate value for B_t. It clearly depends on the latitude of the measurement site. At the magnetic equator ($B_t \approx 30{,}000$ nT) the altitude correction is about 0.015 nT m^{-1}; near the magnetic poles ($B_t \approx 60{,}000$ nT) it is about 0.030 nT m^{-1}. The correction is so small that it is often ignored.

In regional studies the corrections for *latitude* and *longitude* are inherent in the reference field that is subtracted. In a survey of a small region, the latitude correction is given by the north–south horizontal gradient of the magnetic field, obtained by differentiating B_t with respect to polar angle, θ. This gives for the northward increase in B_t (i.e., with increasing latitude)

$$-\frac{1}{r}\frac{\partial B_t}{\partial \theta} = \frac{\mu_0 m}{4\pi} \frac{1}{r^4} \frac{\partial}{\partial \theta} \sqrt{1 + 3\cos^2\theta} = \frac{3B_t \sin\theta \cos\theta}{r(1 + 3\cos^2\theta)} \tag{5.47}$$

The latitude correction is zero at the magnetic pole ($\theta = 0°$) and magnetic equator ($\theta = 90°$) and reaches a maximum value of about 5 nT per *kilometer* (0.005 nT m^{-1}) at intermediate latitudes. It is insignificant in small-scale surveys.

In some land-based surveys of highly magnetic terrains (e.g., over lava flows or mineralized intrusions), the disturbing effect of the magnetized topography may be serious enough to require additional topographic corrections.

5.5.5 Magnetic anomalies

The gravity anomaly of a body is caused by the density contrast ($\Delta\rho$) between the body and its surroundings. The shape of the anomaly is determined by the shape of the body and its depth of burial. Similarly, a magnetic anomaly originates in the magnetization contrast (ΔM) between rocks with different magnetic properties. However, the shape of the anomaly depends not only on the shape and depth of the source object but also on its orientation to the profile and to the inducing magnetic field, which itself varies in intensity and direction with geographical location. In oceanic magnetic surveying the magnetization contrast results from differences in the remanent magnetizations of crustal rocks, for which the Königsberger ratio is much greater than unity (i.e., $Q_n \gg 1$). Commercial geophysical prospecting is carried out largely in continental crustal rocks, for which the Königsberger ratio is much less than unity (i.e., $Q_n \ll 1$) and the magnetization may be assumed to be induced by the present geomagnetic field. The magnetization contrast is then due to susceptibility contrast in the crustal rocks. If k represents the susceptibility of an orebody, k_0 the susceptibility of the host rocks and F the strength of the inducing magnetic field, Eq. (5.17) allows us to write the magnetization contrast as

$$\Delta M = (k - k_0)F \tag{5.48}$$

Some insight into the physical processes that give rise to a magnetic anomaly can be obtained from the case of a vertically sided body that is magnetized by a vertical magnetic field. This is a simplified situation because in practice both the body and the field will be inclined, probably at different angles. However, it allows us to make a few observations that are generally applicable. Two scenarios are of particular interest. The first is when the body has a large vertical extent, such that its bottom surface is at a great depth; the other is when the body has a limited vertical extent. In both cases the vertical field magnetizes the body parallel to its vertical sides, but the resulting anomalies have different shapes. To understand the anomaly shapes we will use the concept of magnetic pole distributions.

5.5.5.1 Magnetic anomaly of a surface distribution of magnetic poles

Although magnetic poles are a fictive concept (see Section 5.2.2.1), they provide a simple and convenient way to understand the origin of magnetic field anomalies. If a slice is made through a uniformly magnetized object, simple logic tells us that there will be as many south poles per unit of area on one side of the slice as north poles on the opposite side; these will cancel each other and the net sum of poles per unit area of the surface of the slice is zero. This is no longer the case if the magnetization changes across the interface. On each unit area of the surface there will be more poles of the stronger magnetization than poles of the weaker one. A quantitative derivation shows that the resultant number of poles per unit area σ (called the surface density of poles) is proportional to the magnetization contrast ΔM.

The concept of the solid angle subtended by a surface element (Box 5.4) provides a qualitative understanding of the magnetic anomaly of a surface distribution of magnetic poles. Consider the distribution of poles on the upper surface with area A of a vertical prism with magnetization M induced by a vertical field B_z, as illustrated in Fig. 5.46a. At the surface of the Earth, distant r from the distribution of poles, the strength of their anomalous magnetic field is proportional to the total number of poles on the surface, which is the product of A and the surface density σ of poles. Equation (5.2) shows that the intensity of the field of a pole decreases as the inverse square of distance r. If the direction of r makes an angle θ with the vertical magnetization M, the vertical component of the anomalous field at P is found by multiplying by $\cos\theta$. The *vertical magnetic anomaly* ΔB_z of the surface distribution of poles is

$$\Delta B_z \propto \frac{(\sigma A)\cos\theta}{r^2} \propto (\Delta M)\Omega \tag{5.49}$$

A more rigorous derivation leads to essentially the same result. At any point on a measurement profile, the magnetic anomaly ΔB_z of a distribution of poles is proportional to the solid angle Ω subtended by the distribution at the point. The solid angle changes progressively along a profile (Fig. 5.46b). At the extreme left and right ends, the radius from the observation point is very oblique to the surface distribution of poles and the subtended angles Ω_1 and Ω_4 are very small; the anomaly distant from the body is nearly zero. Over the center of the distribution, the subtended angle reaches its largest value Ω_0 and the anomaly reaches a maximum. The anomaly falls smoothly on each side of its crest corresponding to the values of the subtended angles Ω_2 and Ω_3 at the intermediate positions. A measurement profile across an equal distribution of "north" poles would be exactly inverted. The north poles create a field of repulsion that acts everywhere to oppose the Earth's magnetic field, so the combined field is less than it would be if the "north" poles were not there. The magnetic anomaly over "north" poles is negative.

5.5.5.2 Magnetic anomaly of a vertical dike

We can now apply these ideas to the magnetic anomaly of a vertical dike. In this and all following examples we will assume a two-dimensional situation, where the horizontal length of the dike (imagined to be into the page) is infinite. This avoids possible complications related to "end effects." Let us first assume that the dike extends to

Box 5.4: Solid angles

A solid angle is defined by the ratio between the area of an element of the surface of a sphere and the radius of the sphere. Let the area of a surface element be A and the radius of the sphere be r, as in Fig. B5.4. The solid angle Ω subtended by the area A at the center of the sphere is defined as

$$\Omega = \frac{A}{r^2} \tag{1}$$

The angle subtended by any surface can be determined by projecting the surface onto a sphere. The shape of the area is immaterial. If an element of area A is inclined at angle α to the radius r through a point on the surface, its projection normal to the radius (i.e., onto a sphere passing through the point) is $A\cos\alpha$, and the solid angle it subtends at the center of the sphere is given by

$$\Omega = \frac{A\cos\alpha}{r^2} \tag{2}$$

A solid angle is measured in units of steradians, which are analogous to radians in planar geometry. The minimum value of a solid angle is zero, when the surface element is infinitesimally small. The maximum value of a solid angle is when the surface completely surrounds the center of the sphere. The surface area of a sphere of radius r is $A = 4\pi r^2$ and the solid angle at its center has the maximum possible value, which is 4π.

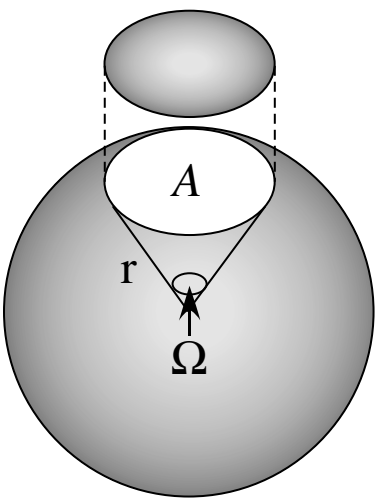

Fig. B5.4 Definition of the solid angle Ω subtended by an area A on the surface of a sphere with radius r.

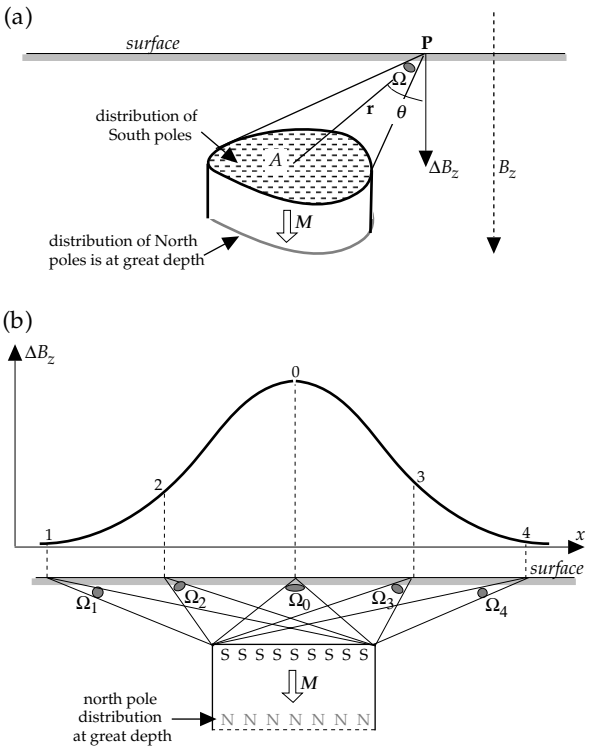

Fig. 5.46 Explanation of the magnetic anomaly of a vertical prism with infinite depth extent. For simplicity the magnetization M and inducing field B_z are both assumed to be vertical. (a) The distribution of magnetic poles on the top surface of the prism subtends an angle Ω at the point of measurement. (b) The magnetic anomaly ΔB_z varies along a profile across the prism with the value of the subtended angle Ω.

very great depths (Fig. 5.47a), so that we can ignore the small effects associated with its remote lower end. The vertical sides of the dike are parallel to the magnetization and no magnetic poles are distributed on these faces. However, the horizontal top face is normal to the magnetization and a distribution of magnetic poles can be imagined on this surface. The direction of magnetization is parallel to the field, so the pole distribution will consist of "south" poles. The magnetized dike behaves like a magnetic *monopole*. At any point above the dike we measure both the inducing field and the *anomalous* "stray field" of the dike, which is directed toward its top. The anomalous field has a component parallel to the Earth's field and so the total magnetic field will be everywhere stronger than if the dike were not present. The magnetic anomaly is everywhere positive, increasing from zero far from the dike to a maximum value directly over it (Fig. 5.46b).

If the vertical extent of the dike is finite, the distribution of north poles on the bottom of the dike may be close enough to the ground surface to produce a measurable stray field. The upper distribution of south poles causes a positive magnetic anomaly, as in the previous example. The lower distribution of north poles causes a negative anomaly (Fig. 5.47b). The north poles are further from the magnetometer than the south poles, so their negative anomaly over the dike is weaker. However, farther along

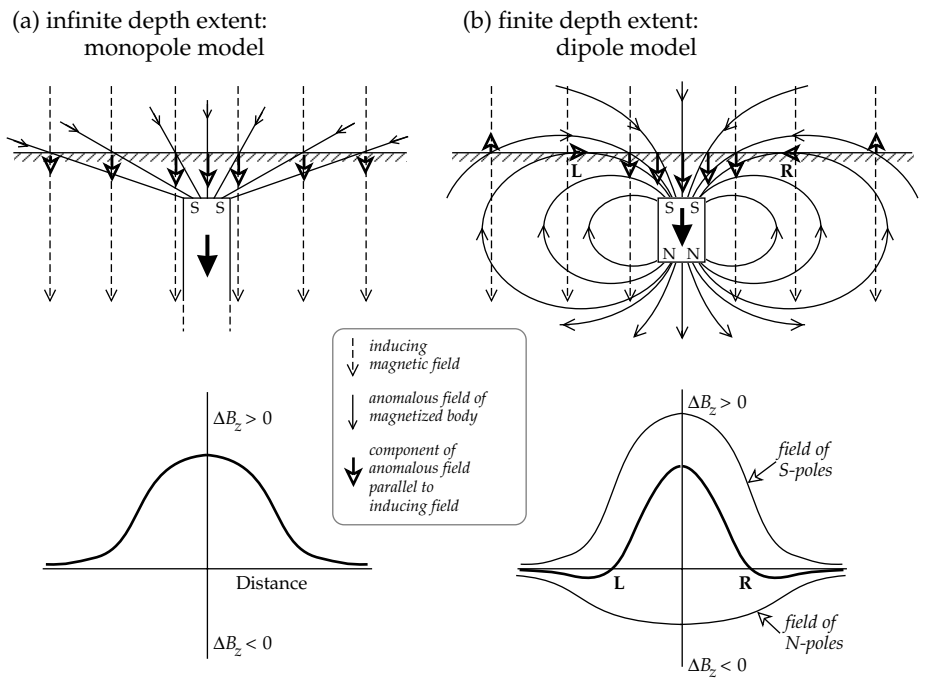

Fig. 5.47 (a) The vertical-field magnetic anomaly over a vertically magnetized block with infinite depth extent is due only to the distribution of poles on the top surface. (b) If the block has finite depth extent, the pole distributions on the top and bottom surfaces both contribute to the anomaly.

the profile the deeper distribution of poles subtends a larger angle than the upper one does. As a result, the strength of the weaker negative anomaly does not fall off as rapidly along the profile as the positive anomaly does. Beyond a certain lateral distance from the dike (to the left of L and to the right of R in Fig. 5.47b) the negative anomaly of the lower pole distribution is stronger than the positive anomaly of the upper one. This causes the magnetic anomaly to have negative side lobes, which asymptotically approach zero with increasing distance from the dike.

The magnetized dike in this example resembles a bar magnet and can be modelled crudely by a *dipole*. Far from the dike, along a lateral profile, the dipole field lines have a component opposed to the inducing field, which results in the weak negative side lobes of the anomaly. Closer to the dike, the dipole field has a component that reinforces the inducing field, causing a positive central anomaly.

5.5.5.3 Magnetic anomaly of an inclined magnetization

When an infinitely long dike is magnetized obliquely rather than vertically, its anomaly can be modelled either by an inclined dipole or by pole distributions (Fig. 5.48). The magnetization has both horizontal and vertical components, which produce magnetic pole distributions on the vertical sides of the dike as well as on its top and bottom. The symmetry of the anomaly is changed so that the negative lobe of the anomaly is enhanced on the side towards which the horizontal component of magnetization points; the other negative lobe decreases and may disappear.

The shape of a magnetic anomaly also depends on the angle at which the measurement profile crosses the dike, and on the strike and dip of the dike. The geometry, magnetization and orientation of a body may be taken into account in forward-modelling of an anomaly. However, as in other potential field methods, the inverse problem of determining these factors from the measured anomaly is not unique.

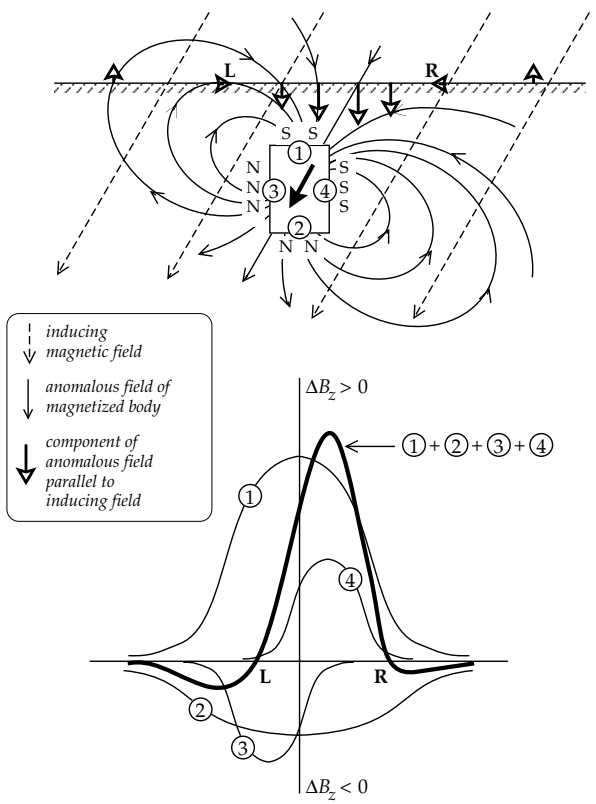

Fig. 5.48 Explanation of the origin of the magnetic anomaly of an infinitely long vertical prism in terms of the pole distributions on top, bottom and side surfaces, when the magnetic field (or magnetization) is inclined.

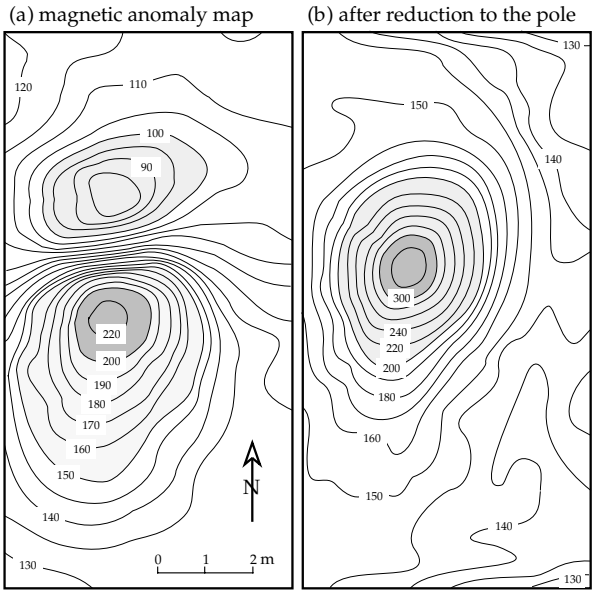

Fig. 5.49 Effect of data-processing by reduction to the pole on the magnetic anomaly of a small vertical prism with an inclined magnetization. In (a) the contour lines define a dipole type of anomaly with regions of maximum and minimum intensity (in nT); in (b) the anomaly after reduction to the pole is much simpler and constrains better the location of the center of the prism (after Lindner *et al.*, 1984).

The asymmetry (or *skewness*) of a magnetic anomaly can be compensated by the method of *reduction to the pole*. This consists of recalculating the observed anomaly for the case that the magnetization is vertical. The method involves sophisticated data-processing beyond the scope of this text. The observed anomaly map is first converted to a matrix of values at the intersections of a rectangular grid overlying the map. The Fourier transform of the matrix is then computed and convolved with a filter function to correct for the orientations of the body and its magnetization. The reduction to the pole removes the asymmetry of an anomaly (Fig. 5.49) and allows a better location of the margins of the disturbing body. Among other applications, the procedure has proved to be important for detailed interpretation of the oceanic crustal magnetizations responsible for lineated oceanic magnetic anomalies.

5.5.5.4 Magnetic anomalies of simple geometric bodies

The computation of magnetic anomalies is generally more complicated than the computation of gravity anomalies. In practice, iterative numerical procedures are used. However, the Poisson relation (Box 5.5) enables the computation of magnetic anomalies for bodies for which the gravity anomaly is known. This is most easily illustrated for vertically magnetized bodies, such as the following examples.

(1) *Sphere.* The gravity anomaly Δg_z over a sphere of radius R with density contrast $\Delta\rho$ and center at depth z (representing a diapir or intrusion) is given by Eq. (2.83), repeated here:

$$\Delta g_z = \frac{4}{3}\pi G\Delta\rho R^3 \frac{z}{(z^2+x^2)^{3/2}}$$

Assuming the same dimensions and a magnetization contrast ΔM_z, the potential of the magnetic anomaly over a vertically magnetized sphere according to the Poisson relation is

$$W = \frac{\mu_0}{4\pi}\left(\frac{\Delta M_z}{G\Delta\rho}\right)\Delta g_z = \frac{1}{3}\mu_0 R^3 \Delta M_z \frac{z}{(z^2+x^2)^{3/2}} \qquad (5.50)$$

By differentiating with respect to x or z we get the horizontal or vertical field anomaly, respectively. The vertical field magnetic anomaly ΔB_z of the sphere is

$$\Delta B_z = -\frac{\partial W}{\partial z} = -\frac{1}{3}\mu_0 R^2 \Delta M_z \frac{\partial}{\partial z}\left(\frac{z}{(z^2+x^2)^{3/2}}\right)$$
$$= -\frac{1}{3}\mu_0 R^2 \Delta M_z \frac{(z^2+x^2)^{3/2} - z(3/2)(2z)(z^2+x^2)^{1/2}}{(z^2+x^2)^3} \qquad (5.51)$$

$$\Delta B_z = \frac{1}{3}\mu_0 R^3 \Delta M_z \frac{(2z^2-x^2)}{(z^2+x^2)^{5/2}} \qquad (5.52)$$

(2) *Horizontal cylinder*. The gravity anomaly Δg_z over a cylinder of radius R with horizontal axis centered at depth z and with density contrast $\Delta\rho$ (representing an anticline or syncline) is given by Eq. (2.93). If the structure is vertically magnetized with magnetization contrast ΔM_z, Poisson's relation gives for the magnetic potential

$$W = \frac{\mu_0}{4\pi}\left(\frac{\Delta M_z}{G\Delta\rho}\right)\Delta g_z = \frac{1}{2}\mu_0 R^2 \Delta M_z \frac{z}{z^2+x^2} \qquad (5.53)$$

The vertical magnetic field anomaly ΔB_z over the horizontal cylinder is

$$\Delta B_z = \frac{1}{2}\mu_0 R^2 \Delta M_z \frac{(z^2-x^2)}{(z^2+x^2)^2} \qquad (5.54)$$

(3) *Horizontal crustal block*. The gravity anomaly for a thin horizontal sheet of thickness t at depth d between horizontal positions x_1 and x_2 (Fig. 2.54 b), extending to infinity normal to the plane of observation, is given by Eq. (2.96). Let the width of the block be $2m$, and let the horizontal position be measured from the midpoint of the block, so that $x_1 = x - m$ and $x_2 = x + m$. Applying Poisson's relation, we get the magnetic potential for a semi-infinite horizontal thin sheet of vertically magnetized dipoles, of thickness t at depth z

$$W = \frac{\mu_0}{4\pi}\left(\frac{\Delta M_z}{G\Delta\rho}\right)\Delta g_z = \frac{\mu_0 \Delta M_z t}{2\pi}$$
$$\times\left[\tan^{-1}\left(\frac{x+m}{z}\right) - \tan^{-1}\left(\frac{x-m}{z}\right)\right] \qquad (5.55)$$

Box 5.5: Poisson's relation

Poisson (1781–1840) observed a relationship between the gravitational and magnetic potentials of a body, which allows a simple method of computing magnetic field anomalies if the gravity anomaly of the body is known. Consider an arbitrary volume V with homogeneous density and vertical magnetization (Fig. B5.5). If the density of the body is $\Delta\rho$ a small element with volume $\mathrm{d}V$ has mass $(\Delta\rho \mathrm{d}V)$. The gravitational potential U at a point on the surface at a distance r from the element is

$$U = -G\frac{\Delta\rho\,\mathrm{d}V}{r} \tag{1}$$

The vertical gravity anomaly Δg_z of the volume element is found by differentiating U with respect to z

$$g_z = -\frac{\partial}{\partial z}\left(-G\frac{\Delta\rho\,\mathrm{d}V}{r}\right) = G\Delta\rho\,\mathrm{d}V\frac{\partial}{\partial z}\left(\frac{1}{r}\right) \tag{2}$$

If the body is vertically magnetized with uniform magnetization ΔM_z, the magnetic moment of the volume element is $(\Delta M_z\,\mathrm{d}V)$. The magnetic moment is directed downward as in Fig. B5.5. The radius vector from the element to a point on the surface makes an angle $(\pi - \theta)$ with the orientation of the magnetization. The magnetic potential W at the point (r, θ) is

$$W = \frac{\mu_0}{4\pi}\frac{\Delta M_z\,\mathrm{d}V\cos(\pi-\theta)}{r^2}$$

$$= -\frac{\mu_0}{4\pi}\frac{\Delta M_z\,\mathrm{d}V\cos\theta}{r^2} = -\frac{\mu_0}{4\pi}\frac{\Delta M_z\,\mathrm{d}V}{r^2}\left(\frac{z}{r}\right) \tag{3}$$

Note the following relationship

$$\frac{\partial}{\partial z}\left(\frac{1}{r}\right) = -\frac{1}{r^2}\frac{\partial r}{\partial z} = -\frac{1}{r^2}\frac{\partial}{\partial z}\sqrt{x^2+z^2} = -\frac{1}{r^2}\left(\frac{z}{r}\right) \tag{4}$$

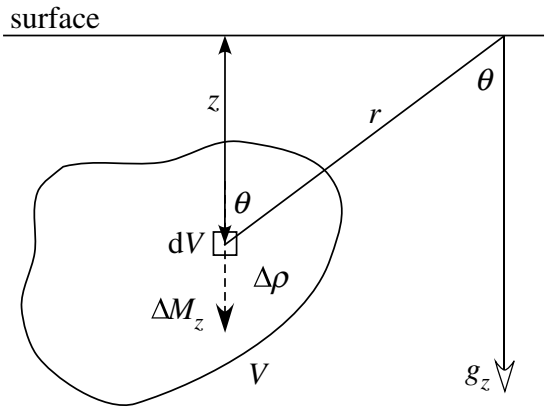

Fig. B5.5 Definition of parameters used in the derivation of Poisson's relation.

Substituting this result in (3) gives

$$W = \frac{\mu_0}{4\pi}\Delta M_z\,\mathrm{d}V\frac{\partial}{\partial z}\left(\frac{1}{r}\right) \tag{5}$$

Comparing Eq. (2) and Eq. (5) and eliminating the volume ΔV we get Poisson's relation:

$$W = \frac{\mu_0}{4\pi}\left(\frac{\Delta M_z}{G\Delta\rho}\right)g_z$$

This derivation for a small element is also valid for an extended body as long as the density and magnetization are both uniform.

Assume that the horizontal crustal block is made up of layers of thickness $t = \mathrm{d}z$. If the top of the block is at depth z_1 and its base at depth z_2, the magnetic potential of the block is found by integrating Eq. (5.55) between z_0 and z_1,

$$W = \frac{\mu_0\Delta M_z}{2\pi}\int_{z_1}^{z_2}\left[\tan^{-1}\left(\frac{x+m}{z}\right) - \tan^{-1}\left(\frac{x-m}{z}\right)\right]\mathrm{d}z \tag{5.56}$$

Differentiating with respect to z gives the vertical magnetic field anomaly over the block:

$$\Delta B_z = -\frac{\partial W}{\partial z} = -\frac{\mu_0\Delta M_z}{2\pi}\int_{z_1}^{z_2}\frac{\partial}{\partial z}\left[\tan^{-1}\left(\frac{x+m}{z}\right) - \tan^{-1}\left(\frac{x-m}{z}\right)\right]\mathrm{d}z \tag{5.57}$$

$$\Delta B_z = \frac{\mu_0\Delta M_z}{2\pi}\left[\tan^{-1}\left(\frac{x+m}{z_1}\right) - \tan^{-1}\left(\frac{x-m}{z_1}\right) - \tan^{-1}\left(\frac{x+m}{z_2}\right) + \tan^{-1}\left(\frac{x-m}{z_2}\right)\right] \tag{5.58}$$

$$\Delta B_z = \frac{\mu_0\Delta M_z}{2\pi}[(\alpha_1 - \alpha_2) - (\alpha_3 - \alpha_4)] \tag{5.59}$$

where the angles α_1, α_2, α_3 and α_4 are defined in Fig. 5.50a. Note that the angles $(\alpha_1 - \alpha_2)$ and $(\alpha_3 - \alpha_4)$ are the *planar* angles subtended at the point of measurement by the top and bottom edges of the vertically magnetized crustal block respectively. This is similar to the dependence of magnetic anomalies of

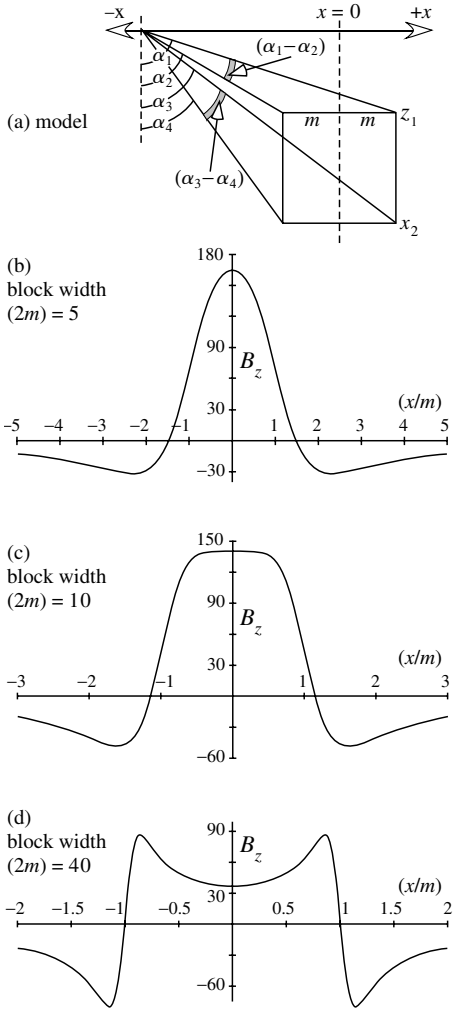

Fig. 5.50 The effect of block width on the shape of the magnetic anomaly over a vertically magnetized thin crustal block. (a) The block has width $w = 2m$, and its top and bottom surfaces are at depths z_1 and z_2, respectively. For each of the calculated anomalies in (b), (c) and (d) these depths are $z_1 = 2.5$ km and $z_2 = 3$ km, and only the width of the block is varied. The amplitude of the anomaly is in arbitrary units.

three-dimensional bodies on *solid* angles subtended by surfaces of the body at the point of observation, as illustrated in Fig. 5.46. As was the case for gravity surveys, magnetic profiles normal to the strike of elongate bodies may be regarded as two-dimensional, as long as the third dimension of the body is large enough for variations normal to the profile to be negligible.

5.5.5.5 Effect of block width on anomaly shape

The effect of the width of a crustal block on anomaly shape is illustrated by use of Eq. (5.59) to model the vertical field magnetic anomaly of a vertically magnetized block with its top at depth 2.5 km and base at depth 3 km. The block is effectively a thin magnetized layer, similar to the source of oceanic magnetic anomalies. Three cases are considered here: a narrow block of width $w = (2m) = 5$ km for which $m/z_1 = 1$, a block of width 10 km ($m/z_1 = 2$), and a wide block of width 40 km ($m/z_1 = 8$).

The narrowest block gives a sharp, positive central anomaly with negative side lobes (Fig. 5.50b), as explained in Section 5.5.5.2. As the block widens with respect to its depth, the top of the central anomaly flattens (Fig. 5.50c), its amplitude over the middle of the block decreases, and the negative side lobes grow. When the block is much wider than the depth to its top (Fig. 5.50d), a dip develops over the center of the block. The positive anomalies are steep sided and are maximum just within the edges of the block, while the null values occur close to the edges of the block. The negative side anomalies are almost as large as the positive anomalies.

The pronounced central dip in the anomaly is due to the limited vertical thickness of the layer. If the layer is very wide relative to its thickness, the central anomaly may diminish almost to zero. This is because the angle $(\alpha_3 - \alpha_4)$ subtended by the magnetized base of the layer is almost (but not quite) as large as the angle $(\alpha_1 - \alpha_2)$ subtended by the top of the layer. For a very large width-to-thickness ratio, the central anomaly is zero, the edge anomalies separate and become equivalent to separate anomalies over the edges of the block.

Examination of Fig. 5.50a shows that the subtended angles $(\alpha_1 - \alpha_2)$ and $(\alpha_3 - \alpha_4)$, and thus the anomaly shape, depend also on the height of the measurement profile above the surface of the block. A low-altitude profile over the block will show a large central dip, while a high-altitude profile over the same block will show a smaller dip or none at all.

In contrast to the example of a thin layer described above, if the crustal block is very thick, extending to great depth, the angle $(\alpha_3 - \alpha_4)$ is zero and the effects of the magnetization discontinuity (or pole distribution) on its base are absent. The shape of the anomaly is then determined by $(\alpha_1 - \alpha_2)$ and is flat topped over a wide block.

5.5.6 Oceanic magnetic anomalies

In the late 1950s marine geophysicists conducting magnetic surveys of the Pacific ocean basin off the west coast of North America discovered that large areas of oceanic crust are characterized by long stripes of alternating positive and negative magnetic anomalies. The striped pattern is best known from studies carried out across oceanic ridge systems (see Fig. 1.13). The striped anomalies are hundreds of kilometers in length parallel to the ridge axis, 10–50 km in width, and their amplitudes amount to several hundreds of nanotesla. On magnetic profiles perpendicular to a ridge axis the anomaly pattern is found to exhibit a remarkable symmetry about the axis of the ridge. The origin of the symmetric lineated anomaly pattern cannot be explained by conventional methods of interpretation based on susceptibility contrast.

Seismic studies indicate a layered structure for the oceanic crust. The floor of the ocean lies at water depths

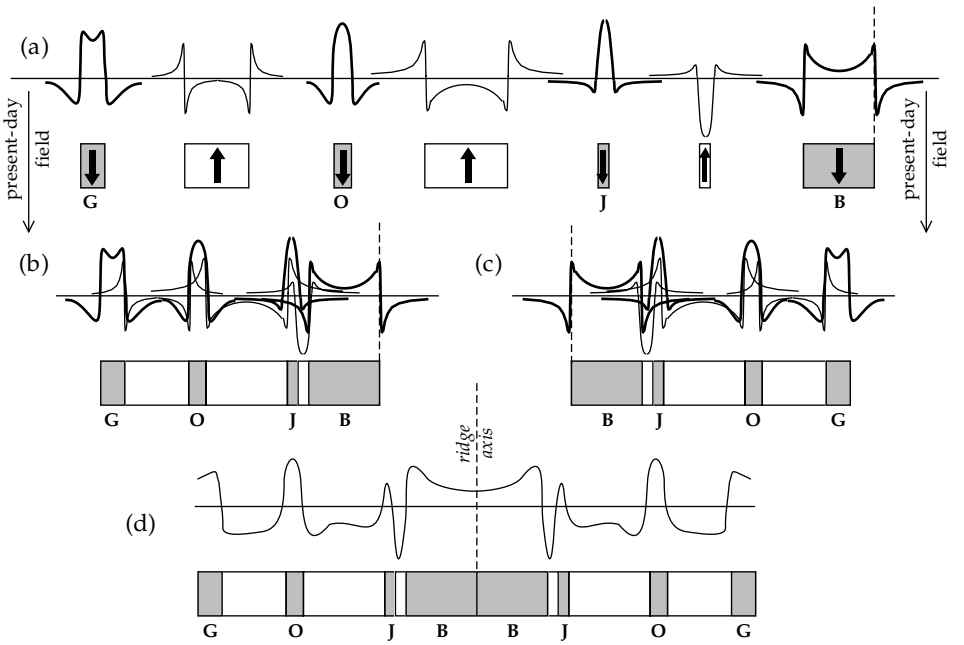

Fig. 5.51 Explanation of the shape of a magnetic profile across an oceanic spreading center: (a) the anomalies of individual oppositely magnetized crustal blocks on one side of the ridge, (b) overlap of the individual anomalies, (c) the effect for the opposite sequence of blocks on the other side of the ridge, and (d) the complete anomaly profile.

of 2–5 km, and is underlain by a layer of sediment of variable thickness, called seismic Layer 1. Under the sediments lie a complex of basaltic extrusions and shallow intrusions, about 0.5 km thick, forming seismic Layer 2A, under which are found the deeper layers of the oceanic crust consisting of a complex of sheeted dikes (Layer 2B) and gabbro (Layer 3). The magnetic properties of these rocks were first obtained by studying samples dredged from exposed crests and ridges of submarine topography. The rocks of Layers 2B and 3 are much less magnetic than those of Layer 2A. Samples of pillow basalt dredged near to oceanic ridges have been found to have moderate susceptibilities for igneous rocks, but their remanent magnetizations are intense. Their Königsberger ratios are commonly in the range 5–50 and frequently exceed 100. Recognition of these properties provided the key to understanding the origin of the lineated magnetic anomalies. In 1963 the English geophysicists F. J. Vine and D. H. Matthews proposed that the *remanent magnetizations* (and not the susceptibility contrast) of oceanic basaltic Layer 2 were responsible for the striking lineated anomaly pattern. This hypothesis soon became integrated into a working model for understanding the mechanism of sea-floor spreading (see Section 1.2.5 and Fig. 1.14).

The oceanic crust formed at a spreading ridge acquires a thermoremanent magnetization (TRM) in the geomagnetic field. The basalts in Layer 2A are sufficiently strongly magnetized to account for most of the anomaly measured at the ocean surface. For a lengthy period of time (measuring several tens of thousands to millions of years) the polarity of the field remains constant; crust formed during this time carries the same polarity as the field. After a polarity reversal, freshly formed basalts acquire a TRM parallel to the new field direction, i.e., opposite to the previous TRM. Adjacent oceanic crustal blocks of different widths, determined by the variable time between reversals, carry antiparallel remanent magnetizations.

The oceanic crust is magnetized in long blocks parallel to the spreading axis, so the anomaly calculated for a profile perpendicular to the axis is two dimensional, as in the previous examples. Consider the case where the anomalies on a profile have been reduced to the pole, so that their magnetizations can be taken to be vertical. We can apply the concept of magnetic pole distributions to each block individually to determine the shape of its magnetic anomaly (Fig. 5.51a). If the blocks are contiguous, as is the case when they form by a continuous process such as sea-floor spreading, their individual anomalies will overlap (Fig. 5.51b). The spreading process is symmetric with respect to the ridge axis, so a mirror image of the sequence of polarized blocks is formed on the other side of the axis (Fig. 5.51c). If the two sets of crustal blocks are brought together at the spreading axis, a magnetic anomaly sequence ensues that exhibits a symmetric pattern with respect to the ridge axis (Fig. 5.51d).

This description of the origin of oceanic magnetic anomalies is over-simplified, because the crustal magnetization is more complicated than assumed in the block model. For example, the direction of the remanent magnetization, acquired at the time of formation of the ocean crust, is generally not the same as the direction of the magnetization induced by the present-day field. However, the induced magnetization has uniformly the same direction in the magnetized layer, which thus behaves like a uniformly magnetized thin horizontal sheet and does not contribute to the magnetic anomaly. Moreover, oceanic rocks have high Königsberger ratios, and so the induced magnetization component is usually negligible in comparison to the remanent magnetization. An exception is when a magnetic

survey is made close to the magnetized basalt layer, in which case a topographic correction may be needed.

Unless the strike of a ridge is north–south, the magnetization inclination must be taken into account. Skewness is corrected by reducing the magnetic anomaly profile to the pole (Section 5.5.5.3). A possible complication may arise if the oceanic magnetic anomalies have two sources. The strongest anomaly source is doubtless basaltic Layer 2B, but, at least in some cases, an appreciable part of the anomaly may arise in the deeper gabbroic Layer 3. The two contributions are slightly out of phase spatially, because of the curved depth profiles of cooling isotherms in the oceanic crust. This causes a magnetized block in the deeper gabbroic layer to lie slightly further from the ridge than the corresponding block with the same polarity in the basaltic layer above it. The net effect is an asymmetry of inclined magnetization directions on opposite sides of a ridge, so that the magnetic anomalies over blocks of the same age have different skewnesses.

5.6 PALEOMAGNETISM

5.6.1 Introduction

A mountain walker using a compass to find his way in the Swiss Alps above the high mountain valley of the Engadine would notice that in certain regions (for example, south of the Septimer Pass) the compass-needle shows very large deviations from the north direction. The deflection is due to the local presence of strongly magnetized serpentinites and ultramafic rocks. Early compasses were more primitive than modern versions, but the falsification of a compass direction near strongly magnetic outcrops was known by at least the early nineteenth century. In 1797 Alexander von Humboldt proposed that the rocks in these unusual outcrops had been magnetized by lightning strikes. The first systematic observations of rock magnetic properties are usually attributed to A. Delesse (1849) and M. Melloni (1853), who concluded that volcanic rocks acquired a remanent magnetization during cooling. After a more extensive series of studies in 1894 and 1895 of the origin of magnetism in lavas, G. Folgerhaiter reached the same conclusion and suggested that the direction of remanent magnetization was that of the geomagnetic field during cooling. By 1899 he had extended his work to the record of the secular variation of inclination in ancient potteries. Folgerhaiter noted that some rocks have a remanent magnetization opposite to the direction of the present-day field. Reversals of polarity of the geomagnetic field were established decisively early in the twentieth century.

In 1922 Alfred Wegener proposed his concept of continental drift, based on years of study of paleoclimatic indicators such as the geographic distribution of coal deposits. At the time, there was no way of explaining the mechanism by which the continents drifted. Only motions of the crust were considered, and the idea of rigid continents ploughing through rigid oceanic crust was unacceptable to geophysicists. There was as yet no way to reconstruct the positions of the continents in earlier eras or to trace their relative motions. Subsequently, paleomagnetism was to make important contributions to understanding continental drift by providing the means to trace past continental motions quantitatively.

A major impetus to these studies was the invention of a very sensitive *astatic magnetometer*. The apparatus consists of two identical small magnets mounted horizontally at opposite ends of a short rigid vertical bar so that the magnets are oriented exactly antiparallel to each other. The assembly is suspended on an elastic fiber. In this configuration the Earth's magnetic field has equal and opposite effects on each magnet. If a magnetized rock is brought close to one magnet, the magnetic field of the rock produces a stronger twisting effect on the closer magnet than on the distant one and the assembly rotates to a new position of equilibrium. The rotation is detected by a light beam reflected off a small mirror mounted on the rigid bar. The device was introduced in 1952 by P. M. S. Blackett to test a theory that related the geomagnetic field to the Earth's rotation. The experiment did not support the postulated effect. However, the astatic magnetometer became the basic tool of paleomagnetism and fostered its development as a scientific discipline. Hitherto it had only been possible to measure magnetizations of strongly magnetic rocks. The astatic magnetometer enabled the accurate measurement of weak remanent magnetizations in rocks that previously had been unmeasurable.

In the 1950s, several small research groups were engaged in determining and interpreting the directions of magnetization of rocks of different ages in Europe, Africa, North and South America and Australia. In 1956 S. K. Runcorn put forward the first clear geophysical evidence in support of continental drift. Runcorn compared the directions of magnetization of Permian and Triassic rocks from Great Britain and North America. He found that the paleomagnetic results from the different continents could be brought into harmony for the time before 200 Ma ago by closing the Atlantic ocean. The evaluation of the scientific data was statistical and at first was regarded as controversial. However, Mesozoic paleomagnetic data were soon obtained from the southern hemisphere that also argued strongly in favor of the continental drift hypothesis. In 1957 E. Irving showed that paleomagnetic data conformed better with geological reconstructions of earlier positions of the continents than with their present-day distribution. Subsequently, numerous studies have documented the importance of paleomagnetism as a chronicle of past motions of global plates and as a record of the polarity history of the Earth's magnetic field.

5.6.2 The time-averaged geomagnetic field

A fundamental assumption of paleomagnetism is that the time-averaged geomagnetic field corresponds to that of

an axial geocentric dipole. The data in support of this important hypothesis come partly from studies of secular variation and partly from paleomagnetic observations in young rocks and sediments.

The dipole and non-dipole parts of the historic geomagnetic field are known to change slowly with time. Spherical harmonic analysis of the geomagnetic field (see Section 5.4.5.1) shows that the axis of the geocentric inclined dipole has drifted slowly westward at about 0.044–0.14° yr^{-1} in the last 400 yr (see Fig. 5.36). This would correspond to a complete circuit about the rotation axis in 2500–8000 yr. The rates of westward drift of the historic non-dipole field are around 0.22–0.66° yr^{-1} (see Fig. 5.37), giving a periodicity of 550–1650 yr. However, it is important to keep in mind that the historic records of the secular variation of the geomagnetic field cover only a fragment of a complete circuit, which is not enough to confirm cyclicity or to estimate a period. The record of earlier magnetic field intensity and direction must be inferred from *archeomagnetism*.

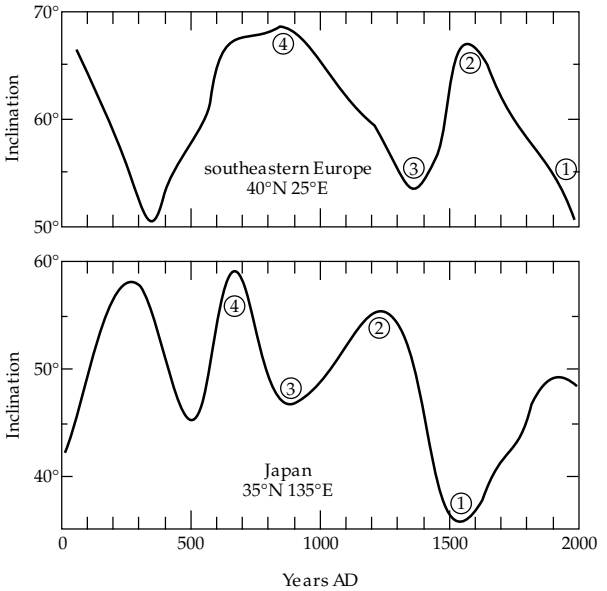

Fig. 5.52 Secular variation of geomagnetic inclination from archeomagnetic studies in southeastern Europe and southwestern Japan (after Merrill and McElhinny, 1983).

5.6.2.1 Archeomagnetic records of secular variation

Paleomagnetism is the study of the geomagnetic field recorded in rock magnetizations; archeomagnetism is the study of the geomagnetic field recorded in dateable historic artefacts. The age of an archeological relict, such as a pot or vase, can often be determined with reliable precision. The pot, and the oven in which it was fired, may carry a thermoremanent magnetization (TRM) acquired during cooling. The direction of the TRM can be measured easily and, if the attitude of the pot during firing is known or can be assumed, the inclination of the ancient magnetic field in which the artefact was made can be deduced. The same considerations apply to lava flows that can be dated from historic records.

The secular record of paleoinclination during the past 2000 yr is available for two regions in which many archeomagnetic studies have been carried out: southeastern Europe and southwestern Japan. These regions are 110° apart in longitude but lie in similar latitude ranges, 35–40°N. Smoothed curves through the observations show pseudo-cyclical changes with several maxima and minima (Fig. 5.52). The shapes of the curves are not distinctive, so correlation of individual extreme values is risky; however, comparison of the four numbered maxima and minima in the last 1400 yr suggests that the extreme values appear to occur about 400 yr earlier in Japan than in Europe. The equivalent period for a full circuit of the globe is 1300 yr. The pseudo-cyclicity is interpreted as the effect of westward drift of foci of the non-dipole field past the sampling site. More detailed analysis of the archeomagnetic data shows that the drift rates vary with the latitude of the observation site (see Fig. 5.37). The mean drift rate is 0.38° longitude per year, which is faster than the rate deduced from recent secular variation.

A subtle magnetic technique devised by Thellier in 1937 permits determination of the intensity of the magnetic field in which an object acquires a TRM. If it is assumed that the field was a dipole field, the strength of the dipole magnetic moment can be inferred. When applied to rocks or ancient artifacts, this type of analysis is called a paleointensity determination. The variation in strength of the geomagnetic field during the past 7000 yr is shown by the results of 3188 paleointensity measurements on dated archeological and geological samples (Fig. 5.53). Older paleointensity data exist, but their number is too small to be included without distorting the record. The number of artifacts decreases as one goes back in time, so to obtain significant mean values the data are grouped in 1000 yr intervals before 2000 BC and in 500 yr intervals after 2000 BC. This introduces a problem, because these time intervals are too short for the geomagnetic field to average to a dipole field. The archeological relict records the total field at the time of cooling, which contains a substantial non-dipole component. However, by combining the 3188 paleointensity data with 13,080 inclination and 16,085 declination data from lake sediments, a global field model has been calculated with Schmidt coefficients (Eq. (5.34)) up to order and degree 10. The coefficients with $n = 1$ from this model give the dipole magnetic moment (Eq. (5.41)). The analysis yields a smooth continuous record of the variation of the strength of the geomagnetic dipole during the past 7000 yr (Fig. 5.53). This record is displaced to slightly lower values than the direct measurements of paleointensity represented by the boxes, because it is free of non-dipole components. The dipole moment has fluctuated in the past 7000 years, but the record is too short to establish whether the changes are cyclical.

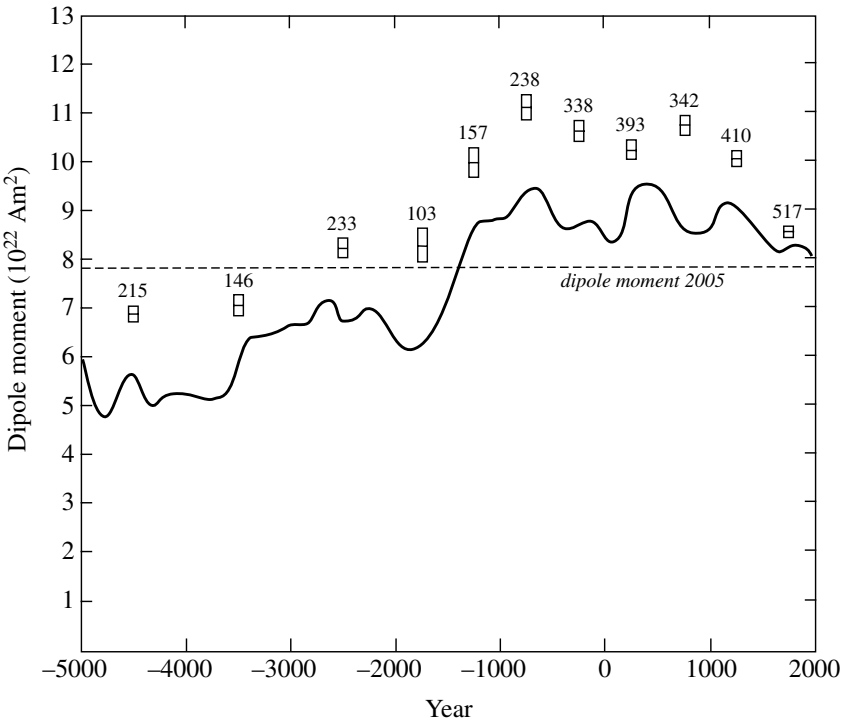

Fig. 5.53 Secular variation of the virtual geocentric dipole moment. The mean paleointensity of each time interval is plotted at the mid-point of each box, whose height represents the 95% confidence limits of the mean. The numbers indicate how many data were averaged in each time interval. The continuous curve is obtained from a global spherical harmonic analysis and the results are smoothed with a spline function (after Korte and Constable, 2005).

Westward drift of the dipole field implies systematic changes in the equatorial components of the dipole. If the changes are approximately cyclical, the mean long-term strength of the equatorial dipole measured at any given site would average to zero within a few multiples of 10^4 yr. Similarly, if the secular variation of the non-dipole field can be assumed to be roughly periodic its mean value should average to zero within a few multiples of 10^3 yr. According to these arguments, the only long-term component of the geomagnetic field that persists and is not averaged to zero within a few tens of thousands of years is the axial dipole component. The long-term equivalence of the Earth's magnetic field with that of a dipole located at the center of the Earth and oriented along the rotation axis is a fundamental tenet of paleomagnetism; it is called the *axial geocentric dipole hypothesis*.

5.6.2.2 The axial geocentric dipole hypothesis

The evidence in support of the axial geocentric dipole hypothesis comes from paleomagnetic studies in modern deep-sea sediments and young igneous and sedimentary rocks. Pelagic sediments are deposited extremely slowly in the deep ocean basins. Sedimentation rates of 1–10 m Ma^{-1} are common. The sediments acquire a post-depositional remanent magnetization (pDRM), which is an accurate record of the depositional field direction. The slow deposition of deep-sea sediments ensures thorough averaging of the magnetic field recorded. For example, at pelagic sedimentation rates a typical one-inch thick sample of deep-sea sediment averages paleomagnetic directions acquired during 2500–25,000 yr of deposition. The test of the axial geocentric dipole hypothesis in modern deep-sea sediments consists of comparing the inclination observed in sediment samples with the inclination expected for the latitude of the site where the sediment was sampled. The relationship between field inclination I, magnetic co-latitude θ and latitude λ was developed in Eq. (5.40) and is shown in Fig. 5.54a. The mean inclinations of remanent magnetization were measured in 52 deep-sea sediment cores of Plio-Pleistocene age taken from sites at different latitudes in the northern and southern hemispheres. The observed inclinations agree well with the values predicted by the theoretical curve for the axial geocentric dipole hypothesis (Fig. 5.54b).

Assuming the direction of the magnetic field recorded at a given site to be that of a dipole field, it is possible to calculate where the geomagnetic pole would need to be in order to produce the observed declination and inclination. This location is called the *virtual geomagnetic pole* (VGP) position. It is useful in computing where the pole lay in ancient times, the so-called *paleomagnetic pole*. The difference between a VGP and a paleomagnetic pole is illustrated by the following example for a recently extruded lava. Each sample from the lava formed in a short interval of time, and the field direction it records will be that of the total geomagnetic field at the site, combining axial dipole, non-dipole and non-axial dipole components. The VGP will therefore not coincide with the rotation axis. If data are collected from several flows of different ages, each will carry a slightly different record of the field. The computed VGP position will be different from flow to flow, and so the distribution of VGP will be scattered. If samples are measured from a large number of recent lava flows covering a long enough period of time

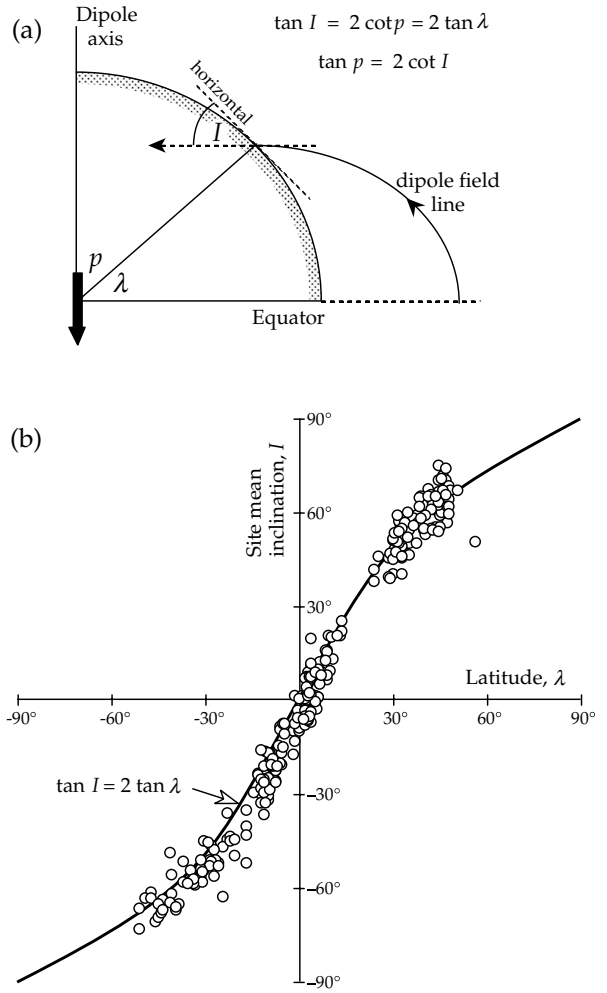

Fig. 5.54 (a) The geocentric axial dipole hypothesis predicts the relationship tan$I = 2\tan\lambda$ between the inclination I of a dipole field and the magnetic latitude λ. (b) The inclinations measured in modern deep-sea sediment cores agree well with the theoretical curve (based on data from Schneider and Kent, 1990).

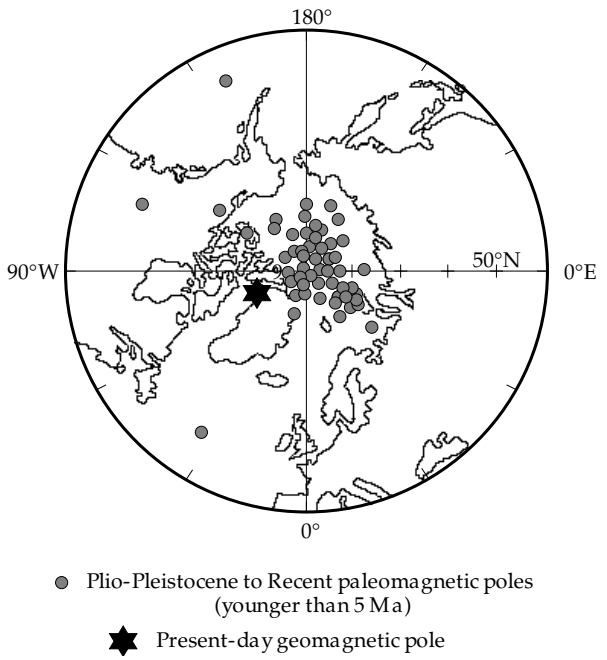

Fig. 5.55 Paleomagnetic pole positions for rocks of Plio-Pleistocene to Recent age (after McElhinny, 1973).

to average the non-dipole and non-axial dipole parts to zero, the mean direction of the collection will correspond to the field of an axial geocentric dipole. The pole position calculated from the mean direction of the collection of flows will agree with the rotation axis. This pole, representing an averaged value of the field, is called a *paleomagnetic pole*. The VGP represents a spot estimate of the field, including non-axial dipole components; the paleomagnetic pole represents an averaged field, corresponding to the axial geocentric dipole.

The paleomagnetic pole positions determined in studies of Plio-Pleistocene to Recent volcanic and sedimentary rocks covering the past 5 Ma lend further support to the axial geocentric dipole hypothesis. The distribution of paleomagnetic poles is clustered around the geographic pole and not around the present-day geomagnetic pole (Fig. 5.55). Statistical analysis shows that the mean of the paleomagnetic poles does not differ significantly from the geographic pole.

The axial geocentric dipole hypothesis maintains that, if data are averaged over a long enough interval of time, the mean paleomagnetic pole position will coincide with the axis of rotation of the Earth. In fact, detailed analysis of Late Tertiary paleomagnetic poles has shown that this hypothesis does not hold exactly. This is because the mean pole position calculated for any field that is symmetric about the rotation axis will lie on the axis, provided the directions are obtained at sites covering a wide range of longitudes. When young paleomagnetic data of the same age are averaged for a particular region, they give a paleomagnetic pole position on the far side of the present-day rotation axis. This "far-sidedness" of paleomagnetic directions is caused by the presence of a small axial geocentric quadrupole, amounting to a few percent of the axial geocentric dipole. The superposition of the axial dipole and quadrupole is equivalent to displacing the center of the dipole about 300 km northward along the rotation axis away from the center of the Earth. This is a second-order effect; to a first approximation the time-averaged paleomagnetic field may be considered to be that of an axial geocentric dipole, and the paleomagnetic pole lies within a few degrees of the rotational pole.

5.6.3 Methods of paleomagnetism

The requirement that the mean paleomagnetic pole position derived for a collection of rocks should represent the axial geocentric dipole is taken into account in the methodology of paleomagnetic analysis. This begins with the sampling of a rock formation on a hierarchical scheme designed to eliminate or minimize non-systematic

errors and to average out the effects of secular variation of the paleomagnetic field. At each hierarchical level, averaging and statistical analysis are carried out on the remanent magnetization vectors. Ideally, a paleomagnetic collection should contain a large number of samples per site. In practice, about 6–10 samples are enough to define the mean direction for a site; the mean values of typically 10–20 sites from the same formation are averaged to get a mean paleomagnetic direction for a formation or region.

A further assumption of paleomagnetism is that the natural remanent magnetization (NRM) of a rock was acquired at the time of formation of the rock (or at a known time in its history), and has since remained unaltered. In fact, the NRM is usually made up of several components acquired at different times, including during the procedures of sampling and preparation. Laboratory techniques must be applied that eliminate the undesirable components and isolate the primary magnetization. This process is loosely called "magnetic cleaning."

The presentation of paleomagnetic directions measured in rock samples is made with the help of stereographic projection. This is a way of plotting three-dimensional directions by projecting them onto a plane. These plots have already been encountered in the analysis of first-motion studies of earthquakes (see Section 3.5.4.2). A direction is identified by the point where it intersects a unit sphere centered at the observation site. This converts a set of directions to a set of points on the surface of a sphere. The intersection point is then projected onto the horizontal plane to give a stereographic plot. This can be done in different ways. The Lambert equal-area projection is usually preferred in paleomagnetism as it avoids visually distorting the dispersion of directions. In geology, all directions are plotted on a stereogram as projections on the lower hemisphere. In paleomagnetic stereograms directions with positive (downward) inclinations are plotted as lower hemisphere projections; directions with negative (upward) inclinations are plotted with a different symbol as upper hemisphere projections.

5.6.3.1 Measurement of remanent magnetization

Measurements of the natural remanent magnetization of rocks with an astatic magnetometer were laborious and time consuming and the instrument has now fallen into disuse. In modern paleomagnetic laboratories more efficient spinner magnetometers and cryogenic magnetometers are in common use.

Spinner magnetometers originally consisted of a large sensor coil containing many turns of wire in which an alternating signal was induced by rotating the sample at high frequency (around 100 Hz) within the coil. Rapid rotation was needed because the voltage induced was proportional to the rate of change of flux in the coil. After phase-lock detection and electronic amplification of the signal, the calibrated output yielded two components of remanence in the plane normal to the rotational axis. The instrument was susceptible to electrostatic build-up but was capable of measuring magnetizations of around 10^{-3} A m^{-1} in 10–15 minutes.

The flux-gate spinner magnetometer is a subsequent refinement in which the sensor coil is replaced with flux-gate sensors. These detect directly the external magnetic fields of the sample. The signal strength is not dependent on rotational speed which could be reduced to about 5–10 Hz. The rotation of the sample gives a sinusoidal output. A large number of cycles can be averaged to reduce noise. The output is commonly digitized and stored in memory in a small on-line computer. The components of magnetization in the plane normal to the rotational axis are then determined by Fourier analysis. A computer-controlled flux-gate spinner magnetometer is capable of measuring a rock magnetization around 5×10^{-5} A m^{-1} in standard samples under optimum conditions. The complete measurement of a sample takes only a few minutes.

The **cryogenic magnetometer** is the most sensitive and rapid instrument in current use. Its sensor consists of a coil immersed in liquid helium. At this temperature (4 K) the coil is superconducting. A small change of magnetic field induces a comparatively large current, which because of the superconducting condition is persistent until the sample is removed. In line with the coil is a Josephson junction, which is a quantum-mechanical device consisting of a very thin element that allows the passage of current in distinct units proportional to a quantum of magnetic flux. By counting the number of flux jumps electronically, the external magnetic field of the rock specimen can be inferred, and from this its magnetization computed. Most cryogenic magnetometers contain orthogonal sets of coils and can measure two or three axes of magnetization simultaneously within a few seconds. The sensitivity of the instrument corresponds to a rock magnetization of 5×10^{-6} A m^{-1} in standard samples.

5.6.3.2 Stepwise progressive demagnetization

The natural remanent magnetization (NRM) of a rock may contain several components, some related to the geological history of the rock and others to the sampling and handling procedures. It is necessary to "magnetically clean" the natural magnetization so that the structure of the NRM can be analyzed and stable components isolated. This is done in a stepwise procedure, in which progressively more and more of the original magnetization is removed. There are two main methods of doing this.

The first method is progressive *alternating field (AF) demagnetization*. An alternating magnetic field can be produced in a coil by passing an alternating current through it. The field fluctuates between equal and opposite peak values. When a rock sample is placed in the alternating magnetic field, the grain magnetic moments with coercivities less than the peak value of the field are remagnetized in a new direction; the field cannot affect a magnetization component with coercivity higher than the peak field. The

intensity of the alternating field is reduced slowly and uniformly to zero. This randomizes the part of the rock magnetization that has coercivities less than the peak value of the alternating magnetic field. The AF demagnetizing coil must be surrounded by magnetic shields or special additional coils to cancel out the Earth's magnetic field; otherwise an anhysteretic remanent magnetization (ARM) is induced along the direction of this field.

The part of the remanence that remains after a demagnetization treatment has been "magnetically cleaned." The direction and intensity of the remanent magnetization are affected. The demagnetization procedure is repeated using successively higher values of the peak alternating field, remeasuring the remaining magnetization after each step, until the magnetization is reduced to zero. Suppose that the NRM of a sample consists of two components AB and BC with different directions and different coercivity spectra (Fig. 5.56a, b). In the early stages of progressive demagnetization (steps 1–3) the "soft" component BC is first reduced to zero. The vector measured after each step in the progressive demagnetization is the sum of the "hard" component, which has not yet been affected by the field used, and the residual part of the soft component. If the direction of the soft component is within 90° of the hard component the intensity decreases during this demagnetization interval; otherwise it may increase (Fig. 5.56c). The direction of the resultant vector changes continually in steps 1–3 (Fig. 5.56d). After removal of the soft component in step 3, higher alternating fields (steps 4–7) progressively reduce the hard component AB. During this stage the intensity decreases constantly but the direction remains consistent with little scatter, defining the "stable end-point" direction of the magnetization.

The effectiveness of the AF demagnetization method is limited by the strongest peak field that can be produced in the demagnetizing coil. This is commonly 0.1 T, although some equipment can reach around 0.3 T. These peak fields are well below the maximum coercivity of pyrrhotite and far below the coercivities of hematite or goethite. Thus AF demagnetization is not effective in demagnetizing components carried by these minerals. The method is most commonly used for rocks that contain magnetite as the main magnetic mineral.

An alternative method of "magnetic cleaning" is progressive *thermal demagnetization*. When a rock sample is heated to a given temperature T, magnetic components that have lower blocking temperatures than T are thermally randomized. If the sample is now cooled in field-free space, this part of the NRM remains demagnetized. In stepwise thermal demagnetization the heating and cooling cycle is repeated with progressively higher maximum temperatures. The progressive destruction of the magnetization reveals the components present in the NRM as in Fig. 5.56. This method is often more effective than AF demagnetization, because it is only necessary to heat a sample above the highest Curie temperature of its constituent minerals to destroy all of the NRM. However, if the rock contains thermally unstable magnetic minerals, irreversible changes may complicate the thermal demagnetization method.

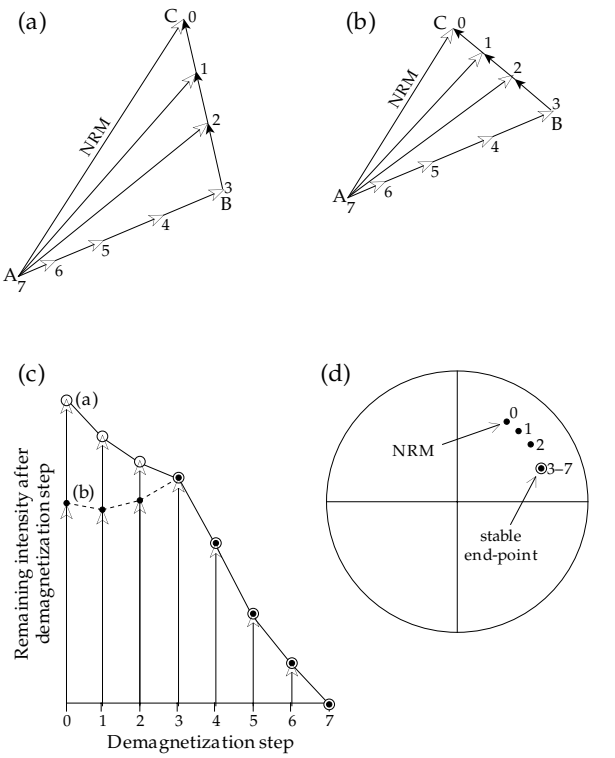

Fig. 5.56 Stepwise demagnetization of a remanent magnetization consisting of two components with different ranges of stability: (a) low stability vector BC demagnetizes before stable stable vector AB; (b) same situation with different angle between AB and BC; (c) variation of intensity for cases (a) and (b); and (d) directional changes on a stereogram. Numbers on points indicate successive demagnetization temperatures in °C.

5.6.3.3 Analysis of magnetization components

The stability of a remanent magnetization during stepwise demagnetization can be demonstrated by plotting the remaining intensity after each step against the corresponding temperature or AF field, as in Fig. 5.56c; the directional stability can be controlled simultaneously by plotting the direction after each step on a stereogram (Fig. 5.56d). However, analysis of magnetization with an intensity plot and stereogram is outmoded. More sophisticated methods treat the magnetization as a vector and analyze the stability of its individual components.

The most powerful method of analysis of the structure and stability of a remanent magnetization involves constructing a vector diagram. The method was introduced by J. D. A. Zijderveld, a Dutch paleomagnetist, in the early 1960s. The magnetization at each stage of demagnetization is resolved into north (N), east (E) and vertical (V) components. Plots are then made of the north component against the east component, and of a horizontal component (north or east) against the vertical component. This is equivalent to projecting the vector onto the

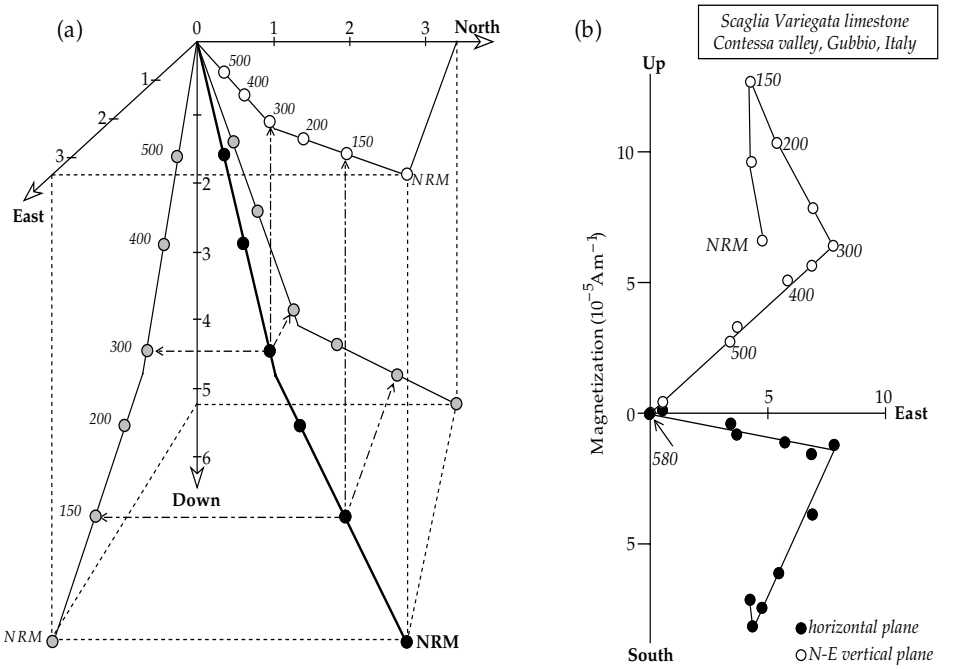

Fig. 5.57 The vector diagram method (Zijderveld, 1967) for analyzing progressive AF or thermal demagnetization. (a) Schematic diagram showing how the components of the vector remaining at each stage of demagnetization are projected as points on three orthogonal planes (horizontal, vertical N–S and vertical E–W). (b) Vector diagram for the thermal demagnetization of a limestone sample. Magnetization components with non-overlapping spectra of thermal blocking temperatures show as linear segments.

horizontal plane and the north–south (or east–west) vertical plane (Fig. 5.57a).

Components of NRM that have distinct spectra of coercivities or blocking temperatures show as linear segments on a vector demagnetization diagram. The example in Fig. 5.57b shows three distinct linear segments on the horizontal and vertical projections. The slopes of the straight lines represent NRM components with different directions. A component removed below 150 °C is directed downward to the north, and so has normal polarity. The component is probably a soft overprint (perhaps a VRM, see Section 5.3.6.5) acquired in the present day or a recent field. A vector removed between 150 °C and 300 °C may represent a more ancient overprint; it is directed in a southerly, upward direction and thus has a reversed polarity. If a stable vector is left after demagnetization of less stable fractions, it is indicated by a straight line to the origin of each half of the vector diagram. This is the case for the component removed from 300 °C to 580 °C. It is interpreted as a stable primary component acquired when the field had reversed polarity.

If more than one magnetization component is present, it is possible that the spectra of coercivity or blocking temperature of the components may overlap partially. During demagnetization of the overlapping components the vector diagram exhibits a curved trajectory. If the spectra overlap completely, no straight segment can be determined. In this case the sample does not have a single stable magnetization component.

5.6.3.4 Statistical analysis of paleomagnetic directions

For the purposes of statistical analysis each paleomagnetic direction in a collection of samples is considered to have equal value and may be regarded as a unit vector. Each vector has unit length but a different direction. The end points of the vectors lie on the surface of a unit sphere and form a distribution of points. The statistical methods for evaluating paleomagnetic directions (or the distribution of points on a sphere) were developed in 1953 by Sir Ronald Fisher. He found that the best estimate of the mean direction of a population of N unit vectors is their vector mean, R. To illustrate this point, consider five paleomagnetic directions, each represented by a unit vector (Fig. 5.58a). Usually the unit vectors are not parallel and when added vectorially their resultant has length $R \leq N$ (Fig. 5.58b); its direction is the best estimate of the mean of the five paleomagnetic directions.

Fisher proposed that the probability density $P(\theta, \kappa)$ of the angle θ between an individual sample direction and the mean direction of the distribution is:

$$P(\theta,\kappa) = \frac{\kappa}{4\pi \sinh \kappa} \exp(\kappa \cos\theta) \tag{5.60}$$

The parameter κ is called the "precision parameter" or "concentration parameter." It describes the dispersion of the directions, and is akin to the inverse of the variance of the distribution. Strictly speaking, κ is a property of an infinitely large population of directions. However, in paleomagnetic investigations only a small number of directions are usually sampled; it is assumed that they are representative for an infinite population. The parameters that are computed are approximate estimates of the true parameters of the population. Fisher showed that the best estimate (k) of the precision parameter κ (valid for $k > 3$) is given by

$$k = \frac{N-1}{N-R} \tag{5.61}$$

where R is the vector sum of the N unit vectors, computed as in Fig. 5.58b. When k (or κ) is zero, the directions are

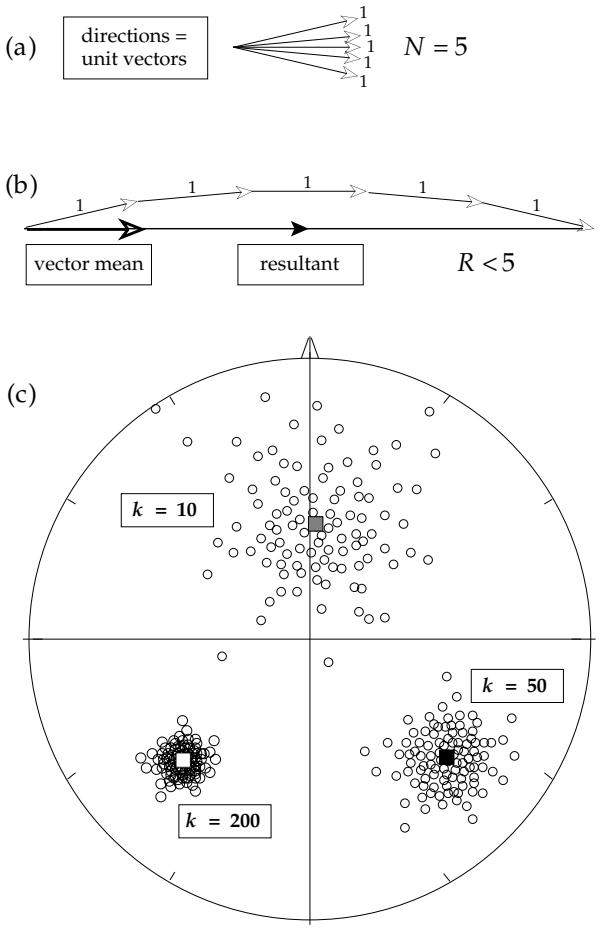

Fig. 5.58 (a) Representation of five magnetization directions as unit vectors. (b) The vector mean direction is that of the resultant vector **R**. (c) Stereograms of some distributions of paleomagnetic directions: the tighter the grouping, the larger the concentration parameter *k*.

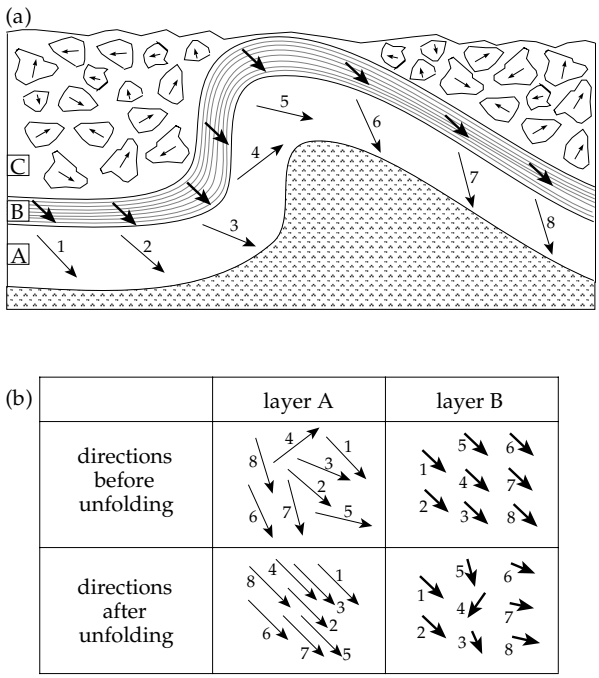

Fig. 5.59 (a) Magnetization directions (arrows) around a fold in stable (A) and unstable layers (B), and in stably magnetized conglomerate cobbles (C). (b) Comparison of directions in the stable layer (A) and unstable layer (B) before and after unfolding.

uniformly or randomly distributed. A badly scattered set of directions has a small value of k; large values of k apply to tightly grouped directions (Fig. 5.58c).

As in other statistical situations, the scatter is a property of the distribution of directions. It is described by the angular standard deviation, which is proportional to $1/\sqrt{k}$. However, it is usually more important to describe how well the mean direction is defined. Keep in mind that we do not know the true mean direction; we have only made an estimate of it, based on the available data. The true mean may differ by several degrees from our estimate. However, if we know that with 95% certainty the true mean lies within, say, 7° of our estimate, we can draw a cone with semi-angle of 7° about the estimated mean direction. The cone is said to define the confidence limits of the mean at the 95% probability level. The size of the confidence limit depends on the number of directions N in the distribution and their dispersion parameter k. The semi-angle of the cone of confidence is denoted α_{95} and is given approximately by

$$\alpha_{95} = \frac{140}{\sqrt{Nk}} \tag{5.62}$$

We could select any level of confidence to describe how well the mean is defined. However, two levels are common in statistics: the 95% (significant) and the 99% (highly significant) levels. In paleomagnetism the level of 95% confidence is used. This means that there is a 95% probability that the true mean of the distribution lies within this cone about the estimated mean direction.

5.6.3.5 Field tests of magnetization stability

If possible, paleomagnetic sampling includes a field test that can establish the stability of the magnetization over geological time. This was especially important in the early days of paleomagnetism when the laboratory techniques of "magnetic cleaning" were not yet available. Pioneering researchers devised some ingenious tests of paleomagnetic stability based on field observations. The fold test and reversals test still serve as the best ways to demonstrate the stability of a remanent magnetization through the aeons of geological time and to verify the timing of its acquisition.

The **fold test** is perhaps the most important paleomagnetic field test. It is applied to samples taken from beds that were originally horizontal and have been tilted by later tectonic effects. If the paleomagnetic direction in the rock is stable, it will experience the same rigid-body rotation as the tilted strata; its direction will vary around the fold (Fig. 5.59a, layer A). This is called a pre-folding magnetization. On the other hand, if the magnetization was acquired by the rock after it was folded, it will have a uniform direction at all points of the fold (Fig. 5.59a, layer B). This is called a

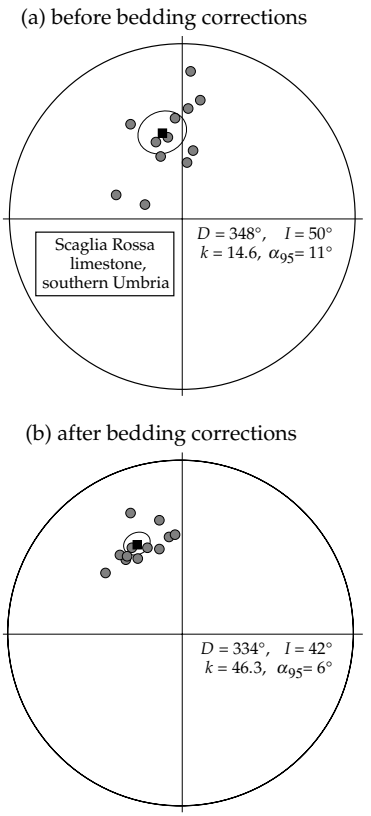

Fig. 5.60 Example of a positive fold test in 12 sites of the Scaglia Rossa limestone from southern Umbria. The directions (a) before correcting for local bedding tilt are more scattered than (b) the corrected directions.

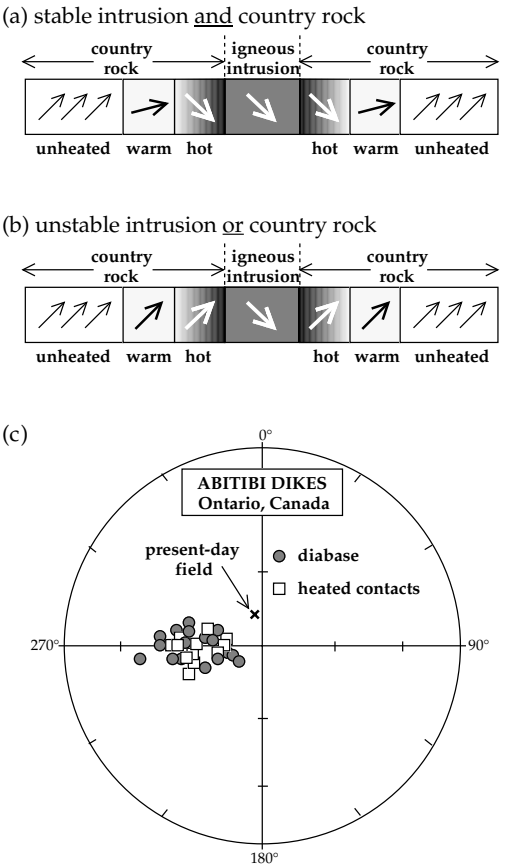

Fig. 5.61 The baked contact test. (a) Magnetization directions of intrusion and country rock when both are stable and (b) when one is unstable. (c) Example of a stable baked contact test for the Abitibi dikes, Ontario, Canada: the directions in the dikes are the same as in the baked country rock and are different from the present-day field direction (after Irving and Naldrett, 1977).

post-folding magnetization. A third situation is common, in which the magnetization is acquired during the tectonic event; in this case the direction of magnetization changes around the fold but by a smaller amount than the folding. This is called a synfolding magnetization.

In practice, the fold test consists of comparing the directions before applying tilt corrections with the directions after unfolding the tilted beds. If samples with a stable magnetization are taken from all parts of the fold, their uncorrected directions should be smeared out. After correction for bedding tilt, the dispersion of directions should be reduced, and the directions should group around a common direction, which is the pre-folding direction of the formation (Fig. 5.59b, layer A). This is called a positive fold test. If the magnetization is unstable or is due to post-folding remagnetization, the tilt corrections will increase the scatter of the distribution of directions (Fig. 5.59b, layer B); this is a negative fold test.

An application of the fold test is shown in Fig. 5.60 for 12 sites of the Scaglia Rossa limestone from the central Apennines in southern Umbria (Italy). The sites were collected on different limbs of long anticlinal structures. Mean directions were computed for about 10–12 "magnetically cleaned" samples at each site. The uncorrected directions are quite scattered, with a confidence cone (α_{95}) equal to 11°. After correcting each site for the local tilt of the bedding the data are much better grouped, and the confidence cone is reduced to 6°. The concentration parameter increases significantly, from 14.6 to 46.3, indicating that the magnetization was acquired before the folding.

The **conglomerate test** is a field test of stability that is rather seldom used. Suppose that we are investigating a limestone formation and that we discover a conglomerate containing cobbles of the limestone (Fig. 5.59a, layer C). Assuming that the cobbles have been randomly re-oriented by the processes of erosion, transport and re-deposition, their paleomagnetic directions, if stable, should be randomly distributed. If a systematic direction is found, the magnetization of the limestone may have a large secondary component.

The **baked contact test** is important in igneous rocks. During intrusion of a dike or sill the adjacent layers of the host rock are baked by contact with the hot lava and acquire a TRM when they cool. In general the magnetic minerals in the lava will differ in composition and grain size from those in the host rock. If samples taken from the lava and contact zone of the host rock have the same magnetization direction (Fig. 5.61a), the lava carries a stable paleomagnetic vector. If they are different (Fig. 5.61b), one of the magnetizations is unstable; alternatively, either

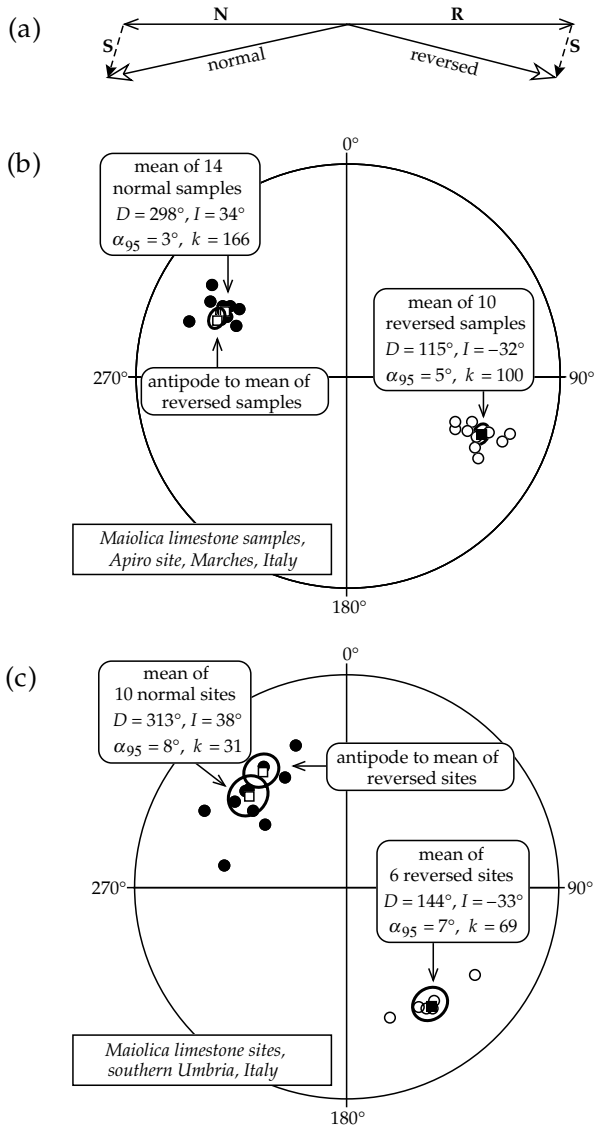

Fig. 5.62 The reversals test. (a) Illustration of how the presence of a secondary component **S** can spoil the anti-parallel directions of normal and reverse magnetizations. (b) A positive fold test for samples of the Maiolica limestone in a site at Apiro (Marches, Italy): the normal and reverse mean directions are almost exactly opposite. (c) Mean directions of normal and reverse polarity Maiolica sites in southern Umbria are not exactly opposite due to local tectonic rotations about vertical axes.

the lava or the baked zone was re-magnetized at a later time. An example of stable magnetizations in Precambrian rocks from the Canadian shield is shown by the agreement between the directions in the Abitibi diabase dikes and the heated contact zone (Fig. 5.61c).

The **reversals test** can be applied when the paleomagnetic samples represent a large enough time interval (>10 ka) to have recorded normal and reversed polarities of the magnetic field. Remanent magnetizations acquired within successive intervals of constant polarity of the Earth's magnetic field should be exactly antiparallel. Let the normal magnetization be represented by the vector **N** and the reversed magnetization by the vector **R** (Fig. 5.62a). The presence of an unremoved secondary component, represented by the vector **S**, will give resultant normal and reversed directions that are no longer antiparallel. If it is possible to clean the directions magnetically, the antipodal normal and reversed directions (**N** and **R**) should be recovered. If magnetic cleaning is inadequate, a residual part of the unremoved secondary component may spoil the antiparallelism.

An example in which the reversals test shows successful "cleaning" is shown in Fig. 5.62b for samples from a single site in the Early Cretaceous Maiolica limestone in central Italy. The vector mean of 14 normal samples has $D_{\mathbf{N}} = 298°$, $I_{\mathbf{N}} = 34°$, and $\alpha_{95} = 3°$; the mean of 10 reversed polarity samples has $D_{\mathbf{R}} = 115°$, $I_{\mathbf{R}} = -32°$, and $\alpha_{95} = 5°$. A simple way to compare how well the sets of normal and reversed polarity directions agree is to invert the mean direction and confidence circle for the reversed group of samples through the origin. The common polarity mean directions differ by only 3°. The mean of each group lies within the confidence limits of the other, so there is no significant difference between the normal and reversed directions.

When the site-mean directions from several sites of the Maiolica limestone are compared throughout a large region of the Umbrian Apennine mountain belt, the antiparallelism of sites with normal and reversed polarities no longer holds. The vector mean of 10 normal sites has $D_{\mathbf{N}} = 313°$, $I_{\mathbf{N}} = 38°$, and $\alpha_{95} = 8°$; the mean of six reversed polarity sites has $D_{\mathbf{R}} = 144°$, $I_{\mathbf{R}} = -33°$, and $\alpha_{95} = 7°$ (Fig. 5.62c). In this case the common polarity mean directions differ by 10°. The mean of each group lies outside the confidence limits of the other, so there is now a significant difference between the normal and reversed directions. Closer examination shows that the mean *inclinations I* of the normal and reversed groups are equivalent, but the *declinations D* are dispersed along a small circle about a vertical pole. The smeared declinations reflect small rotations of each site about a vertical axis, the result of regional tectonism in the area of investigation. This illustrates an important application of paleomagnetism: the description of tectonic rotations that would otherwise be difficult or impossible to observe in the field.

5.6.4 Paleomagnetism and tectonics

Paleomagnetism has made important contributions in documenting local and regional tectonic motions as well as the motions of lithospheric plates. The reason for the failure of the reversals test in Fig. 5.62c was ascribed to local tectonic disturbances within a region. To make use of paleomagnetic data on a larger scale the observed directions must be compared to suitable reference directions. A reference direction can be computed, if it is known where the paleomagnetic pole was in the geological past. The history of paleomagnetic pole positions can be established on a continental scale.

Paleomagnetic results from central and southern Europe document the effects of large-scale tectonics

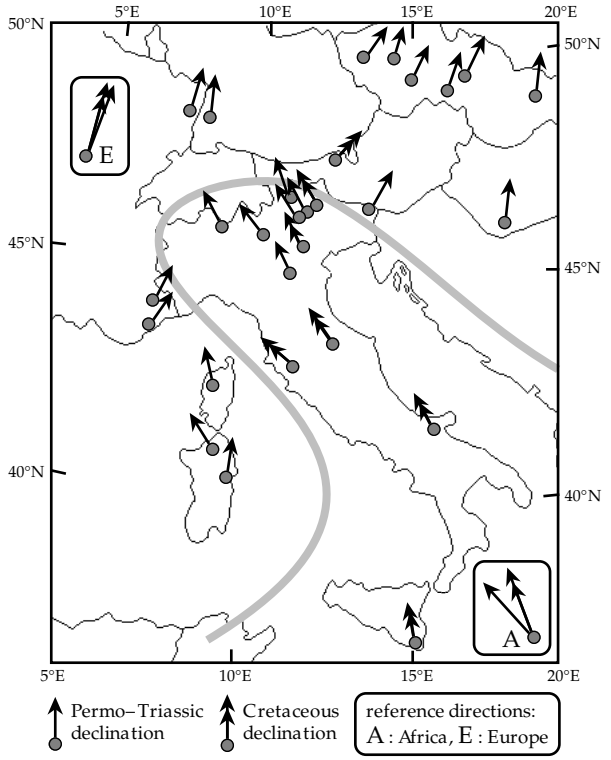

Fig. 5.63 Declinations of Permo-Triassic and Cretaceous rocks from Italy differ systematically from those of Europe north and west of the Alps, but agree well with directions predicted for the African plate. A hypothetical outline of the Adriatic promontory to the African plate is suggested by the shaded line.

(Fig. 5.63). Data of Late Paleozoic to Late Cretaceous age are represented in this analysis. During this long time interval large amounts of motion of the European and African plates have taken place. As a result the inclinations measured at the indicated sites show large variations. However, the reference declinations for sites in Europe do not vary much during this time; this is also true for the African reference declinations. There is a large difference between the north–northeast pointing European declinations and the northwest directed African declinations (Fig. 5.63). The paleomagnetic declinations observed at sites in central and southern Europe show distinct affinities. North and west of a crude line through the Alpine chain the paleomagnetic declinations agree with those expected for the European continent. The declinations observed south of the Alps, on the Italian peninsula and Sicily, are oriented toward the northwest, in agreement with directions expected for the African continent. The pattern of paleomagnetic data supports a tectonic interpretation of the Italian peninsula and adjacent regions of the Adriatic as a northern promontory of the African plate. Although the differences in the declination pattern are striking, there is a certain amount of leeway in the interpretation. This is mainly because the reference directions of Africa are derived from paleomagnetic pole locations that are not very well defined for some time intervals.

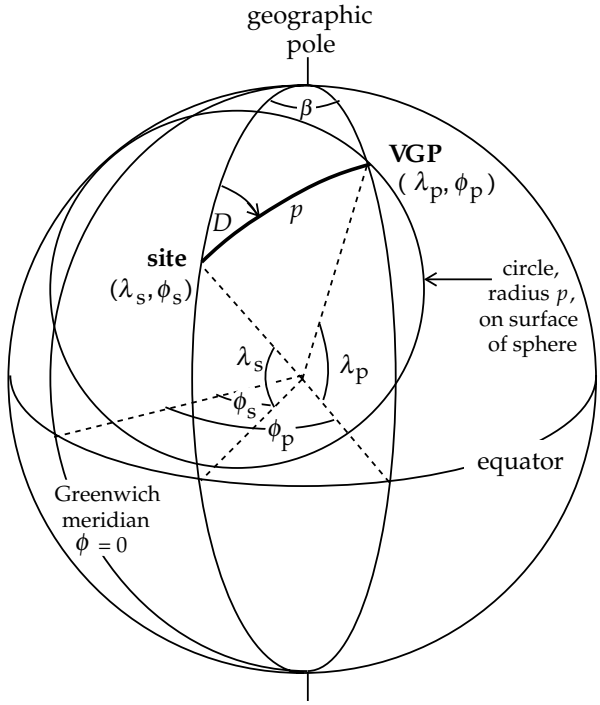

Fig. 5.64 Method of locating the virtual geomagnetic pole (VGP) from the declination *D* and inclination *I* measured at a site (after Nagata, 1961).

5.6.4.1 Location of the virtual geomagnetic pole

Paleomagnetic poles are computed as the average of virtual geomagnetic pole (VGP) positions calculated for a number of samples at a site. The VGP position is where the pole of a geocentric magnetic dipole would need to be in order to give the observed declination D and inclination I of the remanent magnetization measured in the sample. The method of computation of the VGP position is illustrated in Fig. 5.64. First, from the inclination of the magnetization (i.e., the paleofield) we can calculate how far away the VGP was at the time the rock magnetization was acquired. The angular distance to the pole p, assuming a dipole magnetic field, is obtained by using the relationship between inclination and polar angle (Fig. 5.54a).

The value of p determines the radius of a small circle centered on the paleomagnetic sampling site at latitude λ_s and longitude ϕ_s. The circle is the locus of all possible VGP positions that could give the observed inclination I at the site. We next have to decide which point on the small circle is the VGP position. The declination of the remanent magnetization is the angle between geographic north and the horizontal direction to the ancient magnetic pole. In this case the declination defines a meridian (or great circle) which passes through the sampling site and makes an angle D with the north–south meridian (Fig. 5.64). The place where this great circle intersects the small circle with radius p is the location of the virtual geomagnetic pole. Its latitude (λ_p) and longitude (ϕ_p) can be computed exactly from trigonometric formulas (Box 5.6):

$$\sin\lambda_p = \sin\lambda_s \cos p + \cos\lambda_s \sin p \cos D$$

Box 5.6: Virtual geomagnetic pole (VGP) location

The sine and cosine relationships between the sides and angles of spherical triangles (Box 1.4) may be applied to the spherical triangle in Fig. 5.64, its corners corresponding to the site, pole position (VGP) and geographic pole to determine the unknown latitude and longitude of the virtual paleomagnetic pole. The length of the side between the site and the geographic pole, measured in degrees of arc, is $(90–\lambda_s)$, where λ_s is the site latitude. The length of the side between the VGP position and the geographic pole is $(90–\lambda_p)$, where λ_p is the VGP latitude. The length of the third side of the triangle is p. The direction to the VGP position from the site is the declination D, which is opposite the side of length $(90–\lambda_p)$. These values are substituted in the law of cosines (Box 1.4, Eq. (4)) as follows:

$$a = (90 - \lambda_p) \quad \cos a = \sin\lambda_p$$
$$b = (90 - \lambda_s) \quad \cos b = \sin\lambda_s \quad \sin b = \cos\lambda_s \qquad (1)$$
$$c = p \quad A = D$$
$$\sin\lambda_p = \sin\lambda_s\cos p + \cos\lambda_s\sin p\cos D \qquad (2)$$

The great circles through the site and the VGP location meet at the geographic pole where they form an angle, for which there are two possibilities: the acute angle β, or its obtuse equivalent $(180 – \beta)$. As a result, the solution for the longitude ϕ_p of the paleomagnetic pole involves two steps.

First, applying the law of sines (Box 1.4, Eq. (3)) to the spherical triangle gives

$$\frac{\sin\beta}{\sin p} = \frac{\sin D}{\sin(90 - \lambda_p)} \qquad (3)$$

from which the magnitude of the angle β may be obtained

$$\sin\beta = \frac{\sin p \sin D}{\cos\lambda_p} \qquad (4)$$

Next, in order to decide whether the solution requires β or $(180 – \beta)$, the law of cosines is again applied to the spherical triangle, this time for side p, with the following substitutions:

$$a = p \quad A = \beta$$
$$b = (90 - \lambda_s) \quad \cos b = \sin\lambda_s \quad \sin b = \cos\lambda_s \qquad (5)$$
$$c = (90 - \lambda_p) \quad \cos c = \sin\lambda_p \quad \sin c = \cos\lambda_p$$

These give

$$\cos p = \sin\lambda_s\sin\lambda_p + \cos\lambda_s\cos\lambda_p\cos\beta \qquad (6)$$
$$(\cos p - \sin\lambda_s\sin\lambda_p) = \cos\lambda_s\cos\lambda_p\cos\beta \qquad (7)$$

On the right-hand side of Eq. (7), $\cos\lambda_s$ and $\cos\lambda_p$ are always positive, so $\cos\beta$ must take the sign of the left hand side of the equation. This gives the two possibilities for the value of $(\phi_p - \phi_s)$, namely, β or $(180 – \beta)$. Thus,

$$(\phi_p - \phi_s) = \beta \quad \text{for } (\cos p - \sin\lambda_s\sin\lambda_p) \geq 0$$
$$(\phi_p - \phi_s) = 180 - \beta \text{ for } (\cos p - \sin\lambda_s\sin\lambda_p) < 0 \qquad (8)$$

$$\phi_p = \phi_s + \beta, \quad \text{for} \quad \cos p \geq \sin\lambda_s\sin\lambda_p$$
$$\phi_p = \phi_s + 180 - \beta, \quad \text{for} \quad \cos p < \sin\lambda_s\sin\lambda_p \qquad (5.63)$$

where

$$\sin\beta = \frac{\sin p \sin D}{\cos\lambda_p} \qquad (5.64)$$

The longitude of the paleomagnetic pole is here given relative to a fixed meridian in present-day geographic coordinates. The key paleomagnetic parameter is the distance p of the investigated site from the Earth's rotation axis, which was the position of the paleomagnetic pole at the time of formation of the rocks under investigation. At the time of magnetization all locations on the same latitude (i.e., at the same distance p from the rotation axis) were magnetized with zero declination, because the axial dipole field lines through the site lead to the rotation axis. The longitude of the site (its position on the circle of latitude) remains indeterminate. The declination measured later at the site is the expression of any change of azimuthal orientation, which can result, for example, from local tectonic motion or from large-scale continental displacement.

5.6.4.2 Apparent polar wander paths

The observation that paleomagnetic poles obtained from rocks of Pleistocene and Pliocene age are closely grouped about the geographic pole (see Fig. 5.55) is in agreement with the axial geocentric dipole hypothesis. However, when paleomagnetic pole positions are calculated for old rocks from the same continent, they group far away from the geographic pole. This is illustrated by the positions of paleomagnetic poles from the stable European craton. Pliocene and Pleistocene poles group close to the geographic pole but Permian poles are located about 45° away (Fig. 5.65). If the axial dipole hypothesis is valid for rocks of all ages, the pole distributions imply that the geographic pole for Europe in the Permian period (about 250–290 Ma ago) lay far from its present position. An alternative interpretation is that the geographic pole has not changed, but the European continent has moved relative to the pole. This suggests that the position about which the Permian poles now cluster was on the rotation axis in the Permian period. The European continent has subsequently moved to its present-day position with regard to the rotation axis.

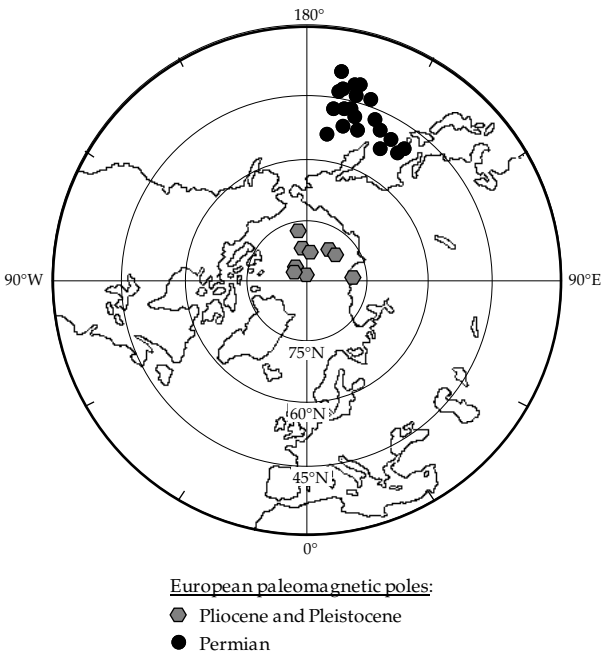

Fig. 5.65 Locations of European paleomagnetic poles. Pliocene and Pleistocene poles (data source: McElhinny, 1973) lie close to the present-day geographic pole, while Permian poles (data source: Van der Voo, 1993) are located at about 45°N in the northwest Pacific Ocean.

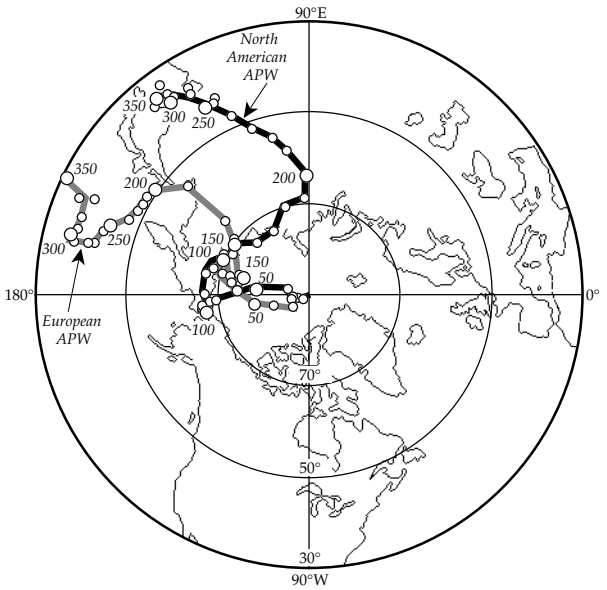

Fig. 5.66 Average apparent polar wander paths for North America and Europe in the past 350 Ma (after Irving, 1977). Numbers on paths are age in Ma.

Paleomagnetic data allow us to resolve the ambiguity. If paleomagnetic pole positions are computed for rocks of different ages from the same continent, they plot systematically along an irregular, curved path. It appears as though the paleomagnetic pole has moved slowly along this path towards the present rotation axis. The apparent motion of the paleomagnetic pole is called *apparent polar wander* (APW) and the path is called an *apparent polar wander path*. The paleomagnetic data from a particular continent define a unique APW path for that continent, and each continent has a different APW path. Thus, we have a European APW path, African APW path, North American APW path, and so on.

A schematic plot of the European and North American APW paths since the Late Paleozoic shows clearly distinct curves (Fig. 5.66). Each APW path lies on the opposite side of the geographic pole from the continent to which it belongs. Keeping the axial geocentric dipole hypothesis in mind, it is obviously impossible that the paleomagnetic pole (i.e., the Earth's rotation axis) could have moved simultaneously along two different APW paths. The two APW paths evidently represent the separate motions of the European and North American continents relative to the rotation axis. They constitute paleomagnetic evidence for "continental drift."

5.6.4.3 Paleogeographic reconstructions using APW paths

A more detailed plot of the two APW paths for the time before the Late Jurassic (Fig. 5.67a) shows strong similarities in their shapes, particularly for the time from the Upper Carboniferous to the Upper Triassic. It is possible to overlay these two segments of the APW paths by moving Europe (including Russia west of the Ural mountains) and North America into different positions relative to each other (Fig. 5.67b). For the time represented by the overlap of the APW paths the two continents formed part of a larger "supercontinent," called *Euramerica*. When the adjacent part of Asia east of the Urals is included, the continents in the northern hemisphere form an earlier landmass called *Laurasia*. The present separation of the APW paths (Figs. 5.66, 5.67a) is interpreted as evidence for relative plate tectonic motion between Europe and North America that has taken place since the end of the interval for which the APW paths overlap well, i.e., since the Early Jurassic.

In order to bring the two APW paths into coincidence we have to move Europe relative to North America (or vice versa) so as to close the present gap between the continents. As shown in Section 1.2.9, the relative motion of plates on the surface of the spherical Earth is equivalent to a relative rotation about an *Euler pole of rotation*. The computer-generated "Bullard" fit of the 500 fathom contour lines on opposites sides of the North Atlantic ocean (see Section 1.2.2.2) can be obtained by displacing Europe toward North America by a clockwise rotation through 38° about the Euler pole located at 88.5°N 27.7°E, which by coincidence is very close to the present-day geographical pole (Fig. 5.67a). The APW path of a continent is constrained to move with the continent. If the European APW path is also rotated by 38° clockwise about the same Euler pole, the observed overlap of the Upper Carboniferous to Upper Triassic sections of the European and North American APW paths is obtained. Later segments of the paths diverge, indicating relative

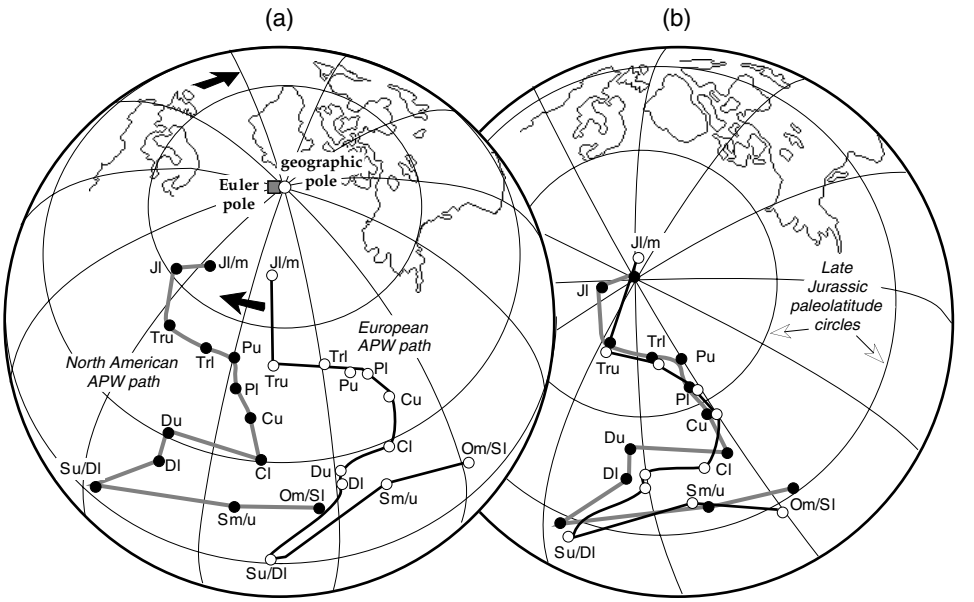

Fig. 5.67 (a) The Ordovician to Jurassic segments of the North American and European APW paths. (b) The same APW paths after rotating Europe by 38° clockwise about the Euler rotation pole at 88.5°N 27.7°E, marked by the square symbol in (a) (after Van der Voo, 1990).

motion between the continents. The Late Jurassic pole position corresponds to the Earth's rotation axis at that time. Circles of paleolatitude about the North American paleomagnetic pole emphasize the paleogeographic reconstruction of the relative positions of Europe and America in the Late Jurassic.

The interpretation of APW paths is not always as clear-cut as in this example. Consider the situation of the paleomagnetic pole P for continental plate C, which is rotated through an angle Ω about the Euler pole of rotation, E. First, let the plate lie between the paleomagnetic pole and the rotation pole (Fig. 5.68a). The rotation of the plate from C to C′ causes the paleomagnetic pole P to move to P′. The arc PP′ of the polar motion is longer than the arc CC′ of the true plate motion. Next, consider what happens when the paleomagnetic pole lies between the plate and the Euler pole (Fig. 5.68b). In this case the plate moves through a large distance but the paleomagnetic pole moves only a small distance. In the extreme case where the paleomagnetic and Euler poles coincide, the plate rotation does not move the paleomagnetic pole at all. Under these special conditions plate motion leaves no trace in the APW path of the plate.

Clearly, the interpretation of an APW path as a record of plate motion relative to the geographic axis must be made with caution. The rate of motion of the pole along an APW path cannot be simply equated with the rate of motion of the parent continent or global plate. It follows that similarity of APW paths does not imply a unique solution for former relative plate positions. However, if two continents once belonged to the same plate for some length of time, they should have acquired the same APW path for this time. Matching the present APW paths of the continents for the time they were on the same plate should give a unique reconstruction of the earlier positions of the continents relative to each other. To avoid

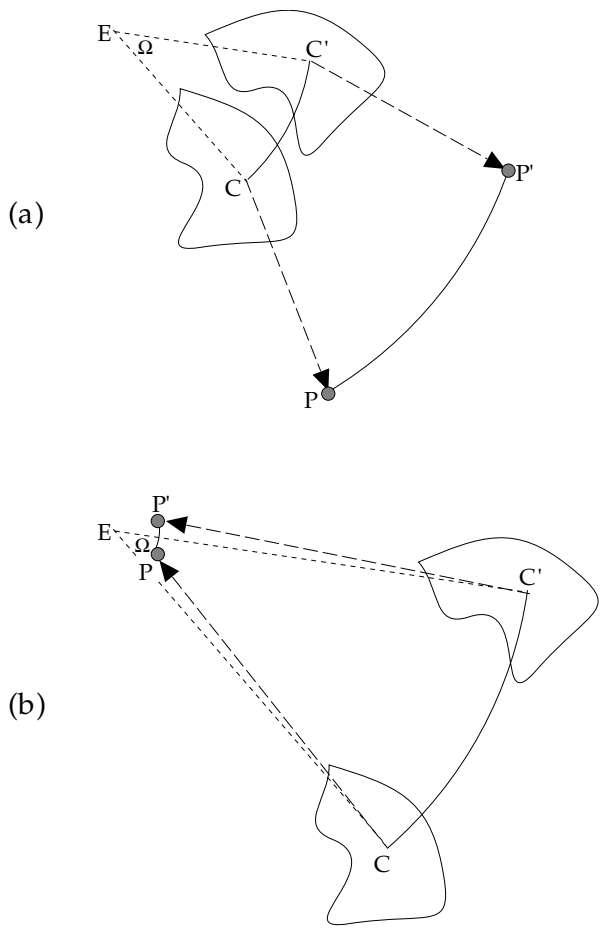

Fig. 5.68 Rotation of a continental plate C about an Euler pole E displaces the paleomagnetic pole P (a) by a large amount, if P is further from E than the continent C, and (b) by only a small amount when P lies close to E.

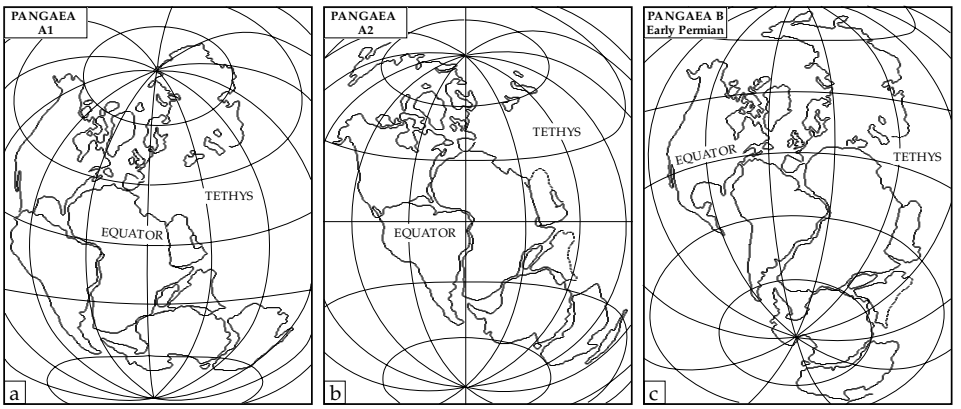

Fig. 5.69 The configurations of Pangaea models A1, A2 and B based on the matching of coastlines and the optimizing of paleomagnetic data (after Morel and Irving, 1981).

ambiguities, additional independent evidence (such as paleoclimatic data, or computer matching of coastlines) must be utilized in conjunction with paleomagnetic data for making such reconstructions.

5.6.4.4 Paleomagnetism and continental drift

The nineteenth century geologist Eduard Suess deduced the existence of a great Late Paleozoic continent, which he called Gondwanaland (Section 1.2.1). It was composed of Africa, Antarctica, Arabia, Australia, India and South America. In 1912, Wegener went a step further by postulating that all the present continents lay close together during the Late Paleozoic, forming a single great continent that he called Pangaea. Wegener's concept was based on paleoclimatic evidence, the matching of Carboniferous coal belts and of regions of Paleozoic glaciation in the different continents. Subsequently, additional geological evidence for the existence of Gondwanaland and Pangaea during the Late Paleozoic and Early Mesozoic accumulated from the fields of sedimentology, paleontology and tectonics. The earlier great continents were presumed to have dispersed to their present-day location by the process of *continental drift*. Unfortunately, Wegener was unable to offer a satisfactory driving mechanism for continental drift, and some of his ideas were found to be extreme. Scepticism among geophysicists and geologists brought Wegener's theories into disrepute.

Interest in continental drift was re-awakened in the 1950s by the development of paleomagnetism. Soon thereafter some of the most convincing paleomagnetic evidence for continental drift was obtained from the "southern continents." Researchers found that Mesozoic paleomagnetic pole positions of the same age from these continents were very dissimilar. In landmark contributions E. Irving showed that the paleomagnetic poles of the southern continents were incompatible with the present-day arrangement of these continents, but that they agreed much better when the continents were rearranged to conform with a Gondwanaland reconstruction. Numerous paleomagnetic investigations have subsequently provided a rich database that can be used to test the validity of reconstructions of former great continents at different times in their history.

The reconstructions are generally not made on paleomagnetic evidence alone. Usually, a model is proposed, based on geometrical or geological grounds. The congruity of paleomagnetic pole positions from the separate continents is then evaluated in their reconstructed positions. The model is adjusted iteratively until a configuration of the continents is obtained that gives minimum dispersion of the paleomagnetic poles.

The evaluation of paleomagnetic data from the Gondwanic continents, North America and Europe lends convincing support to the reconstructions and thereby to the continental drift hypothesis. From the Carboniferous to the Triassic, contemporary paleomagnetic poles from the individual continents do not agree when the continents are in their present positions, but are more consistent when the great continent is reconstructed. In fact, the paleomagnetic data are of high enough quality to suggest refinements to the purely geometric reconstructions. The Pangaea model in Fig. 5.69a corresponds closely to computer-assisted matches of the continental coastlines (see Section 1.2.2.2); it is referred to as Pangaea A1. It places the east coast of North America adjacent to the coast of northwest Africa. This configuration is supported well by Late Triassic and Early Jurassic paleomagnetic poles. It is the generally accepted model of Pangaea immediately prior to its breakup in the Early Jurassic. However, older paleomagnetic data of Permian and Carboniferous age (around 280 Ma) are less compatible with the Pangaea A1 model. Results of Late Permian to Middle Triassic age agree much better with a configuration referred to as Pangaea A2 (Fig. 5.69b), first proposed by R. Van der Voo and R. French in 1974. In this model, North America is much closer to South America and its eastern coast is opposite to western Africa. The transition from the Late Permian Pangaea A2 to the Late Triassic Pangaea A1 configuration requires a large dextral shear between the continents in this time interval.

Pangaea may have had yet another configuration earlier in its history. In 1977 E. Irving showed that results of Carboniferous and Early Permian age agree better for a Pangaea configuration in which the east coast of North America is adjacent to the west coast of South America (Fig. 5.69c). This model, Pangaea B, is possible because

paleomagnetic longitudes are much more poorly constrained than paleolatitudes. The change from Early Permian Pangaea B to Late Permian Pangaea A2 requires a huge dextral megashear between Laurasia and Gondwana.

The models Pangaea A1, A2 and B are each consistent with paleomagnetic data for the different times of the reconstructions, which span about 100 Ma. None of the models accounts for the apparent polar wander paths of the individual continents over the whole interval of time from Early Permian to Late Triassic or Early Jurassic. Instead, the differences between the models imply that Pangaea was not a static great continent for this entire time interval, but that internal motions took place between the constituent continents.

Paleomagnetic data can be used to reconstruct the relative positions of continents during any time interval with enough good paleomagnetic data. APW paths (e.g., Fig. 5.66) can be determined fairly precisely by averaging the best available pole positions in 20–40 Ma time windows. Optimum fitting of APW paths of different continents allows reconstructions to be made for the time represented by the matching segments (Fig. 5.67). When this procedure is applied to paleomagnetic data covering the last 375 Ma, a picture of continental drift since the Middle Devonian is obtained (Section 1.2.2.3). According to this scenario, the supercontinents Laurasia and Gondwana, which were still separated by the Hercynian Ocean (Fig. 5.70) in the Devonian, collided in the Carboniferous to form Pangaea. The paleomagnetic reconstruction of continental drift for older epochs becomes tenuous because reliable paleomagnetic data become scarcer. The derivation of durable reconstructions for the Early Paleozoic and Precambrian will be a long and painstaking process.

The positions of continents since the breakup of Pangaea can also be obtained from analysis of APW paths. However, more precise reconstructions can be made by using a different form of paleomagnetic data, namely the record of geomagnetic polarity. Sea-floor spreading has imprinted this record in the oceanic crust, creating lineated magnetic anomalies. Matching coeval anomalies allows us to trace the motions of the lithospheric plates since the Middle Jurassic and describe the drift of the continents which they transport.

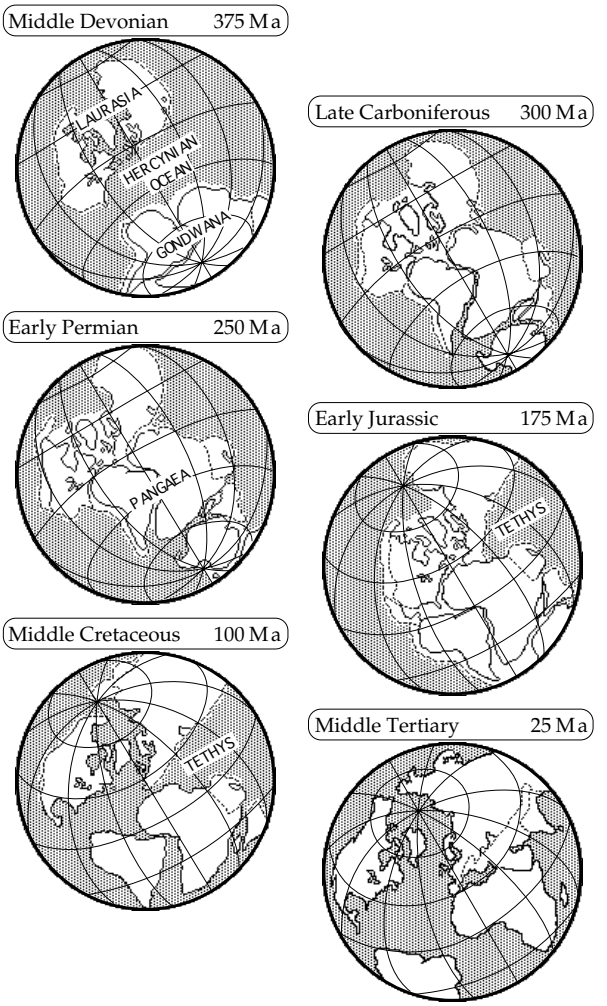

Fig. 5.70 Continental drift since the Devonian is illustrated by reconstructions of the positions of the major continental blocks at different times based on paleomagnetic data (after Irving, 1977).

5.7 GEOMAGNETIC POLARITY

5.7.1 Introduction

The earliest demonstration that the geomagnetic field has changed polarity in the past was made by the French scientists P. David and B. Brunhes. In 1904–6 they described the magnetic properties of young lava flows in the Massif Central region of France. They found that clays baked by the lava flows had the same direction of remanent magnetization as the lavas. Moreover, when the magnetization direction in the lava was opposite to that of the present-day field, the same was the case in the baked clay. The opposite polarities were interpreted as evidence that the geomagnetic field can reverse its polarity.

A Japanese scientist, M. Matuyama, was the first to associate the polarity of remanent magnetization in lavas with their age, determined stratigraphically. In 1929 he reported finding young Quaternary lavas with magnetization directions close to the present-day field direction, whereas the directions in older Quaternary and Pleistocene lavas were clustered about an antipodal direction. He also found that one of three samples of Miocene basalt was magnetized oppositely to the other two. Matuyama's interpretation was that geomagnetic polarity had changed several times during Late Tertiary time.

The idea that geomagnetic polarity could change was controversial, and for many years sceptics sought alternative interpretations. Scientists realized that the observed reversed polarities might have a mineralogical explanation. Indeed, some ferromagnetic minerals, because of their

composition and structure, can acquire a thermoremanent magnetization exactly opposite to the field direction. This mechanism is called self-reversal of magnetization. It has been described in lavas in which the ferromagnetic minerals are particular forms of titanohematite. Fortunately, it is a rather rare phenomenon. Most records of polarity reversals have been found to be a feature of the geomagnetic field.

To envisage what a reversal of geomagnetic polarity means, imagine that the geomagnetic dipole inverts its direction. At present the axial geocentric dipole points from the northern hemisphere towards the southern hemisphere; a polarity reversal would orient the dipole in the opposite direction. At each point on the surface the magnetic inclination I changes sign and the declination D changes by 180°; for example, a normal direction $\{I = 40°, D = 30°\}$ might change to a reverse direction $\{I = -40°, D = 210°\}$. A polarity reversal is a global event, experienced simultaneously all over the Earth. Thus, geomagnetic reversals provide a convenient means of stratigraphic correlation and dating.

5.7.1.1 Geomagnetic polarity transitions

The change of polarity from one sense to the opposite one is called a *polarity transition*. Paleomagnetic records of polarity transitions have been observed in radiometrically dated lava sequences and in deep-sea sediments with known deposition rates. These records indicate that the duration of a polarity transition is about 3.5–5 ka. This is much shorter than the length of the interval of constant polarity before or after the transition, which may last for hundreds of thousands or millions of years.

It is not yet known for sure how the geomagnetic field behaves during a polarity transition. The dipole field is dominant before and after a transition, but it is not certain that this is the case during the transition. Detailed analyses of field behavior during a polarity transition usually show a notable decrease in field intensity (Fig. 5.71); this is observed in volcanic and sedimentary records of reversals. Possibly the dipole component disappears, granting more importance to higher-order quadrupole or octupole field configurations. There seems to be stronger evidence that, even though its intensity decreases, the transitional field is still dominantly that of a dipole. If this can be assumed, the position of the virtual geomagnetic pole (VGP) of the transitional dipole field can be calculated. During a polarity transition the VGP position changes progressively. It appears to move systematically relative to the Earth's rotation axis, defining a path from one polar region to the opposite one. The transitional paths of many reversals appear to define two longitudinal belts, one over the Americas and an antipodal belt over Southeast Asia. However, many other transitions do not pass over these two belts. It has not been established conclusively that a path over the Americas or Southeast Asia is a preferred feature of polarity transitions.

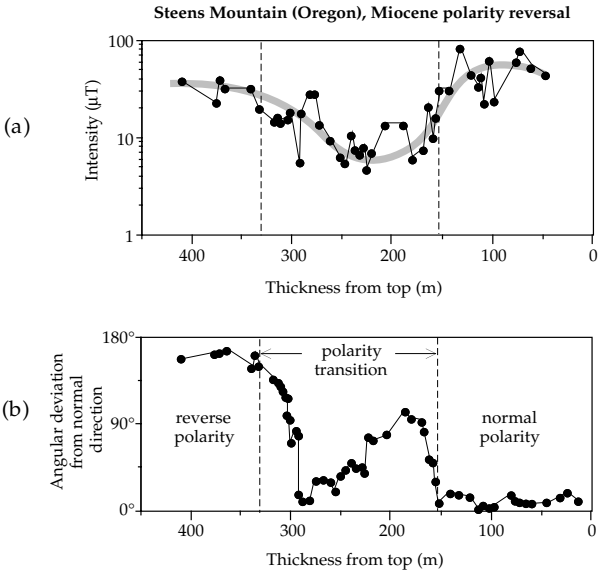

Fig. 5.71 The record of a reversed-to-normal Miocene polarity transition at Steens Mountain, Oregon. (a) The paleointensity record during the transition and (b) the directional record, shown as the angular deviation from the normal paleomagnetic direction outside the transition (after Prévot *et al.*, 1985).

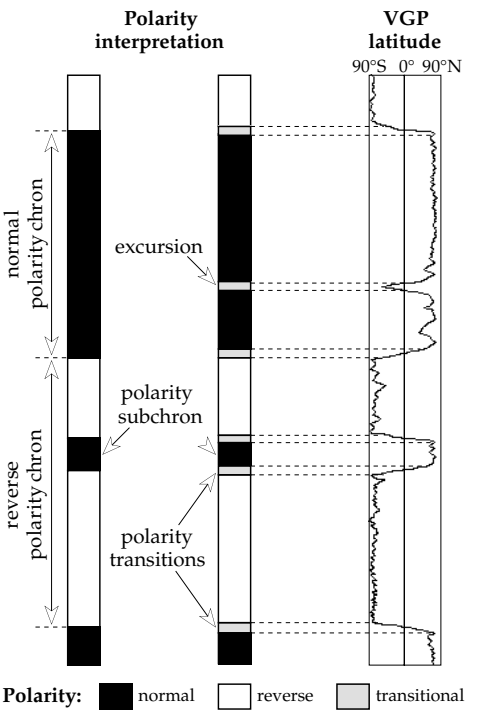

Fig. 5.72 Definition of polarity chrons, subchrons and transitions (modified after Cox, 1982, and Harland *et al.*, 1990).

5.7.1.2 Geomagnetic polarity intervals

Long intervals of constant normal or reversed polarity, originally called polarity *epochs*, are referred to as *polarity chrons* (Fig. 5.72); they last typically from 50 ka to 5 Ma. The polarity chrons are interrupted at irregular intervals by shorter *polarity subchrons* (originally called *events*) lasting for 20–50 ka. At times the polarity record

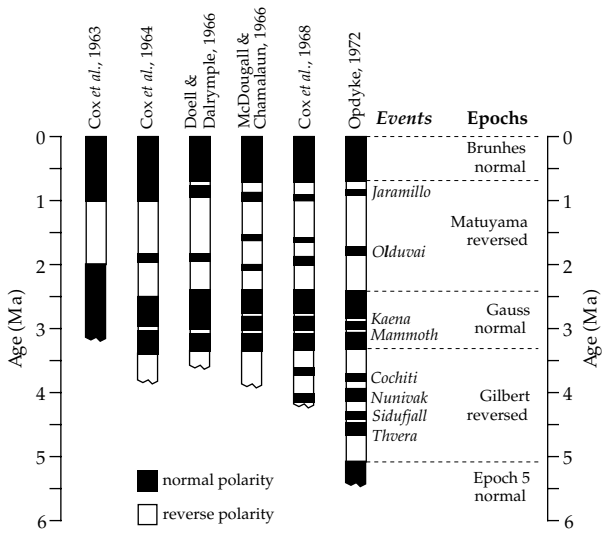

Fig. 5.73 Progressive evolution and refinement of the magnetic polarity timescale.

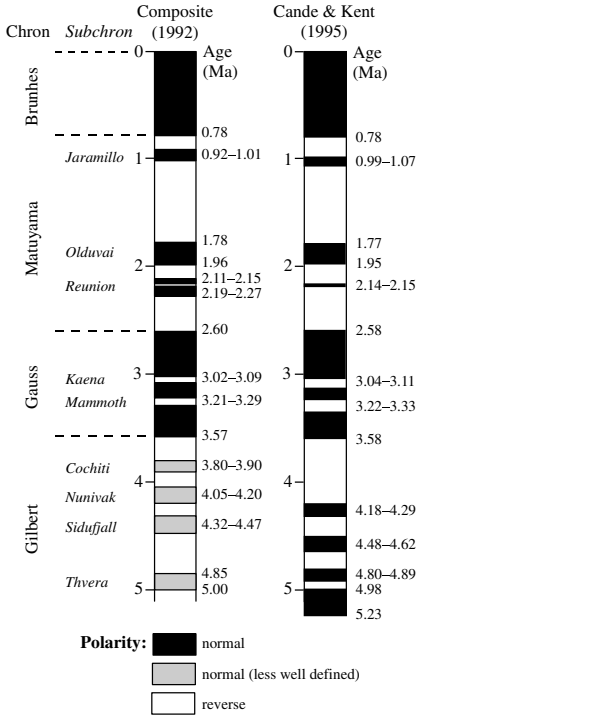

Fig. 5.74 *Left*: a composite radiometric timescale for the past 5 Ma, compiled from several sources (Mankinen and Dalrymple, 1979; Spell and McDougall, 1992; McDougall *et al.*, 1992). *Right*: a polarity timescale for the same time interval obtained from marine magnetic anomalies, dated by correlation to radiometrically dated tie-points as well as by astrochronological ages based on Milankovitch cyclicities (Cande and Kent, 1992, 1995).

shows large departures of the magnetic pole from normal or reversed polarity, but the polarity does not change completely; the pole wanders into equatorial latitudes but returns to its initial location on the rotation axis. The departure is short lived, lasting less than 10 ka, and the phenomenon is called a magnetic *excursion*. The irregular pattern of polarity intervals in any sequence provides a kind of geological fingerprint which can be used under favorable circumstances to date and correlate some types of sedimentary rocks. This procedure is called magnetic polarity stratigraphy, or *magnetostratigraphy*.

5.7.2 Magnetostratigraphy in lavas and sediments

In the 1950s the methods of dating rocks took a giant step forward with the development of improved techniques for dating rocks radiometrically. The potassium–argon method (Section 4.1.4.4) was applied to the determination of accurate ages for Pliocene and Pleistocene lava samples from flows that were also sampled for paleomagnetic purposes. The polarity of the thermoremanent magnetization of the lava was found to correlate with its age. There were distinct intervals of time in which the field polarity was the same as at present, and these were separated by intervals of exactly opposite polarity. At first the data were sparse, and in the earliest interpretations it was thought that the field changed polarity quite regularly, roughly once every million years (Fig. 5.73). Gradually, however, a more complex history evolved. Long *epochs* of a given polarity were found to contain much shorter *events* of opposite polarity. The polarity epochs were named after important investigators of paleomagnetic polarity (Brunhes, Matuyama) and geomagnetism (Gauss, Gilbert) while the polarity events were named after the geographical location where they were first discovered (Jaramillo creek in New Mexico, Olduvai gorge in Africa, etc.). Countless studies of magnetic polarity in radiometrically dated lavas have established the history of geomagnetic polarity in the last 5 Ma (Fig. 5.74). If the polarity record in a rock sequence can be identified, its age can be determined by comparison with the dated sequence. For this reason a dated polarity sequence is called a *geomagnetic polarity timescale*.

There is a practical limit to the application of this technique. As can be seen by quick inspection, some of the polarity events last less than 50 ka. If a reasonable precision of 1–2% is assumed for potassium–argon dating, the error in determining the age of a lava sample that is about 5 Ma old amounts to 50–100 ka. This is longer than the duration of many short events. The dating error makes it impossible to associate the lava sample unambiguously with the correct polarity event. Extension of the magnetic polarity timescale beyond 5 Ma requires other methods.

In the middle 1960s the polarity record from lavas was augmented by a large amount of high-quality data acquired from young deep-sea sediments. The deep ocean basins provide a tranquil depositional environment, where sediments are deposited at rather uniform rates. Marine geologists routinely take cores of sediment with a special coring device (see Fig. 4.26) for sedimentological, geophysical and paleontological studies. The magnetostratigraphy

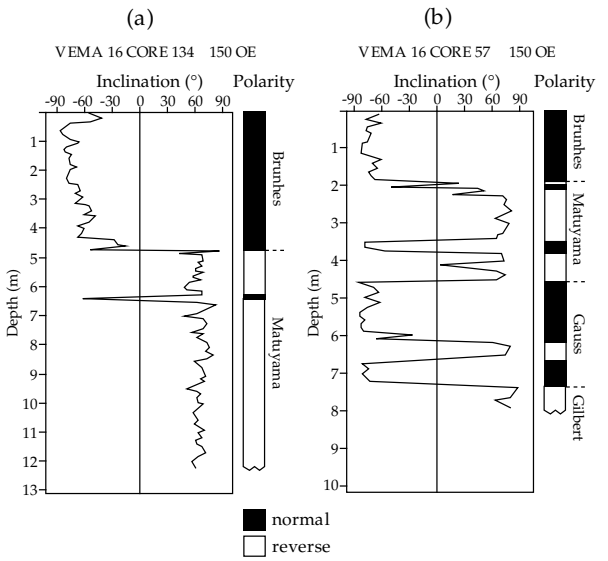

Fig. 5.75 Variations in magnetic inclination and inferred polarity with depth in two deep-sea sediment cores (based on data from Opdyke *et al.*, 1968).

of a core is studied by measuring the direction of magnetization in small oriented samples from different depths in the core. Although deep-sea cores have vertical axes, they are not oriented in azimuth, so the declinations can only be determined relative to an arbitrary reference value. Polarity determinations are often based only on the inclination records. The boundaries between normal and reverse magnetozones are interpolated at the depths where the inclination is zero (Fig. 5.75). In equatorial cores, where inclinations are nearly zero, the relative changes in declination often give a good polarity record. The polarity records of numerous cores correlate well with the sequence found in contemporaneous young lavas. The sediment magnetic polarity records are independent of lithology; the same reversal occurs at different depths from core to core because of different sedimentation rates (Fig. 5.76). By correlating reversals with the radiometrically dated lava record, the sediment ages at the reversal depths are obtained. From the depths and ages it is a simple matter to calculate the incremental sedimentation rates in the core. In addition to providing sedimentation rates, magnetic polarity stratigraphy also yields the absolute ages of the first and last appearances of key fossils, and so gives absolute dates for paleontological fossil zones. A recent innovation is the use of astrochronology, based on the identification of Milankovitch cycles (Section 2.3.4.5), to provide refined dating of sediments and their polarity record.

The magnetostratigraphic data from deep-sea sediment cores eliminated the lingering doubt that reversals observed in lavas may be due to a self-reversal mechanism. Lavas and sediments acquire their magnetizations by quite different mechanisms; the thermoremanent magnetization of a lava is acquired rapidly during cooling from high temperature, whereas the depositional or post-depositional remanent magnetization in a sediment is acquired slowly at constant ambient temperature. Although a self-reversal mechanism might be invoked to cast doubt on polarity changes in lavas, the argument is invalid for the remanence of deep-sea sediments. The common polarity sequence in lavas and sediments can only be explained as a record of the alternations of polarity of the Earth's magnetic field. Moreover, the same pattern of reversals is found regardless of geographical location, emphasizing that reversals are a global phenomenon.

5.7.3 Marine magnetic anomalies and geomagnetic polarity history

The striped magnetic anomaly patterns formed at oceanic ridges contribute to the compelling geophysical evidence in favor of the theory of global plate tectonics (see Section 1.2.5). Marine magnetic surveys and independent investigations of the rock magnetic properties of marine rocks and sediments have identified the source of the magnetic anomalies to be the basaltic Layer 2A of the oceanic crust.

Seismic evidence indicates that the oceanic crust has a vertically stratified structure (see Fig. 3.85). The uppermost part, seismic Layer 1, consists of a layer of slowly accumulating marine sediments; the thickness of the sediments increases progressively away from the ridge crest. The sediments are so weakly magnetic that they are essentially transparent to the Earth's magnetic field. The seismic Layer 2A consists of a 500 m thick layer of oceanic basalts that are extruded as submarine lava flows or intruded as dikes. These basalts are strongly magnetic and are chiefly responsible for the strong magnetic anomalies observed at the ocean surface. The metamorphosed basalts of the underlying Layer 2B are too weakly magnetic to have much signature. The rocks of the deeper gabbroic Layer 3 may be sufficiently magnetic to add to the skewness of the magnetic anomalies.

5.7.3.1 Marine magnetic anomalies

The origin of marine magnetic anomalies was explained by the Vine–Matthews–Morley hypothesis in 1963 (Section 1.2.5.1). Oceanic basalts were found to have strong and stable remanent magnetizations. Their Königsberger ratios are much larger than unity, so the remanent magnetizations are more important than the magnetization induced by the present-day geomagnetic field. The conventional method of interpreting surveyed magnetic anomalies assumed that the anomaly was due to the *susceptibility contrast* between adjacent crustal blocks. According to the Vine–Matthews–Morley hypothesis the oceanic magnetic anomalies arise from the contrast in *remanent magnetizations* between adjacent, oppositely magnetized crustal blocks. The remanent magnetization is acquired thermally by the basalts in oceanic crustal Layer 2A.

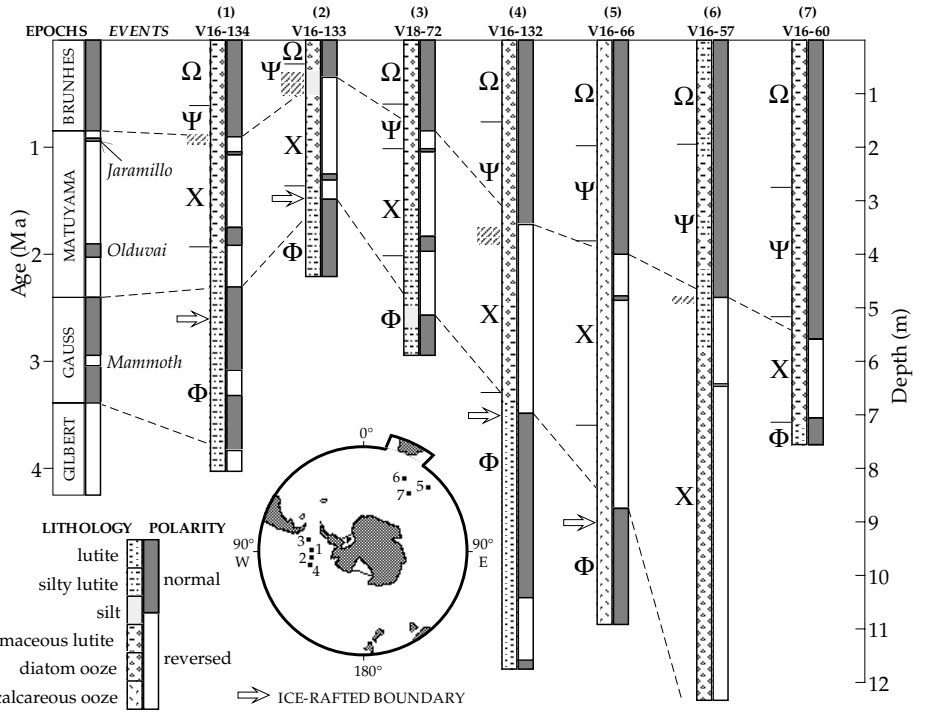

Fig. 5.76 Magnetic reversals in Antarctic deep-sea sediment cores correlate with the radiometric polarity timescale. This allows fossil zones (Greek letters) to be dated. Tie-lines between reversals illustrate the effects of different sedimentation rates (based on data from Opdyke *et al.*, 1968).

The main magnetic mineral in oceanic basalts is titanomagnetite (Section 5.3.2.1). A basaltic lava is initially at a temperature well above 1000 °C. Its titanomagnetite grains frequently have skeletal structures, indicating that they cooled and solidified so rapidly that there was not enough time for the formation of normal crystals. Eventually the temperature of the lava sinks below the Curie point of the titanomagnetite (around 200–300 °C) and the lava acquires a thermoremanent magnetization (TRM) in the direction of the Earth's magnetic field at that time. Basalts formed contemporaneously along an active spreading ridge acquire the same polarity of magnetization. Long thin strips of similarly magnetized crust form on opposite sides of the spreading center. These elongated "crustal blocks" may be hundreds of kilometers in length parallel to the ridge axis and several tens of kilometers wide normal to the ridge, while Layer 2A – the strongly magnetic upper part – is only 0.5 km thick.

Sea-floor spreading persists for millions of years at an oceanic ridge. During this time the magnetic field changes polarity many times. The alternating field polarity leaves some blocks of oceanic crust normally magnetized while their neighbors are reversely magnetized. When the total intensity of the field is measured from a survey ship or aircraft, an alternating sequence of positive and negative anomalies is observed (see Fig. 1.13), which can be interpreted in terms of the crustal magnetization. The anomalies can be correlated almost linearly between parallel profiles across a ridge system; consequently, the stripe-like anomalies are often referred to as *magnetic lineations*.

5.7.3.2 Uniformity of sea-floor spreading

Each anomaly in a set of magnetic lineations derives from a crustal block (or stripe) that formed at a ridge and was subsequently transported away from the spreading center. A magnetized crustal block forms during a period of sea-floor spreading when the geomagnetic polarity was constantly normal or reversed, and therefore represents a polarity chron or subchron. The width of a particular block depends on the duration of the chron and the spreading rate at the ocean ridge.

The spreading rate can be determined easily close to a ridge (see Section 1.2.5.2). The edges of the magnetized crustal stripes correspond to the occurrences of polarity reversals, which can be correlated directly with the radiometrically dated sequence for the last 3–4 Ma determined in lavas on the continents or islands. A plot of the distance of a given polarity reversal from the spreading axis against the age of the reversal is nearly linear near the ridge; the slope of a best-fitting straight line gives the average *half-rate of spreading* at the ridge (see Fig. 1.15). This is half the full rate of plate separation, assuming that sea-floor spreading has been symmetric on each side of the ridge, which is often the case.

Accumulated evidence from marine magnetic profiles allows us to assess the constancy of sea-floor spreading at different ridge systems. It is thought to have been uniform for the longest time in the South Atlantic. A plot of the distance to a given anomaly in the South Atlantic against the distance to the same anomaly in the Indian, North Pacific and South Pacific oceans contains several long linear segments, representing constant rates of sea-floor spreading in both oceans defining the line (Fig. 5.77). A

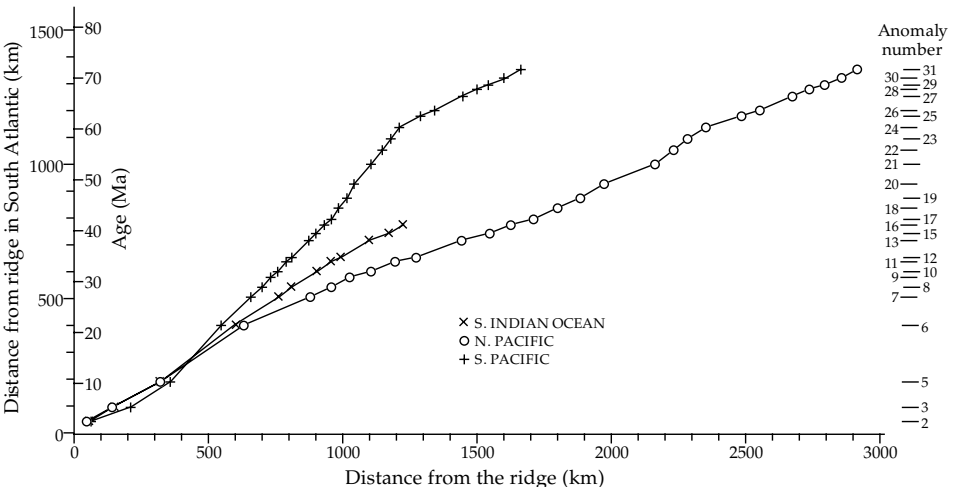

Fig. 5.77 Distances of anomalies from the ridge axis in the South Atlantic plotted against distances to the same anomalies from spreading centers in the Indian, North and South Pacific Oceans (after Heirtzler *et al.*, 1968).

change in gradient indicates a change in spreading rate in one ocean relative to the other. The plot does not exclude a synchronous worldwide change of spreading rate in all oceans, but this would be a rather unlikely occurrence. Clearly the rate of sea-floor spreading changes from time to time, but for long intervals it is a remarkably constant process.

5.7.3.3 The marine record of geomagnetic polarity history

Investigations of magnetic anomalies in all major oceanic areas have given a clear, consistent record of the history of geomagnetic polarity during the past 155–160 Ma. It consists of two sequences of polarity reversals represented by magnetic lineations and a long interval of constant normal polarity (Fig. 5.78). The sequences of chrons derived from magnetic lineations have been confirmed by magnetostratigraphic research.

The most prominent positive magnetic anomalies are numbered in turn from the youngest (anomaly 1 at an active ridge axis) to the oldest (anomalies 33–34 in the Late Cretaceous). The associated polarity chrons are identified by the same number and a letter to indicate the polarity. The polarity chrons in the latest sequence fall largely in the Cenozoic (see Fig. 4.2) and are identified by a leading letter C, which may be taken to stand for either "chron" or "Cenozoic." The current Brunhes normal polarity interval corresponds to chron C1N; the reversed interval older than it is labelled chron C1R. Anomaly 2 corresponds to the normal Olduvai event, which interrupts the reversed Matuyama interval and is identified as polarity chron C2N; the reversed interval older than C2N is called polarity chron C2R, etc. The current reversal sequence began in the Late Cretaceous. The oldest normal polarity chron in the sequence is C33N; it is preceded by reversed polarity chron C33R, which ended a long interval (lasting about 35 Ma) in which no polarity reversals took place. This interval in which the geomagnetic field had a constant normal polarity is variously

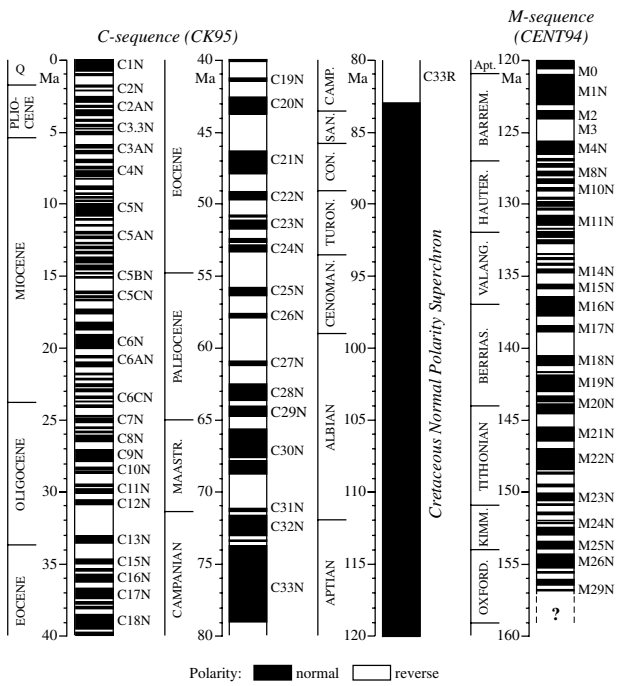

Fig. 5.78 The geomagnetic polarity timescale since the late Jurassic, derived from the interpretation of marine magnetic anomalies and calibrated by coordinated magnetostratigraphy and biostratigraphy. The polarity record of the C-sequence anomalies for the past 85 Ma (CK95) was revised by Cande and Kent (1995); the M-sequence record from 120 Ma to 157 Ma (CENT94) is that of Channell *et al*. (1995). The record of reversals prior to about 155 Ma is uncertain.

called the Cretaceous Quiet Interval, the Cretaceous Normal Polarity Superchron, or chron C34N.

A phase of alternating polarity giving lineated magnetic anomalies precedes the Cretaceous Quiet Interval. It began late in the Middle Jurassic and continued until the middle of the Early Cretaceous. These Late Mesozoic oceanic anomalies are referred to as the M-sequence. To distinguish them from the later sequence the numbered chrons are identified by a leading letter M. The youngest anomalies M0–M8 are numbered sequentially regardless of the magnetization polarity; older than M9 normal and

reverse polarity chrons are paired, as for the Cenozoic. The oldest securely identified chron in the sequence is M29N. Some older anomalies with low amplitudes have been interpreted as polarity chrons, but it has not yet been established that they represent polarity reversals rather than geomagnetic intensity fluctuations.

The oldest regions of the modern oceans correspond to oceanic crust formed approximately 180 Ma ago, when Pangaea broke up and the current episode of sea-floor spreading was initiated. The marine magnetic anomalies over these areas have subdued amplitudes and they do not form lineations. Either no reversals happened during the period of initial spreading or the oceanic crust has not been able to retain the record. The character of the geomagnetic field during this part of the Early Jurassic has not yet been definitively established.

5.7.4 Geomagnetic polarity timescales

The interpretation of marine magnetic anomalies provides the most continuous and reliable record of geomagnetic polarity since the Middle Jurassic. The length of the record greatly exceeds the length of the securely established, radiometrically dated magnetic polarity timescale, which covers only about the past 5 Ma. Thus, it is not possible to date most of the marine magnetic anomalies by direct correlation with a radiometrically dated polarity sequence. Knowledge of the spreading rate at a ridge system provides an alternative way of determining the age of the oceanic crust. Assuming that the rate of sea-floor spreading at the spreading center is constant, the age of a given anomaly can be computed by dividing its distance from the spreading center by the spreading rate. However, this is an unsatisfactory method because the extrapolation is many times longer than the baseline. A further method of dating the polarity record is by establishing the same polarity sequence in sedimentary rocks that are dated paleontologically. This has been achieved in several investigations of the magnetic polarity stratigraphy in pelagic carbonate rocks. Using known absolute ages of major stage boundaries as tie-levels, the ages of magnetic polarity chrons that are too old to be dated directly are calculated by interpolation.

5.7.4.1 Magnetostratigraphic calibration of polarity sequences

The correlation of the radiometrically dated polarity sequence in continental lavas (Fig. 5.74 left) with the magnetic anomaly record near to a spreading ridge was the original method used to date young marine magnetic anomalies. Subsequently, the polarity record was refined by detailed analysis of marine magnetic anomaly sequences. The polarity reversals were located in sediments where they could be dated precisely by counting Milankovitch cycles in the sediments. The combination of improved marine magnetic record and astrochronological

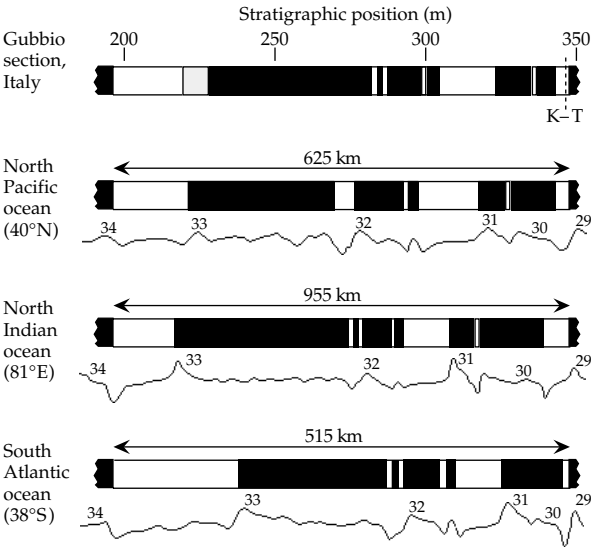

Fig. 5.79 Crustal magnetization patterns for anomalies 29–34 interpreted from magnetic profiles in the Indian, North Pacific and South Atlantic oceans, and comparison with the magnetic polarity stratigraphy in the Gubbio Bottaccione section (after Lowrie and Alvarez, 1977). K–T indicates the position of the Cretaceous–Tertiary boundary, which falls within reversed polarity chron C29R.

dating gave a more reliable polarity timescale for 0–5 Ma (Fig. 5.74 right).

The independent confirmation and dating of older marine magnetic anomalies required combined magnetostratigraphical and paleontological studies in suitable rock formations. The dating of anomalies 29–34, which are the oldest found in the Cenozoic to Late Cretaceous sequence, illustrates this method. Along magnetic profiles in the Indian, North Pacific and South Atlantic oceans, the shapes of anomalies 29–34 are very different because of the different directions of the survey profiles and the orientations of the spreading axes. However, interpretation of the anomalies gives nearly identical crustal magnetization patterns (Fig. 5.79).

The Scaglia Rossa pelagic limestone in the Umbrian Apennines of Central Italy was deposited almost continuously from the Late Cretaceous to the Eocene. Rock magnetic analysis showed that the limestone contained an easily defined stable component of characteristic remanent magnetization. Samples were taken at approximately 0.5–1 m stratigraphic intervals in a long section through the limestone exposed in the Bottaccione gorge near Gubbio. The declinations and inclinations of the stable magnetization, after simple tectonic corrections, were used to calculate the latitude of the virtual geomagnetic pole (VGP) during deposition of the limestone. In times of normal polarity the VGP latitude is near 90°N, during reversed polarity it is near 90°S. The fluctuations of VGP latitude clearly define magnetozones of normal and reversed polarity (Fig. 5.80). The Gubbio polarity record in a 200 m thick section of pelagic limestone correlates almost perfectly with the oceanic polarity sequence derived from anomalies 29–34, measured in

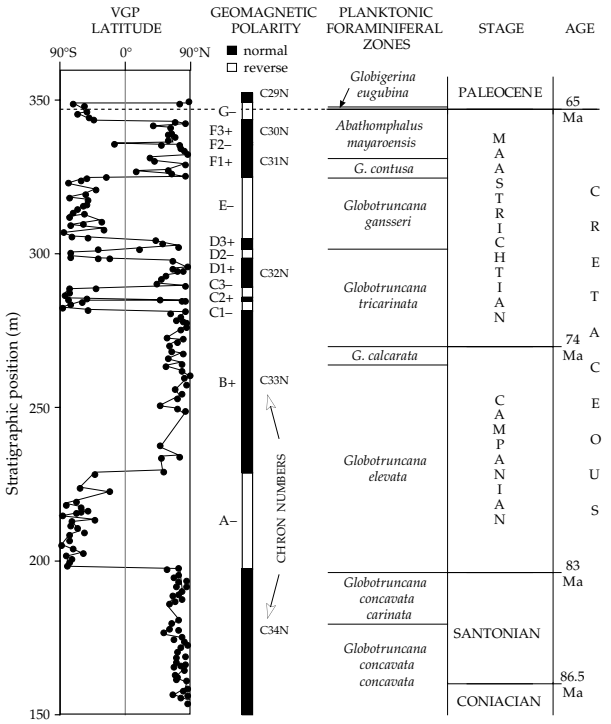

Fig. 5.80 Magnetostratigraphy and biostratigraphy in the Bottaccione section at Gubbio, Italy (after Lowrie and Alvarez, 1977).

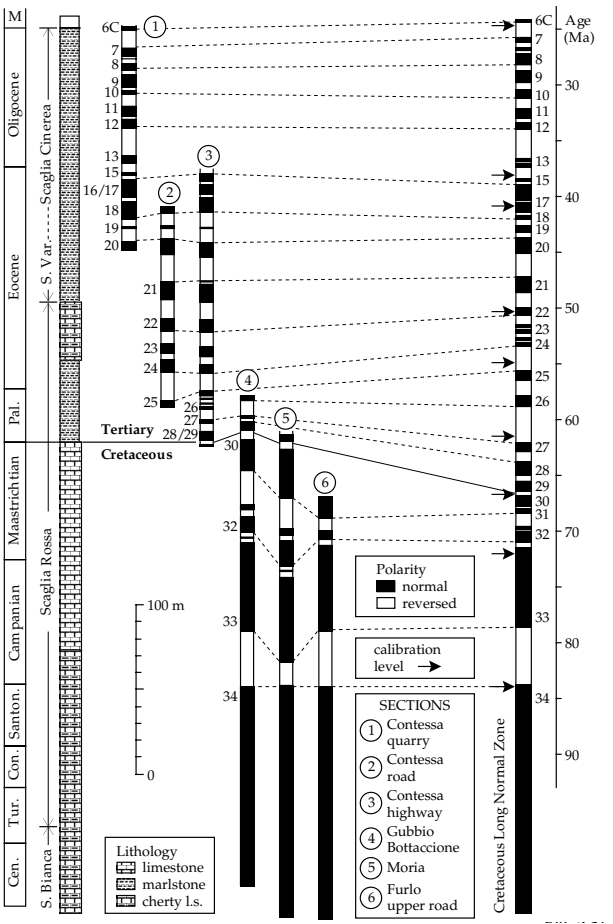

Fig. 5.81 Confirmation and calibration of the oceanic magnetic reversal record in Paleogene and Cretaceous magnetostratigraphic sections in Umbria, Italy (after Lowrie and Alvarez, 1981).

different oceans on profiles that are hundreds of kilometers long (Fig. 5.79). The limestone magnetostratigraphy confirms independently this part of the oceanic magnetic polarity record.

Paleontological studies in the Gubbio section gave the locations of important planktonic foraminifera zones and enabled the positions of the major stage boundaries to be located relative to the polarity sequence. The absolute ages of some important stage boundaries are known from independent radiometric and stratigraphic work. This enabled calculation of the absolute ages of the polarity reversals in the Gubbio section and, by correlation, the ages of the corresponding parts of the ocean floor. For example, the Santonian–Campanian boundary (with an age of about 83 Ma) lies close to the old edge of the reversed polarity chron C33R; the geologically important Cretaceous–Tertiary boundary (age 65 Ma) falls within reversed polarity chron C29R.

In this way the geomagnetic polarity sequence in the Late Cretaceous and Paleogene has been confirmed in magnetostratigraphic sections, and the locations of many major and minor stage boundaries have been correlated to the polarity sequence paleontologically (Fig. 5.81). Reliable absolute ages are available for some of the stage boundaries, which can then be used as calibration levels. The ages of magnetic reversals between the dated tie-points are computed by interpolation, giving a numerical geomagnetic polarity timescale (see Fig. 5.78). In the same way, overlapping magnetostratigraphic sections of Early Cretaceous and Late Jurassic age have permitted independent confirmation and dating of the M-sequence polarity record.

5.7.4.2 *Reconstruction of plate tectonic motions*

Once the ages of magnetic anomalies are known, a map showing the positions of dated anomalies is equivalent to a chronological map of the ocean basins (Fig. 5.82). The different rates of sea-floor spreading are evident from the separations of the isochrons. The oldest domains of the oceans (about 180 Ma) are found in the Atlantic ocean adjacent to the coastlines of North America and Africa, and in the North Pacific ocean. They are very much younger than the oldest rocks from the continents, which are up to 3.6 Ga old. The oceanic crust has been entirely produced since the onset of sea-floor spreading and the anomaly patterns reflect plate motions.

The past motions of the major plates can be obtained in some detail from the anomaly ages given by a geomagnetic polarity timescale. The relative positions of the continents at any time since the late Mid-Jurassic can be reconstructed by matching coeval marine magnetic anomalies formed at the same spreading center. The procedure is similar to the reconstruction of supercontinents

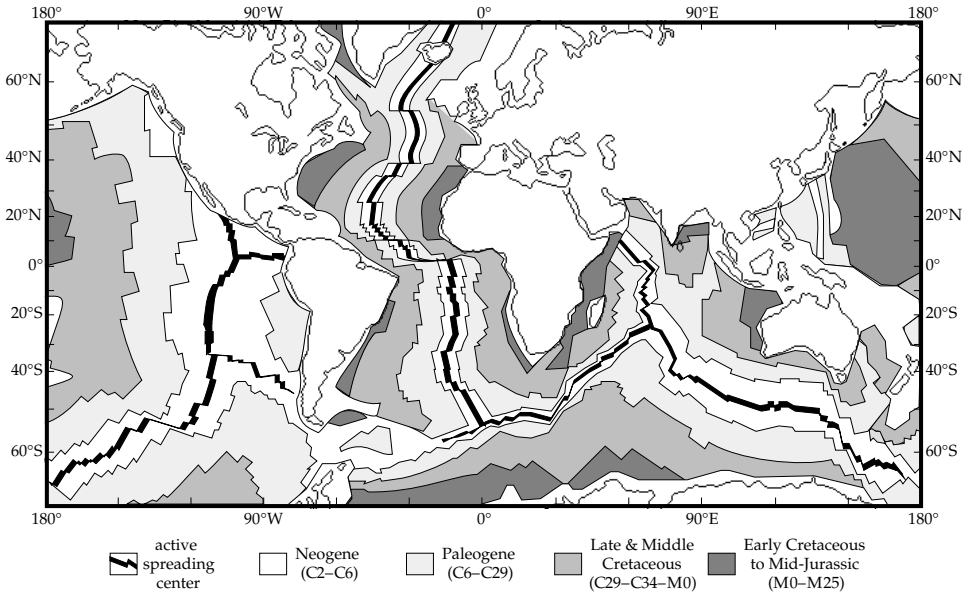

Fig. 5.82 Map of the age of oceanic crust, as interpreted from marine magnetic anomalies (simplified after Scotese *et al.*, 1988).

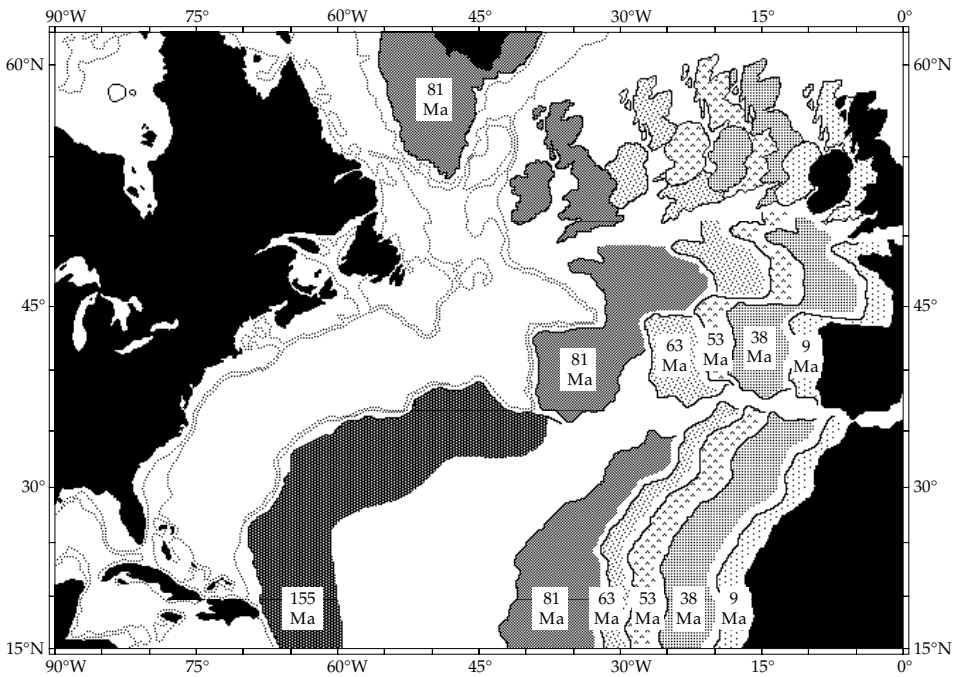

Fig. 5.83 Reconstruction of the history of opening of the North and Central Atlantic oceans. The figure shows the relative positions of Europe and Africa with respect to North America at specific times before the present (after Pitman and Talwani, 1972).

by matching coastlines, 500 fathom depth contours or apparent polar wander paths.

The method is illustrated by the sea-floor spreading between North America and Africa in the Central Atlantic (Fig. 5.83). Anomaly 33 forms a long stripe on each side of the Mid-Atlantic Ridge and subparallel to it. The anomaly is due to the magnetization contrast between chron C33N and the reverse polarity chron C33R which marks the end of the Cretaceous Quiet Interval. Its age is about 81 Ma. The anomaly on the west side of the ridge was formed at the same time as the anomaly on the east side, when the newly formed crust was magnetized at the ridge axis. If the African and North American plates are moved closer together until the east and west anomalies overlap, or until they match along their lengths with minimum misfit, the continents will be brought into the same positions relative to each other that they occupied around 81 Ma ago. By repeating this process of matching dated anomalies it is possible to reconstruct the successive relative positions of the African and North American plates as they separated.

Marine magnetic anomalies in the North Atlantic can be used likewise to describe the relative plate motions between Europe and North America. A picture evolves of the separate histories of separation of Africa and Europe from North America. The differences between the European–North American and African–North American

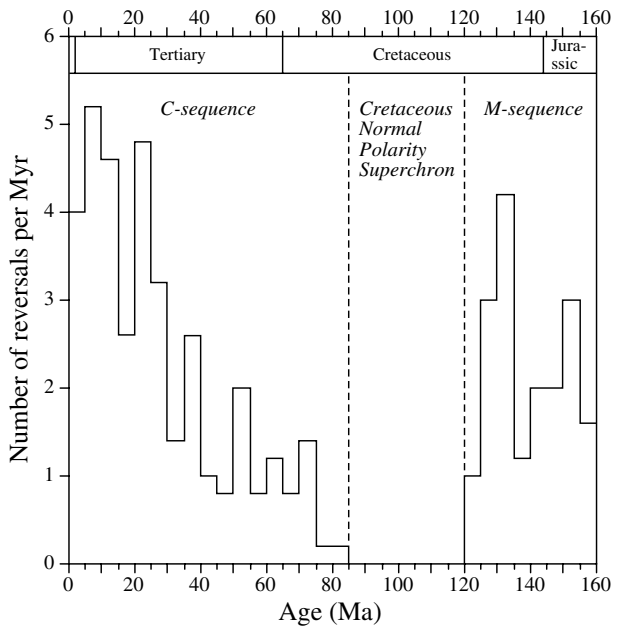

Fig. 5.84 The number of geomagnetic polarity reversals per Myr during the last 160 Myr, computed in 4 Myr intervals from the composite reversal record in Fig. 5.78.

plate motions permit the history of relative motion between Africa and Europe to be inferred. In the Late Cretaceous and Early Tertiary Africa moved eastwards in a giant shear motion relative to Europe, but since the Middle Tertiary the motion of Africa has been one of convergence and collision with the European plate. This is compatible with the formation of the Alpine fold belt and the present-day seismicity in the Alpine region.

5.7.5 Frequency of polarity reversals

Visual examination of the magnetic polarity record in Fig. 5.78 shows that the rate of polarity reversals has been quite variable in the last 160 Ma. A simple way to portray the reversal rate is to count the numbers of reversals in successive bins of equal duration (e.g., 4 Myr) and compute the average number per Myr. The plot of reversal rate against age (Fig. 5.84) is uneven, but has some distinct features.

The reversal frequency during the M-sequence averaged about 3–4 reversals/Myr. From about 130 Ma ago the reversal rate slowed down until the beginning of the Cretaceous Normal Polarity Superchron (CNPS) at about 121 Ma ago. There were no reversals for the following 38 Myr. After the end of the CNPS about 83 Ma ago the reversal rate was at first very low, but gradually speeded up. It reached a peak of about 5 reversals/Myr in the Late Miocene, about 10 Ma ago, and has since decreased slightly to about 4 reversals/Myr. The current interval of normal polarity (known as the Brunhes or chron C1N) has lasted 0.78 Myr, which is much longer than the mean length of polarity chrons in the Late Tertiary.

In 1968 A. Cox theorized that reversals are random events, triggered by unknown mechanisms that affect the fluid motions in the Earth's liquid outer core. With a random reversal process there would be no continuity between successive reversals; as soon as a reversal was completed, the next one would be as likely to occur immediately as at any time later. Because there would be no waiting period, this type of mechanism would generate a large number of very short polarity chrons and a small number of long chrons. The frequency distribution of polarity chron durations should decrease exponentially with increasing chron duration. In fact this model does not fit the observed lengths of polarity intervals precisely. The polarity sequence contains comparatively few short chrons, a lot of medium duration chrons and few long chrons. This may imply that the process that causes reversals is not completely random. A distinct length of time may elapse after a reversal for the fluid motions to recover sufficiently to allow the next reversal to happen. However, the mechanism that causes a reversal is inadequately understood.

5.7.6 Early Mesozoic and Paleozoic reversal history

Because of the availability of the excellent marine magnetic anomaly record, it has been possible to construct a well dated history of geomagnetic polarity in the last 155–160 Ma (see Fig. 5.78). The determination of a geomagnetic polarity timescale for eras older than the Middle Jurassic is more complicated, because no comparable oceanic record exists. Paleomagnetic results show numerous reversals during the Triassic, but the Permian and Late Carboniferous were dominated by reversed polarity. A long interval of constant reversed polarity – the Kiaman interval – is a distinctive feature of the Paleozoic polarity record. Earlier in the Paleozoic reversals were common. Although magnetostratigraphic investigations of many formations are in progress, no unique record of the polarity succession is available for the Early Mesozoic or Paleozoic.

At present it is only possible to analyze Paleozoic polarity history in terms of the bias toward normal or reverse polarity. The polarity bias broadly defines superchrons (Fig. 5.85). When as many reversed as normal magnetizations are found it is assumed that the field polarity has been reversing; the interval is called a mixed polarity superchron. The Late Cretaceous and Cenozoic and the Triassic illustrate mixed polarity superchrons. Sometimes, for unknown reasons, the polarity was constant for long intervals. This was the case during the Cretaceous Quiet Interval, which in terms of polarity bias is called the Cretaceous Normal Polarity Superchron. The Kiaman reversed polarity interval is the same as the Permo-Carboniferous Reversed Polarity Superchron. The derivation of a more detailed history of geomagnetic polarity for Early Mesozoic and Paleozoic time is a massive task for paleomagnetists and biostratigraphers. Because of the absence of a marine magnetic record each polarity sequence will have to be confirmed by repetition in several magnetostratigraphic

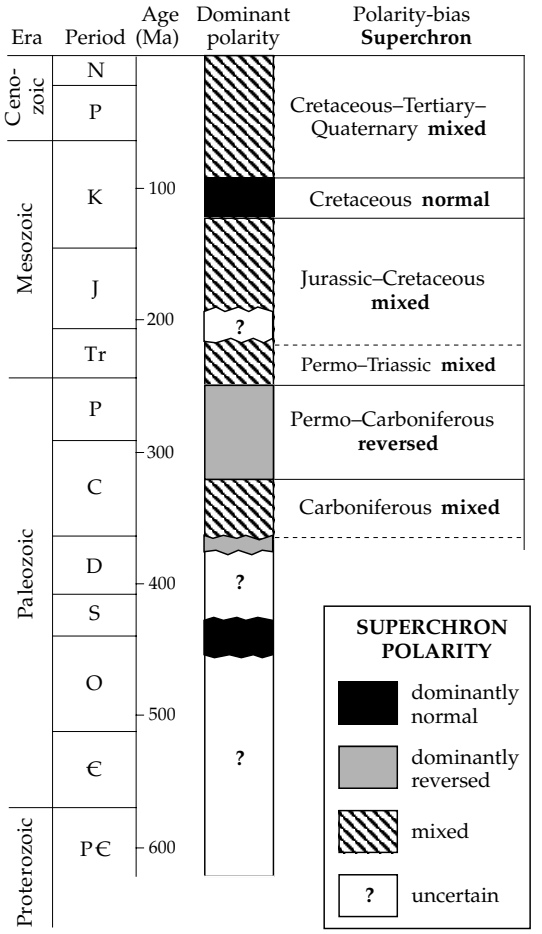

Fig. 5.85 Geomagnetic polarity bias superchrons in the Paleozoic, Mesozoic and Cenozoic (after Harland *et al.*, 1982).

sections before it can be accepted as globally significant and representative of dipole field behavior.

5.8 SUGGESTIONS FOR FURTHER READING

Introductory level

Butler, R. F. 1992. *Paleomagnetism: Magnetic Domains to Geologic Terranes*, Boston, MA: Blackwell Scientific.

Campbell, W. H. 2001. *Earth Magnetism: A Guided Tour Through Magnetic Fields*, San Diego, CA: Harcourt/Academic Press.

Campbell, W. H. 2003. *Introduction to Geomagnetic Fields*, Cambridge: Cambridge University Press.

Mussett, A. E. and Khan, M. A. 2000. *Looking into the Earth: An Introduction to Geological Geophysics*, Cambridge: Cambridge University Press.

Intermediate level

Evans, M. E. and Heller, F. 2003. *Environmental Magnetism: Principles and Applications of Enviromagnetics*, New York: Academic Press.

Lillie, R. J. 1999. *Whole Earth Geophysics: An Introductory Textbook for Geologists and Geophysicists*, Englewood Cliffs, NJ: Prentice Hall.

Sleep, N. H. and Fujita, K. 1997. *Principles of Geophysics*, Oxford: Blackwell Science.

Tauxe, L. 2002. *Paleomagnetic Principles and Practice*, Dordrecht: Kluwer Academic Publishers.

Advanced level

Blakely, R. J. 1995. *Potential Theory in Gravity and Magnetic Applications*, Cambridge: Cambridge University Press.

Cox, A. (ed) 1973. *Plate Tectonics and Geomagnetic Reversals*, San Francisco, CA: W. H. Freeman.

Dunlop, D. J. and Özdemir, Ö. 1997. *Rock Magnetism: Fundamentals and Frontiers*, Cambridge: Cambridge University Press.

McElhinny, M. W. and McFadden, P. L. 2000. *Paleomagnetism: Continents and Oceans*, New York: Academic Press.

Merrill, R. T., McElhinny, M. W. and McFadden, P. L. 1996. *The Magnetic Field of the Earth: Paleomagnetism, the Core, and the Deep Mantle*, New York: Academic Press.

Opdyke, N. D. and Channell, J. E. T. 1996. *Magnetic Stratigraphy*, San Diego, CA: Academic Press.

Van der Voo, R. 1993. *Paleomagnetism of the Atlantic, Tethys and Iapetus Oceans*, Cambridge: Cambridge University Press.

5.9 REVIEW QUESTIONS

1. What is the evidence that the geomagnetic field originates inside the Earth?
2. Why is the geomagnetic field at the Earth's surface mainly a dipole field?
3. What is the non-dipole geomagnetic field? How large is it compared to the dipole field at the Earth's surface? Is its importance relative to the dipole field greater or less at the core–mantle boundary?
4. What is the magnetosphere? How does it originate?
5. What are the Van Allen belts? How are they formed?
6. Why do electrically charged particles from the solar wind have curved paths in the Earth's magnetic field?
7. The geomagnetic field has a large anomaly over the South Atlantic, where its intensity is weakened by about 20%. What effects could this anomaly have on extra-terrestrial radiation that impinges on the Earth? What might be the consequences for (a) Earth-orbiting satellites, (b) astronauts, (c) passengers and crew in high-flying aircraft.
8. What is the ionosphere? What effect does it have on the magnetic field measured at the Earth's surface?
9. What is a *magnetic storm*? What is its cause and what are its effects?
10. Describe the principle of operation of (a) the fluxgate magnetometer, and (b) the proton-precession magnetometer.

11. Which corrections must be made to magnetic survey measurements in order to define a magnetic anomaly?
12. Describe how the magnetic anomaly of a very wide, vertically magnetized thin sheet varies with position from one side of the sheet to the other. Where is the anomaly largest and where is it smallest?
13. What are diamagnetism, paramagnetism, ferromagnetism, ferrimagnetism, and antiferromagnetism?
14. Which type of magnetism is exhibited by (a) quartz, (b) calcite, (c) clay minerals, (d) magnetite, and (e) hematite?
15. What is remanent magnetization? What types of remanent magnetization are possible in (a) sedimentary, (b) metamorphic, and (c) igneous rocks? Explain how they originate.
16. Explain what is wrong with the following explanation of the origin of thermoremanent magnetization (TRM): "When cooled below the Curie point the magnetite grains align with the magnetic field to give a TRM."
17. What are (a) the declination and (b) the inclination of the magnetic field at a given location? What is the direction of the magnetic field at the magnetic equator?
18. What is implied if the inclination of the remanent magnetization of a rock differs from the inclination of the magnetic field at the same location? What is implied if the declinations differ?
19. How might a rock acquire more than one component of remanent magnetization?
20. How can the original direction of remanent magnetization be identified in a rock that has more than one magnetization component?
21. What is the *geocentric axial dipole* (GAD) hypothesis and why is it important for paleomagnetism?
22. What is an apparent polar wander (APW) path? Why is it an *apparent* path? How are APW paths for different continents interpreted in terms of global tectonics?
23. What is magnetic polarity stratigraphy? How is a magnetic polarity stratigraphy calibrated for young rocks and for old rocks?
24. How do oceanic magnetic anomalies originate? Explain the survey procedure that might be used to measure them.
25. What is a geomagnetic polarity timescale (GPTS)? How is a GPTS constructed and calibrated?

5.10 EXERCISES

1. Assuming that the geomagnetic field corresponds to a geocentric axial dipole, calculate the latitude of a site where the field inclination is 45°.
2. With the same assumption, calculate the inclination of the geocentric axial dipole field at latitude 45°N.
3. The magnetic moment of the Earth's geocentric dipole is 7.7674×10^{22} A m^2. Assuming an axial dipole, calculate the total geomagnetic field intensity as a function of latitude. What is the latitudinal variation of the total field in nT km^{-1} at 30°N?
4. Compute the inclination and declination of the magnetic field that would be observed in Boulder, Colorado (40°N, 105°W) if the Earth's field corresponded to a perfect geocentric dipole whose axis penetrates the Earth's surface at 80°N, 72°W.
5. Show that, for a small displacement along a meridian of magnetic longitude at magnetic latitude 45°N, the change of inclination is exactly 4/5 the change in latitude.
6. The north magnetic pole is at 77°N 102°W, the south magnetic pole is at 66°S 139°E.
   (a) Why are the poles not antipodal (exactly opposite)?
   (b) What is the closest distance between the center of the Earth and the straight line joining the poles?
7. Measurements of the magnetic field elements at a geomagnetic observatory gave the following results: N-component 27,000 nT; E-component −1800 nT; V-component −40,000 nT.
   (a) Is the observatory in the northern or southern hemisphere?
   (b) What is the total field intensity at the site?
   (c) What are the local values of inclination and declination of the field?
8. The IGRF for 2005 gives the values of the Gauss coefficients for the dipole and quadrupole components of the geomagnetic field shown in the following table.

Gauss coefficients [nT]			
g_1^0	–29,557	g_2^0	−2,341
g_1^1	−1,672	g_2^1	+ 3,047
h_1^1	+ 5,080	h_2^1	−2,595
		g_2^2	+ 1,657
		h_2^2	−517

   The mean squared value, R_n, of the intensity of the geomagnetic field at the Earth's surface due to the component of degree n is given by

$$R_n = (n+1)\sum_{m=0}^{n}\left((g_n^m)^2 + (h_n^m)^2\right)$$

   (a) Calculate the root mean square intensity of the dipole component of the field at the Earth's surface.
   (b) Calculate the corresponding intensity of the quadrupole component and express it as a percentage of the dipole field intensity.
9. The values of the Gauss coefficients in the previous exercise are given for the Earth's surface. Recalculate

the root mean square intensities of the dipole and quadrupole field components at the core–mantle boundary (Earth's radius 6371 km, core radius 3485 km).

10. What are the values of n and m in the designation Y_n^m for the spherical harmonic functions illustrated in Fig. B5.3.2 in Box 5.3? Sketch how these patterns would appear on the opposite side of the reference sphere to the one you are looking at?

11. In an aeromagnetic survey at a flight altitude of 2000 m above sea-level, the maximum total field anomaly over an orebody was 30 nT. In a repeated measurement at 2500 m altitude the maximum amplitude of the anomaly was 20 nT. Calculate the depth of the orebody below sea-level assuming (i) a monopole source and (ii) a dipole source for the anomaly.

12. The vertical field magnetic anomaly ΔB_z over a vertically magnetized anticline (represented by a horizontal cylinder) is given by Eq. (5.54). Draw a sketch of the anomaly on a profile normal to the structure. Observe the horizontal positions where the anomaly is zero.
    (a) Calculate the horizontal positions where the anomaly has extreme values.
    (b) Calculate the peak-to-peak values of the anomaly.

13. Assume that the core of an anticline is made of basalt, the host formation is limestone, and the rocks are vertically magnetized with susceptibilities given by the median values in Fig. 5.13.
    (a) Compute the induced magnetization contrast when the vertical magnetic field intensity is 40,000 nT.
    (b) If the anticline is modelled by a horizontal cylinder whose radius is one fifth the depth of its axis, calculate the maximum amplitude of the vertical field anomaly over the structure.

14. Assuming the gravity anomaly over an anticline as given by Eq. (2.94), apply the Poisson relationship (Box 5.5) to obtain the *horizontal* field magnetic anomaly ΔB_x of a vertically magnetized anticline with radius R and magnetization contrast ΔM_z.

15. The north (N), east (E) and vertical (V) components of a magnetization can be calculated from its intensity (M), declination (D) and inclination (I) using the following relationships:

$$N = M\cos I\cos D$$

$$E = M\cos I\sin D$$

$$V = M\sin I$$

In the progressive thermal demagnetization of a sample of Cretaceous limestone for a paleomagnetic study the remanent magnetizations given in the table were measured at different temperatures T.

T [°C]	M [10^{-5} A m^{-1}]	D [°]	I [°]
200	5.08	60.8	60.1
300	3.87	62.1	59.8
400	3.02	61.2	62.1
500	2.10	62.2	61.6
550	1.18	63.1	60.9

    (a) Calculate the north (N), east (E) and vertical (V) components of the magnetizations at each demagnetization stage.
    (b) Plot the N-components against the E-components, fit a straight line, and determine the optimum declination for the stable magnetization direction.
    (c) Plot the V-components against either the N- or E-components, fit a straight line, and compute the optimum inclination for the stable magnetization direction.
    (d) The straight lines do not pass through the origin of the plot. What does this imply?

16. In the same paleomagnetic study, the following stable directions of remanent magnetization, corrected for the dip of bedding in the limestone formation, were measured in five samples from the same site:

Sample	D [°]	I [°]
SR-04	329.7	40.6
SR-05	336.6	24.7
SR-07	326.2	46.0
SR-10	321.1	40.9
SR-12	322.7	44.9

    (a) Calculate the direction cosines (λ_N, λ_E, λ_V) of the north, east and vertical components of each stable direction, using the relationships

$$\lambda_N = \cos I\cos D$$

$$\lambda_E = \cos I\sin D$$

$$\lambda_V = \sin I$$

    (b) Add up the values for each direction cosine. Let the sums be X, Y and Z, where

$$X = \sum\lambda_N \quad Y = \sum\lambda_E \quad Z = \sum\lambda_V$$

Calculate the vector sum of the directions, R, and the declination D_{m} and inclination I_{m} of the mean direction using the relationships

$$R = \sqrt{X^2 + Y^2 + Z^2}$$

$$\tan D_{\mathrm{m}} = Y/X \qquad \sin I_{\mathrm{m}} = Z/R$$

    (c) Using the computed value of R, calculate the precision parameter k of the data and the 95% confidence error (α_{95}) for the mean direction.

17. The samples analyzed in the previous exercise were gathered at a site in Italy with latitude 43.4°N, longitude 12.6°E. Calculate the latitude and longitude of the paleomagnetic pole position for the Italian limestone.

18. Assume that the location of the Late Cretaceous paleomagnetic pole for the European plate is at 72°N, 154°E and the corresponding pole for the African plate is at 67°N, 245°E.
    (a) Calculate the expected 'European' and 'African' directions at the Italian site in the previous exercise.
    (b) Compare the expected directions with the observed directions and explain how the paleomagnetic results from the Italian limestone should be interpreted.